Process of Evaporation from a Dry Bare Soil

Tsutomu YAMANAKA

A Dissertation Submitted to
the Doctoral Program in Geoscience,
the University of Tsukuba
in Partial Fulfillment of the Requirements for
the Degree of Doctor of Philosophy in Science

January, 1998

Contents

Abstract

Attempts have been made in the previous studies to model the bare soil evaporation or its restriction during soil drying. Recently, the concept of surface resistance, which is the resistance to the vapor transfer in the soil, was introduced and being widely accepted as useful concept to understand or represent the restriction of evaporation by soil moisture deficit. However, there remained several unsettled questions, such as the structure and the temporal variation of the evaporation zone.

In the present study, the microscopic physical process of bare soil evaporation, including evaporation beneath the soil surface and water transport in the liquid and vapor phases, is presented with an emphasis on the dry surface layer (DSL) phenomena. To investigate the above processes, field observations on micrometeorology and soil hydrology were carried out at three representative bare lands which consist of different types of soils, with a preliminary investigation by means of numerical simulation.

Conclusions from the present study are as follows:

(1) Evaporation of soil water takes place at the bottom boundary of the DSL throughout a day, and also occurs within the DSL in the forenoon. The former is caused by a deficit of or insufficient liquid water supply from deeper soil layers, and the latter is introduced by large change in the condition of equilibrium between the liquid and vapor phases of water in the DSL with diurnal variation of solar radiation.

(2) For coarse-textured soils having low specific water capacity, the phase of water transported upward changes in a narrow zone around the bottom boundary of the DSL, and the amounts of evaporation and condensation occurring within the DSL are small. In contrast, for fine-textured soils having high specific water capacity, the liquid water transport is not negligible in the DSL, and the two types of evaporation tend to combine over a wider zone.

(3) Degree of the restriction of evaporation during soil drying largely depends on the depth of the dominant part of the evaporation zone. The movement of the dominant part

of the evaporation zone affects the partitioning of available energy both in inter-diurnal and diurnal time scales, and induces a change in diurnal variation patterns of energy fluxes at the soil surface.

(4) A redefinition of the DSL is needed as the layer in which a reduction of relative humidity occurs due to lack of or insufficient liquid water supply from deeper soil layers and the layer has whitish color relative to that of the underlying soil.

Key words: bare soil evaporation, restriction of evaporation, surface resistance, evaporation zone, dry surface layer (DSL)

List of Tables

List of Figures

List of Symbols

Symbol	Definition	Unit
A	logarithmic value of roughness Reynolds number	—
A_T	amplitude of the surface temperature wave	K or °C
a	empirical parameter in Equations (3.7) and (3.8)	1/m
a_v	ratio of the eddy diffusivity for water vapor and the eddy viscosity under neutral conditions (= 1.0)	—
Bo	Bowen ratio ($\equiv H/LE$)	—
Bo_{after}	afternoon-averaged Bowen ratio	—
Bo_{fore}	forenoon-averaged Bowen ratio	—
C	volumetric heat capacity of the soil	J/m^3K
C_1	volumetric heat capacity of the soil in the Layer 1	J/m^3K
C_E	bulk transfer coefficient for vapor transfer	—
C_H	bulk transfer coefficient for sensible heat transfer	—
C_l	volumetric heat capacity of liquid water	J/m^3K
C_m	volumetric heat capacity of soil mineral	J/m^3K
c_A	empirical parameter in Equation (3.10)	—
c_B	empirical parameter in Equation (3.10)	—
c_C	empirical parameter in Equation (3.10)	—
c_D	empirical parameter in Equation (3.10)	—
c_E	empirical parameter in Equation (3.10)	—
c_p	specific heat of the air under constant pressure	J/kgK
D_{av}	molecular diffusivity of water vapor in the air	m^2/s
D_{avi}	molecular diffusivity of water vapor for isotopic species i in the air	m^2/s

D_{lei}	effective isotopic diffusivity in liquid phase for species i	m^2/s
D_{ve}	effective vapor diffusivity in the soil	m^2/s
d	dumping depth ($\equiv (2\lambda/C\omega)^{1/2}$)	m
d_0	zero-plane displacement height	m
d_1	dumping depth for the Layer 1	m
d_2	damping depth for the Layer 2	m
E	rate of evaporation	kg/m^2s
E^*	referenced evaporation rate over a period between time steps	kg/m^2s
E_{eq}	equilibrium evaporation defined by Equation (2.19)	kg/m^2s
E_{node}	evaporation rate at a calculation-node	kg/m^2s
E_{sat}	evaporability defined by Equation (2.10)	kg/m^2s
E_{pen}	evaporation rate derived by Penman equation (Equation (2.5))	kg/m^2s
E_t	threshold rate of evaporation controlled by soil moisture profile	kg/m^2s
e_a	vapor pressure of the air	hPa
e_s	vapor pressure of the air at the soil surface level	hPa
$e_{sat}(T)$	saturation vapor pressure at temperature T	hPa
F_b	flux determined by Bowen ratio /energy balance method	W/m^2
F_m	flux estimated by the energy balance model	W/m^2
F_b	flux determined by profile method	W/m^2
$f(z)$	depth function defined by Equation (A.3)	m
f_e	enhancement factor for additive vapor diffusion process in the soil	—
G	soil heat flux	W/m^2
G_0	conductive heat flux into the soil at the soil surface	W/m^2

G_1	conductive heat flux from the Layer 1 to the effective evaporation zone	W/m^2
G_2	conductive heat flux from the effective evaporation zone to the Layer 2	W/m^2
G_c	conductive heat flux in the soil	W/m^2
G_{plate}	conductive heat flux measured by heat flux plate	W/m^2
g	gravitational acceleration	m/s^2
H	sensible heat flux	W/m^2
H^*	referenced sensible heat flux over a period between time steps	W/m^2
h	relative humidity	—
h_a	relative humidity in the atmosphere	—
h_s	relative humidity of the air at the soil surface level	—
h_x	difference between i-th and $(i+1)$-th approximate values for x	—
h_y	difference between i-th and $(i+1)$-th approximate values for y	—
J_1	water flux at the depth of 1 cm	kg/m^2s
J_5	water flux at the depth of 5 cm	kg/m^2s
J_b	water flux across the bottom boundary of the surface soil layer	kg/m^2s
J_h	heat flux in the soil	W/m^2
J_l	liquid water flux	kg/m^2s
J_v	vapor flux	kg/m^2s
K	unsaturated hydraulic conductivity	m/s
K_{sat}	saturated hydraulic conductivity	m/s
k	the von Kármán's constant $(= 0.4)$	—

LE	latent heat flux ($\equiv lE$)	W/m^2
LE_h	latent heat flux estimated from specific humidity gradient in the DSL by using Equation (7.2)	W/m^2
l	latent heat for vaporization	J/kg
M_{dw}	mass of distilled water added to soil sample for measuring water quality of soil water	kg
M_s	mass of soil particles	kg
M_w	mass of liquid water	kg
M_{ws}	mass of wet soil sample used for measuring water quality of soil water	kg
m	empirical parameter in Equations (3.7) and (3.8)	—
n	empirical parameter in Equations (3.7) and (3.8)	—
P	precipitation	mm
p	atmospheric pressure (= 1013.15)	hPa
Q_n	available energy ($\equiv R_n - G$)	W/m^2
q	specific humidity	kg/kg
q_s	specific humidity of the air at the soil surface level	kg/kg
R	gas constant for water vapor (= 461.5)	J/kgK
R_i	Richardson number	—
R_{ld}	downward long-wave radiation (or atmospheric radiation)	W/m^2
R_{lu}	upward long-wave radiation (or terrestrial radiation)	W/m^2
R_n	net radiation	W/m^2
R_n^*	referenced net radiation over a period between time steps	W/m^2
R_{sd}	downward short-wave radiation (or solar radiation)	W/m^2
R_{su}	upward short-wave radiation	W/m^2
r	correlation coefficient	—

r_{av}	aerodynamic resistance to vapor transfer in the atmosphere ($\equiv 1/C_E u$)	s/m
r_c	canopy resistance in Equation (2.15)	s/m
r_s	surface resistance in Equation (2.12) or (2.16)	s/m
r_{sv}	resistance to vapor transfer in the surface soil	s/m
r_s^*	modified surface resistance in Equation (2.13) or (2.17)	s/m
S	change rate of heat storage in the soil	W/m^2
S_1	change rate of heat storage in the Layer 1	W/m^2
Sc	Schmidt number ($\equiv \nu/D_{av}$; $= 0.595$ in the lower atmosphere)	—
S_{s-p}	change rate of heat storage in a soil layer between the soil surface and heat flux plate	W/m^2
s	slope of saturation vapor pressure curve	hPa/K
T	temperature	K or °C
T^*	referenced temperature over a period between time steps	K or °C
$\bar{T}$	mean soil temperature	K or °C
T_2	deep soil temperature	K or °C
T_a	air temperature	K or °C
T_e	temperature at the (effective) evaporation zone	K or °C
T_{max}	monthly averaged daily maximum temperature	°C
T_{min}	monthly averaged daily minimum temperature	°C
T_s	soil surface temperature	K or °C
t	time	s
t_{ls}	local standard time (LST)	hr
u	wind velocity	m/s
u_*	friction velocity	m/s
W	change rate of water storage in the surface soil layer	kg/m^{2}s

W_{0-1}	change rate of water storage in the surface soil layer of 1 cm thickness	kg/m^{2}s
W_{0-5}	change rate of water storage in the surface soil layer of 5 cm thickness	kg/m^{-2}s
w	gravimetric water content	kg/kg
x	variable	—
y	variable	—
z	depth	m
$\bar{z}$	penetration depth ($\equiv \rho_{vsat} D_{ve}/\rho_l E$)	m
$\hat{z}_i$	decay length ($\equiv D_{lei}/E$)	m
z_0	surface roughness length	m
z_{0+}	roughness Reynolds number ($\equiv u_* z_0/\nu$)	—
z_{0m}	roughness length for momentum transfer	m
z_{0v}	roughness length for vapor transfer	m
$z_{0v,r}$	value obtained by Equation (6.8)	m
$z_{0v,s}$	value obtained by Equation (6.10)	m
z_a	reference level in the atmosphere	m
z_e	depth of the (effective) evaporation zone	m
z_{ef}	depth of the evaporation front	m
z_w	depth of water table	m
α	surface moisture availability parameter used in Equation (2.8)	—
α_{PT}	empirical constant used in Equation (2.18)	—
α_i^*	equilibrium isotope fractionation factor for species i	—
α_s	albedo of the soil surface	—
β	surface moisture availability parameter used in Equation (2.11)	—

β'	evaporation ratio ($\equiv E/E_{pen}$)	—
β_0	weighting factor ($\equiv (u_*/100 - 2)/18$)	—
γ	psychometric constant ($\equiv c_p/l$)	hPa/K
ΔT_s	change in surface temperature	K
Δt	time interval	s
$\Delta q_{sat}(T)$	change in saturation specific humidity	kg/kg
$\Delta\theta$	change in volumetric water content	m^3/m^3
δ_{DSL}	thickness of the DSL	cm
δ_i	isotopic delta value for species i	$^\circ/_{oo}$
δ_i^a	isotopic delta value of the vapor in the atmosphere	$^\circ/_{oo}$
δ_i^{res}	isotopic delta value of input water	$^\circ/_{oo}$
δ_i^{ef}	isotopic delta value of soil water at the evaporating front	$^\circ/_{oo}$
δ_s	thickness of the surface soil layer	m
ϵ_i^*	equilibrium enrichment ($\equiv 1 - \alpha_i^*$)	—
ε_s	emissivity of the soil surface	—
η_i	diffusion ratio excess ($\equiv D_{av}/D_{avi} - 1$)	—
θ	volumetric water content	m^3/m^3 or %
$\bar{\theta}$	average volumetric water content over z_{ef} to z	m^3/m^3
θ_{0-1}	volumetric water content of the surface soil layer of 1 cm thickness	m^3/m^3 or %
θ_{0-5}	volumetric water content of the surface soil layer of 5 cm thickness	m^3/m^3 or %
θ_1	representative volumetric water content in the Layer 1	m^3/m^3
θ_2	representative volumetric water content in the Layer 2	m^3/m^3
θ_{ad}	(volumetric) water content at air-dry condition	m^3/m^3
θ_d	(volumetric) water content of the deep soil layer	m^3/m^3

θ_{fc}	(volumetric) water content at field capacity	m^3/m^3
θ_r	residual (volumetric) water content	m^3/m^3
θ_s	(volumetric) water content of the surface soil layer	m^3/m^3
θ_{sat}	saturated (volumetric) water content	m^3/m^3
θ_{wilt}	(volumetric) water content at wilting point	m^3/m^3
λ	thermal conductivity of the soil	W/mK
λ_1	thermal conductivity of the soil in the Layer 1	W/mK
λ_2	thermal conductivity of the soil in the Layer 2	W/mK
λ_s	thermal conductivity of the surface soil	W/mK
ν	kinematic viscosity	m^2/s
ρ	density of the air	kg/m^3
ρ_b	dry bulk density of the soil	kg/m^3
ρ_l	density of liquid water	kg/m^3
ρ_v	density of water vapor	kg/m^3
ρ_{vsat}	saturation vapor density	kg/m^3
σ	Stefan-Boltzmann constant ($= 5.6697 \times 10^{-8}$)	W/m^2K^4
X	ion concentration as milliequivalents per unit volume of soil matrix	$meq/m^3(soil)$
χ	ion concentration in the sample water	meq/l
Ψ	water potential	m
$\Psi_{sm}(\zeta)$	stability correction function for momentum transfer	—
$\Psi_{sv}(\zeta)$	stability correction function for water vapor transfer	—
ψ	matric potential	m
ψ^*	referenced matric potential over a period between time steps	m
ψ_s	matric potential of the water in the surface soil	m
ω	angular frequency of oscillation	1/s

List of Abbreviations

Abbreviation	Definition
ASL	atmospheric surface layer
DSL	dry surface layer
GCM	general circulation model
IOD	intensive observation day
MAD	mean absolute difference
OTD	ordinary temperature distillation
RMSD	root mean square difference

Chapter 1

Introduction

1.1 Objectives

In general, specific humidity of the air contacting with the surface of a fairly wet soil can be taken as the saturation value at the temperature of the soil surface. Therefore, the rate of evaporation from a wet soil-surface can hardly depend on the soil moisture conditions. During the soil drying, however, specific humidity at the soil surface is reduced below the saturation value, and then the evaporation is restricted strongly depending on the soil moisture conditions.

In the last two decades, many investigators have attempted to quantify the effect of soil drying on the restriction of evaporation, and numerous formulas for representing it have been proposed. In those attempts, the concept of surface resistance, which is the resistance to the vapor transfer in the soil, has been widely accepted as an useful concept to understand or represent the restriction of evaporation. However, there remained several unsettled questions, such as the structure of the evaporation zone (the zone where the vaporization of water takes place), and its dependency on soil types or atmospheric conditions.

On the other hand, it is well known that the dry surface layer (DSL) is formed at bare soil surface during soil drying. It has often been pointed out that the restriction of evaporation

is closely related to the formation of the DSL. However, there are few investigations on the relationship between the evaporation zone and the DSL for soils other than sand. Therefore, for a deeper understanding and quantification of the restriction of evaporation during soil drying, more detailed process-studies on evaporation, including the structure of evaporation zone and its relation to the DSL, should be carried out for various types of soils under various atmospheric conditions.

In the present study, the microscopic physical process of evaporation from a dry bare soil is presented based on the field observations carried out at the three representative bare lands commonly found in the world. More specifically, the objectives of this study can be summarized as follows:

1. To make clear the spatial distribution and temporal behavior of the evaporation zone.

2. To elucidate the relationship between the temporal and spatial structure of the evaporation zone and the soil physical properties.

3. To evaluate the effect of the structure of the evaporation zone on the restriction of evaporation and surface energy balance variation.

1.2 Outline of the present study

A brief description of the background of this study and the review of related researches are given in Chapter 2. Chapter 3 presents the structure of the evaporation zone simulated by a numerical model, as a preliminary investigation. Description of field observation data is given in Chapter 4, and some characteristics of the observation results are described in Chapter 5, as basic information to be referenced for the subsequent analyses. Chapter 6 presents the results of the analysis from aspect of energy exchange between the soil and the atmosphere. Chapter 7 gives analysis from aspect of water movement in the soil. In Chapter 8, the restriction of evaporation is investigated quantitatively by applying a

model to the field observation results. Finally, discussion and conclusions are presented in Chapters 9 and 10, respectively.

Chapter 2

Review of the literature

2.1 Significance of the study of bare soil evaporation

Evaporation from the land surface into the atmosphere is one of the most important components of the hydrological cycle. It represents the return flow of water received from rainfall back to the atmosphere. It has been of great interest to various fields of science and social activity, since it is not only a process of water transport but also a process of energy transport in the form of latent heat flux.

In the field of water resources management, evaporation is a subject of great concern, particularly in arid and semi-arid lands, as a main process of the loss of water available for human activity [Kayane, 1967]. According to the estimates of water balance components of the continents of the world by Lvovitch [1973], total amount of evaporation (including transpiration) from the surfaces of the continents occupies approximately 65 % of the total precipitation to there. In Africa and Australia, the values reach up to 80 and 69 %, respectively. Other researchers [e.g., Baumgartner and Reichel, 1975; Korzoun et al., 1977] also gave almost similar estimates (see Table 1). Evaporation is also closely related with the quality of water resources as well as their quantity. For instance, evaporation of soil water involves not only loss of water but also the danger of water- and soil-salinizations,

Table 1 Some estimates of the mean evaporation and precipitation for the continents (unit: mm/year) (after Brutsaert [1982] but slightly modified).

	Europe	Asia	Africa	North America	South America	Australia Oceania	Antarctica	Reference
Evaporation	415	433	547	383	1065	510	-	Lvovitch
Precipitation	734	726	686	670	1648	736	-	(1973)
Evaporation	375	420	582	403	946	534	28	Baumgartner and Reichel (1975)
Precipitation	657	696	696	645	1564	803	169	
Evaporation	507	416	587	418	910	511	0	Korzoun et al.
Precipitation	790	740	740	756	1600	791	165	(1977)

in regions where annual rainfall is low and groundwater table is at a shallow depth [e.g., Hillel, 1980, p. 110].

In atmospheric sciences, evaporation is important as a source of moisture and as a factor affecting the thermal conditions of the bottom boundary of the atmosphere. For example, many numerical studies have shown that the large scale atmospheric circulation and the rainfall are sensitive to the distribution and amount of evaporation from the land surface [e.g., Walker and Rowntree, 1977; Shukla and Mintz, 1982; Yeh et al., 1984]. Numerical experiments by Rowntree and Bolton [1983] showed that effects of soil moisture (and thus evaporation) anomalies in a given area on rainfall or air temperature and humidity can propagate into adjacent land areas. Yasunari et al. [1991] pointed out the significance of snow melt and of the subsequent evaporation of soil water as a mechanism of an apparent inverse correlation between the Eurasian snow cover extent in winter and the strength of Indian monsoon in the following summer.

In agriculture or plant ecology, evaporation is an important process since it affects the thermal and moisture conditions of soils. Germination and early seedling growth are sensitive to the moisture conditions of soils, and thus are often doomed during their most vulnerable stage by the rapid soil-drying due to evaporation [Hillel, 1971]. Soil temperature also affects numerous ecosystem-processes including dynamics of soil organisms, plant-root growth, seed germination, nutrient uptake, and decomposition [Whitford, 1989; Kemp et al., 1992]. For example, Shimada et al. [1997] pointed out a possibility that evaporation and its controls of the thermal conditions of soils had strongly affected the formation of current ecosystems in Sri Lanka. Thus, it is quite essential for various scientific fields to understand the process of evaporation and to evaluate or predict accurately its amount.

Evaporation from land surface consists of evaporation from open water surfaces, bare soil surfaces, and snow covers, evaporation of intercepted water on plant leaves and artificial structures, transpiration from vegetation, and others. Evaporation from bare soil surfaces is the most dominant component particularly in arid lands. According to the literature

[Kondo, 1994, p. 5], forests, grasslands (including agricultural lands), and deserts (including semi-deserts) occupy 34.0, 31.0, and 32.1 %, respectively, of land area on the earth (not including the Antarctic Continent). Although not all deserts and semi-deserts are completely bare land, the agricultural lands remain largely bare during approximately a half of year in case of annual field crops. Furthermore, soil surface is partly exposed even in forests and grasslands. Considering these situations, the role of bare soil evaporation is quite large at the global scale.

In addition, many forests and grasslands are being lost due to deforestation and desertification, and bare lands are extending year by year [e.g., Furley, 1994; Goudie, 1994]. Once land surface becomes bare, the growth of plants becomes difficult due to increase of temperature variation and severe dry conditions of the soil, and then land degradation progresses. Therefore, bare soil evaporation and its effect on the thermal and moisture conditions of soils need to be more intensively investigated.

2.2 Factors affecting bare soil evaporation

By taking bulk transfer approach, the rate of evaporation (E) from bare soil surface is represented as

$$E = \rho C_E u(q_s - q_a) \tag{2.1}$$

$$= \frac{0.622\rho C_E u}{p}(e_s - e_a), \tag{2.2}$$

where ρ is the density of air, C_E the bulk transfer coefficient, u the wind velocity at a reference level z_a, q the specific humidity, p (= 1013.15 hPa) the atmospheric pressure, e the vapor pressure, and the subscripts s and a refer to the soil surface and the level z_a, respectively. Bulk transfer coefficient under neutral atmospheric stability conditions can be expressed as [Brutsaert, 1982, p. 202]

$$C_E = \frac{a_v k^2}{ln(z_a/z_{0v})ln(z_a/z_{0m})}, \tag{2.3}$$

where a_v ($= 1.0$) is the ratio of the eddy diffusivity for water vapor and the eddy viscosity under neutral conditions, k ($= 0.4$) the von Kármán's constant, and z_{0v} and z_{0m} are the roughness length for vapor and momentum transfers, respectively.

In general, equation of surface energy balance is given as

$$R_n = LE + H + G, \tag{2.4}$$

where R_n is the net radiation, LE ($\equiv lE$) the latent heat flux, l the latent heat for vaporization, E the evaporation rate, H the sensible heat flux, and G the soil heat flux.

By assuming that the soil surface is sufficiently wet (i.e., e_s is given by saturation value $e_{sat}(T_s)$, where T_s is the soil surface temperature) and by replacing approximately $(e_{sat}(T_s) - e_{sat}(T_a))/(T_s - T_a)$ by the slope of saturation vapor pressure curve (s) at the air temperature T_a, combination of Equations (2.2) and (2.4) gives so-called Penman's [1948] equation, as follows (slightly modified [Brutsaert, 1982, pp. 216-217]):

$$E_{pen} = \frac{s}{s+\gamma} Q_n + \frac{\gamma}{s+\gamma} \frac{0.622 \rho C_E u}{p} (e_{sat}(T_a) - e_a), \tag{2.5}$$

where E_{pen} is the evaporation rate derived by Penman equation, Q_n ($\equiv R_n - G$) the available energy, γ the psychometric constant, $e_{sat}(T_a)$ the saturation vapor pressure of the air, e_a the vapor pressure in the air at z_a. The term $(e_{sat}(T_a) - e_a)$ is often called as the saturation deficit or the vapor pressure deficit.

The Penman equation indicates what factors are affecting the evaporation from wet soil surface, as summarized below:

- Available energy
- Wind velocity
- Air temperature
- Vapor pressure deficit

- Roughness of the surface

The net radiation can be broken down into several components as follows:

$$R_n = (1 - \alpha_s)R_{sd} + \varepsilon_s R_{ld} - \varepsilon_s \sigma T_s^4 \tag{2.6}$$

where R_{sd} is the downward short-wave radiation (or solar radiation), α_s the albedo of the soil surface, R_{ld} the downward long-wave radiation (or atmospheric radiation), ε_s the emissivity of the surface, and σ ($= 5.6697 \times 10^{-8}$ Wm/^{2}K^4) the Stefan-Boltzmann constant.

The soil heat flux can be represented by the following equation as the first approximation for the simple case of a homogeneous semi-infinite soil whose surface temperature varies sinusoidally [Sellers, 1965, pp. 135-138]:

$$G = A_T(\omega C\lambda)^{1/2} \sin(\omega t + \frac{\pi}{4}) \tag{2.7}$$

where A_T is the amplitude of the surface temperature wave, ω the angular frequency of oscillation (2π/(24 hours) for the diurnal cycle, 2π/(365 days) for the annual cycle), C the volumetric heat capacity of the soil, λ the thermal conductivity of the soil, and t the time. The parameter $(C\lambda)^{1/2}$ has been called as the conductive capacity [Priestley, 1959; Petterssen, 1959], as the thermal property [Johnson, 1954; Sellers, 1965], as the soil product [Haltiner and Martin, 1957], as the thermal contact coefficient [Businger and Buettner, 1961; van Wijk and Derksen, 1963], and as the thermal inertia [e.g., Pohn et al., 1974; Pratt and Ellyett, 1979; Carson et al., 1980; van de Griend et al., 1985]. The term *thermal inertia* will be used in this study since it is widely used at present particularly in the field of remote sensing.

From Equations (2.6) and (2.7), factors affecting available energy can be summarized as follows:

- Solar and atmospheric radiation
- Albedo of the surface

- Emissivity of the surface
- Surface temperature and its amplitude
- Thermal inertia (volumetric heat capacity and thermal conductivity)

Among these factors, the surface albedo and the thermal inertia can largely change during soil drying. Note that although the surface temperature can also change, it is not an independent variable: surface temperature changes depending on the change in other factors.

The relationship between the surface albedo and the water content of surface soil layer has been derived by numerous researchers [e.g., Maruyama, 1962; Idso et al., 1975; Hwang, 1985; Passerat de Silans et al., 1989; Kondo et al., 1992; Fukumoto and Hirota, 1994]. Based on the results of those researches, it can probably be summarized that the soil drying can introduce the change in surface albedo of approximately 0.15. Thus, the decrease in available energy of 150 W/m^2 can be introduced by an effect of decrease in albedo due to soil drying when $R_{sd} = 1000$ W/m^2.

The heat capacity of the soil can be theoretically expressed as a function of soil water content [e.g., de Vries, 1963; Campbell, 1985]. The relationship between soil thermal conductivity and soil water content has been investigated, for example, by de Vries [1963], Kimball et al., [1976], Sepaskhah and Boersma [1979], Kasubuchi [1982], and Yamanaka et al. [1994]. Figure 40 of Sellers [1965] or Figure 7 of van de Griend et al. [1985] indicate that the decrease of 50 to 60 % in thermal inertia can be introduced by soil drying under usual soil water conditions. This suggests that the increase in soil heat flux of 55 W/m^2 (i.e., decrease in available energy) can be introduced by the decrease in thermal inertia resulting from soil drying when soil heat flux under wet conditions is equal to 100 W/m^2. However, in reality, the soil heat flux does not decrease during soil drying, because the amplitude of surface temperature wave increases due to soil drying and acts as counter effect. According to the data of Hwang (1985), the increase of 36 % in soil heat flux was

introduced by the decrease of volumetric water content from 0.38 to 0.23 under identical radiation conditions.

Under considerably dry conditions of the soil, the decrease of evaporation can be induced without the mechanisms mentioned above (i.e., without the changes in surface albedo and in thermal inertia) because the specific humidity at the surface no longer is the saturation value at the surface temperature. In other words, under those situations, actual rate of evaporation is reduced below a potential rate. The effect of the decrease of surface humidity on the evaporation reduction is often expressed as the decrease of (surface) moisture availability [Barton, 1979] (or evaporation opportunity [Ward, 1967], evapo(transpi)ration efficiency [Kim et al., 1996]).

Consequently, soil dryness (or soil moisture condition) affects evaporation through the following factors:

- Surface albedo
- Thermal inertia
- Surface moisture availability

As mentioned above, the effect of the change in surface albedo on the available energy is larger than that of the change in thermal inertia in common situations. On the other hand, Yamanaka et al. [1995b] showed that the change of surface albedo due to soil drying introduces the reduction of 15 % in evaporation rate while the change in surface moisture availability introduces the reduction of 70 % in evaporation rate. Therefore, of these three factors, surface moisture availability may be the most important.

In the present study, the term *effect of soil drying on the restriction of evaporation* is used in a limited sense as the effect concerning the reduction of surface moisture availability, not including the variation of surface albedo and thermal inertia.

2.3 Parameterization of evaporation and its relation to soil moisture

In meteorology and climatology, numerous parameterization schemes of bare soil evaporation have been proposed for the modelling of the global climate or for the satellite remote sensing of a terrestrial environment. In parameterizing the bare soil evaporation, one of the difficulties lies on how to consider or represent the surface moisture availability. Except for several approaches, most schemes have introduced additional empirical parameters in the formulas of evaporation for wet surface and those have been related to the water content of surface soil layer of a few centimeters thickness.

Numerous schemes previously proposed can be divided into several groups based on the type of their basic formula and the type of parameter representing the surface moisture availability. It should be noted that the symbols used are not identical to those in original referenced papers.

2.3.1 Classification of existing parameterization schemes

A) Bulk equation based scheme

A1. Alpha type In Equation (2.1), surface specific humidity q_s is replaced with the $\alpha q_{sat}(T_s)$, and evaporation rate can be expressed as

$$E = \rho C_E u(\alpha q_{sat}(T_s) - q_a), \tag{2.8}$$

where α is one of the parameters representing surface moisture availability and is equivalent to the surface relative humidity h_s.

Barton [1979] derived experimentally a relationship between α and water content of surface soil layer. Yasuda and Toya [1981] and Noilhan and Planton [1989] also reported similar relationship but adopted different forms of function.

On the other hand, when a thermodynamic equilibrium locally exists between the liquid and vapor phases of water in the soil pore, the relative humidity h of pore air is theoretically derived by the following equation [Philip and de Vries, 1957; Edelfsen and Anderson, 1943, p. 260]

$$h = exp(\frac{\Psi g}{RT}), \tag{2.9}$$

where Ψ is the water potential, which can be replaced by the matric potential ψ when osmotic potential can be ignored, g the gravitational acceleration, R the gas constant for water vapor, and T the temperature in Kelvin. Milly [1982] confirmed that the assumption of the thermodynamic equilibrium is justified within the soil except for a special case, such as artificially high infiltration rates into coarse soils. Contrary to this, Connel and Bell [1993] introduced a parameter representing the rate of vapor-liquid phase change into their numerical model. Nevertheless, in their companion paper [Connel et al., 1993], the improvement of the prediction accuracy by considering the phase-change rate was not obvious.

Philip [1957], Sasamori [1970], Nappo [1975], McCumber and Pielke [1981] and Camillo et al. [1983] extended the application of Equation (2.9) to the soil surface: they used the equation in calculation of α. Kondo et al. [1990], however, found out that the relationship between α and water content of surface soil layer of 2-cm thickness depended on wind velocity and air humidity. Their result indicates that it is not appropriate to relate α to the water content of the soil layer of, at least, a few centimeters thickness. This problem exists not only in the theoretical approach based on Equation (2.9) but also in the empirical approaches of Barton [1979] and others.

It should be noted, however, that the result of Kondo et al. [1990] does not necessarily deny validity of Equation (2.9). The problem comes from the inappropriate choice of the thickness of surface soil layer, rather than the application of Equation (2.9) itself. Wind tunnel experiments of Yamanaka et al. [1995a] showed the possibility that α can be

accurately estimated by Equation (2.9) if one uses the water content or water potential of a sufficiently thin surface soil layer.

A-2. Beta type So-called evaporability [Manabe, 1969] (E_{sat}) is defined by the following equation:

$$E_{sat} = \rho C_E u(q_{sat}(T_s) - q_a). \tag{2.10}$$

In estimating the energy balance of the earth's surface, Budyko [1956] introduced the following simple scheme:

$$E = \beta E_{sat}, \tag{2.11}$$

where β is one of the surface moisture availability parameters, and is usually given by a function of soil water content. Manabe [1969] used the scheme in his general circulation model (GCM) for simulating the global climate. Deardorff [1977] applied the scheme to a bare soil surface and verified its validity from comparison of predicted soil moisture variation with observed result. Lee and Pielke [1992] proposed a more realistic function for β based on observed data for two different soils.

However, it has been revealed recently that β depends on wind velocity as well as soil water content [Kondo et al., 1990; Fukumoto and Hirota, 1994]. In addition, a negative correlation between actual evaporation and wind velocity was also reported [Chanzy and Bruckler, 1993; Yamanaka and Takeda, 1994a and 1994b]. The negative correlation cannot be simulated by using the β approaches. In other words, fictitious variation can be introduced in evaporation rate estimated by using the β as a function of soil water content only, depending on the variation of wind velocity.

A3. Surface resistance type By assuming that the evaporation takes place within the soil and that the surface humidity is determined by the balance between vapor transport in the atmosphere and that in the soil, evaporation rate can be expressed as

$$E = \rho_a(q_{sat}(T_s) - q_a)/(r_{av} + r_s), \tag{2.12}$$

where $r_{av}(\equiv 1/C_E u)$ is the resistance to vapor transfer in the atmosphere, and r_s the surface resistance (resistance to vapor transfer in the surface soil). Numerous formulas for representing the surface resistance by the water content of surface soil layer have been proposed [e.g., Sun, 1982; Passerat de Silans, 1986; Kondo et al., 1990; van de Griend and Owe, 1994]. Those formulas were experimentally obtained. As used in the SiB (simple biosphere model) [Sellers et al., 1986] which has been accepted as a powerful sub-model of GCM, this r_s approach may be one of the most widely used schemes now. However, it was reported that the relationship between r_s and surface water content varies in the course of a day [Camillo and Gurney, 1986; Daamen and Simmonds, 1996]. Yamanaka et al. [1997] also showed that the relationship slightly depends on radiation conditions. This is caused by ignoring the difference between the soil surface temperature and the temperature at which the vaporization of soil water actually takes place (i.e., evaporation zone). As a result, evaporation rate estimated by this scheme may have a fictitious correlation with radiation change.

Choudhury and Monteith [1988] proposed the following non-empirical scheme:

$$E = \rho(q_{sat}(T_e) - q_a)/(r_{av} + r_s^*), \tag{2.13}$$

where T_e is the temperature at the evaporation zone within the soil, and r_s^* is the modified surface resistance considering the difference between T_e and T_s. While r_s is usually estimated empirically from surface water content, r_s^* is obtained non-empirically from the depth of evaporation zone (z_e). Yamanaka et al., [1997] demonstrate the validity of the r_s^* approach by their wind tunnel experiments for a uniform fine sand. In their experiments, r_s^* did not depend on radiation conditions and other atmospheric conditions.

B) Penman equation based scheme

B1. Beta type As mentioned in the previous section, Penman equation does not give the actual rate of evaporation from dry soils. Therefore, for estimating actual evapora-

tion (E, or actual evapotranspiration) from potential evaporation derived from Penman equation (E_{pen}, or potential evapotranspiration), it is necessary to take into account the evaporation ratio [e.g., Kayane, 1967; Nakagawa, 1984] ($\beta' \equiv E/E_{pen}$). If one obtains the relationship between the evaporation ratio and soil water content, actual evaporation is estimated from known atmospheric variables and soil water content by using the following relationship:

$$E = \beta' E_{pen}. \tag{2.14}$$

Many types of function for the evaporation ratio have been proposed [e.g., Veihmeyer and Hendrickson, 1955; Thornthwaite and Mather, 1955; Budyko, 1956; Holmes, 1959; Marlatt et al., 1961]. Recently, Chanzy and Bruckler [1993] proposed a more realistic function based on detailed observations in three types of bare soil. In their function, the evaporation ratio depends on soil type and wind velocity as well as soil water content.

Although Equation (2.11) is quite similar to (2.14), it should be noted that the both are not identical as explained, for example, by Milly [1992]. The difference between β and β' originates in the difference between E_{sat} and E_{pen}. The E_{sat} is calculated by using the surface temperature at an actual dry surface. On the other hand, although the Penman equation does not use the surface temperature, it implicitly uses the surface temperature for a hypothetically wet surface (i.e., which is cooled by evaporation at potential rate). Therefore, E_{pen} is equal to E_{sat} for actual wet surface, but differs for dry surface ($E_{sat} \gg E_{pen}$). Thus, the function for β' is not identical to that for β.

B2. Surface resistance type Penman-Monteith equation [Monteith, 1973, p. 197] for vegetated surfaces is expressed as

$$E = \frac{sQ_n + \rho c_p (e_{sat}(T_a) - e_a)/r_{av}}{s + \gamma(r_{av} + r_c)/r_{av}}, \tag{2.15}$$

where r_c is the canopy resistance which includes stomata resistance and the effects of canopy structure on vapor transfer inside the canopy. When this equation is applied to a bare soil

surface, r_c can be replaced by r_s, and thus Equation (2.15) is rewritten as

$$E = \frac{sQ_n + \rho c_p(e_{sat}(T_a) - e_a)/r_{av}}{s + \gamma(r_{av} + r_s)/r_{av}}. \tag{2.16}$$

The resistance r_s in this equation is essentially identical to r_s in Equation (2.12).

On the other hand, Budogovsky [1964] and Menenti [1984] independently proposed the following equation similar to Penman-Monteith equation (slightly modified [Yamanaka and Takeda, 1994a]),

$$LE = \frac{sr_{av}Q_n + \gamma l\rho(q_{sat}(T_e) - q_a) - sc_p\rho z_e G/\lambda_s}{sr_{av} + \gamma(r_{av} + r_s^*) + sc_p\rho z_e/\lambda_s} \tag{2.17}$$

where λ_s is the thermal conductivity of the surface soil. The resistance r_s^* in this equation is essentially identical to r_s^* in Equation (2.13). Experiments of Yamanaka et al. [1995b] showed a good agreement between the evaporation rate estimated by this scheme and that measured by a weighing lysimeter.

C) Priestley and Taylor equation based scheme Instead of Penman equation, Priestley and Taylor [1972] suggested the use of the following empirical equation (hereafter referred to as P-T equation) for calculating evaporation from wet surface under conditions of minimal advection:

$$E = \alpha_{PT} E_{eq} \tag{2.18}$$

where α_{PT} is an empirical constant ($\simeq 1.26$), and E_{eq} is the equilibrium evaporation [Slatyer and McIlroy, 1961] expressed as

$$E_{eq} = \frac{s}{s + \gamma} Q_n \tag{2.19}$$

Davies and Allen [1973] treated the parameter α_{PT} as a variable, and obtained an empirical relationship between the α_{PT} and water content of surface soil based on measurements for cropped surface. Barton [1979] also obtained the similar relationship for a bare soil surface. Owe and van de Griend [1990] carried out a more detailed investigation on the relationships for both vegetated and bare soil surfaces.

One of the most important advantages of this approach is that there is no need for the knowledge of the bulk transfer coefficient or the aerodynamic resistance. However, because P-T equation is one of the alternatives to Penman equation, it can be said that there are similar problems as appeared in Penman equation-based approaches (e.g., systematic error due to atmospheric conditions).

D) Threshold formulation scheme In the threshold formulation method [Mahfouf and Noilhan, 1991], evaporation rate is assumed to be determined by the water flux E_t from bellow when E_t is less than E_{sat}, namely as

$$E = \min(\rho_l E_t, E_{sat}) \tag{2.20}$$

where E_t is the threshold rate of evaporation controlled by soil moisture profile, and ρ_l is the density of liquid water. Several formulations of E_t have been proposed [e.g., Mahrt and Pan, 1984; Dickinson, 1984; Wetzel and Chang, 1987; Abramopoulos et al., 1988].

This concept probably is right if one chooses proper time scale. The E_t is, however, difficult to be simply parameterized by using water content of one or two soil layers. Actually, the water flux within a soil usually varies in the vertical direction and E_t is a mere measure of water supply to the evaporation zone. Mahfouf and Noilhan [1991] stated that threshold methods strongly underestimated evaporation and could not predict a diurnal cycle of evaporation in their comparative study of various formulations of evaporation.

2.3.2 Problems concerning the methodology of parameterization

The parameterization schemes for bare soil evaporation mentioned above are summarized in Table 2. Except for the non-empirical surface-resistance approaches (i.e., z_e based approaches), all approaches are based on the water content of surface soil layer of a few centimeters thickness. One of the main defects in the water content based approaches is

Table 2 Summary of parameterization schemes for bare soil evaporation proposed by previous studies.

Type	Formula	Parameter		Reference
Bulk-alpha	Eq. (2.8)	$\alpha = \exp(\psi_s g/RT_s)$		Philip [1957] and others
	〃	$\alpha = c_1 w_s/(w_s+c_2)$	$w_s < 0.375$	Barton [1979]
		$= 1$	$w_s \geqq 0.375$	
	〃	$\alpha = c_1 \theta_s/(c_2 \theta_s+c_3)$	$\theta_s < 0.36$	Yasuda and Toya [1981]
		$= 1$	$\theta_s \geqq 0.36$	
	〃	$\alpha = (1/2)(1-\cos(\pi\theta_s/\theta_{fc}))$	$\theta_s < \theta_{fc}$	Noilhan and Planton [1989]
		$= 1$	$\theta_s \geqq \theta_{fc}$	
Bulk-beta	Eqs. (2.11), (2.10)	$\beta = \theta_s/\theta_{fc}$	$\theta_s \leqq \theta_{fc}$	Deardorff [1977]
		$= 1$	$\theta_s > \theta_{fc}$	
	〃	$\beta = (1/4)(1-\cos(\pi\theta_s/\theta_{fc}))^2$	$\theta_s < \theta_{fc}$	Lee and Pielke[1992]
		$= 1$	$\theta_s \geqq \theta_{fc}$	
Bulk - surface resistance	Eq. (2.12)	$r_s = c_1 + c_2(\theta_s/\theta_{sat})^{c_3}$		Sun [1982], Sellers et al. [1986]
	〃	$r_s = c_1 \exp(c_2 \theta_s/\theta_{sat})$		Passerat de Silans[1986]
	〃	$r_s = c_1(\theta_{sat} - \theta_s)^{c_2}/D_{av}$		Kondo et al.[1990]
	〃	$r_s = 10\exp(c_1(c_2 - \theta_s))$		van de Griend and Owe [1994]
	Eq. (2.13)	$r_s^* = z_e/D_{ve}$		Choudhury and Monteith [1988]
Penman-beta	Eq. (2.14)	$\beta' = [\exp(c_1\theta_s+c_2)]/[1+\exp(c_1\theta_s+c_2)]c_3+(1-c_3)$		Chanzy and Bruckler [1993]
Penman-surface resistance	Eq. (2.16)	$r_s = c_1\theta_s+c_2$		Daamen and Simmonds [1996]
	Eq. (2.17)	$r_s^* = z_e/D_{ve}$		Budogovsky [1964], Menenti [1984]
P-T equation	Eqs. (2.18), (2.19)	$\alpha_{PT} = c_1 [1-\exp(c_2 w_s)]$		Barton [1979]
	〃	$\alpha_{PT} = c_1+c_2 \exp(c_3\theta_s/\theta_{fc})$		Owe and van de Griend [1990]
Threshold formulation	Eq. (2.20)	$E_t = 2D(\theta_s - \theta_{ad})/\delta_s + K$		Mart and Pan [1984]
	〃	$E_t = c_1\theta_d/\theta_{sat}(c_2)^{0.5}$		Dickinson [1984]
	〃	$E_t = c_1[(\theta_d^{c_3+4} - \theta_{wilt})^{c_3+3}[\theta_d(c_2+4)-\theta_{wilt}(c_2+3)]]/c_3$		Wetzel and Chang [1987]
	〃	$E_t = D\theta_s\pi^2/4\delta_s$		Abramopoulos et al. [1988]

α, β, r_s, r_s^*, β', α_{PT}, and E_t are the parameters representing surface moisture availability or effect of evaporation restriction; c_1, c_2, and c_3 are the empirical constants or semi-empirical variables; ψ_s, the matric head at soil surface level, R_v, the gas constant for water vapor; T_s, the soil surface temperature; w_s, the gravimetric water content of surface soil layer; θ, the volumetric water content (suffix s denotes value of surface soil layer; *fc*, value at field capacity; *sat*, value at saturation; *ad*, value at air-dry; *d*, value of deep soil layer; and *wilt*, value at wilting point); D_{av}, the molecular diffusivity of water vapor in the air; z_e, the depth of evaporation zone; D_{ve}, the effective vapor diffusivity in the soil; δ_s the thickness of the surface soil layer.

that the water content is not uniformly distributed vertically within a surface soil layer and its inhomogenity varies depending on atmospheric conditions. In other words, even though the water content of surface soil is identical, surface moisture availability may not be identical. In addition, the relationship between the surface moisture availability parameters and surface water content depends on the types of soils. However, it is considerably difficult to obtain the relationships for various soil types by means of in *situ* measurements.

Consequently, the further requirements for the parameterization can be summarized as follows:

- To avoid the systematic errors introduced by the variations in atmospheric conditions.
- To reflect the difference in soil types by considering basic properties of soils.

On the other hand, although the z_e based approaches may satisfy these requirements [Yamanaka et al., 1997], the structure and the dynamic behavior of the evaporation zone have not been elucidated very well. Therefore, more detailed studies on the process of evaporation, particularly the process of phase-transition of water within a soil, should be carried out. Although, in practice, there are needs for simple parameterization rather than accurate but complex parameterization, further understanding of the process of evaporation would also help an optimum simplification of its parameterization.

2.4 Process of bare soil evaporation and its restriction mechanism

2.4.1 General explanation

In the field of soil physics, the process of soil drying have been recognized to have two distinct stages based on the variation in evaporation rate under constant external conditions (see Figure 1).

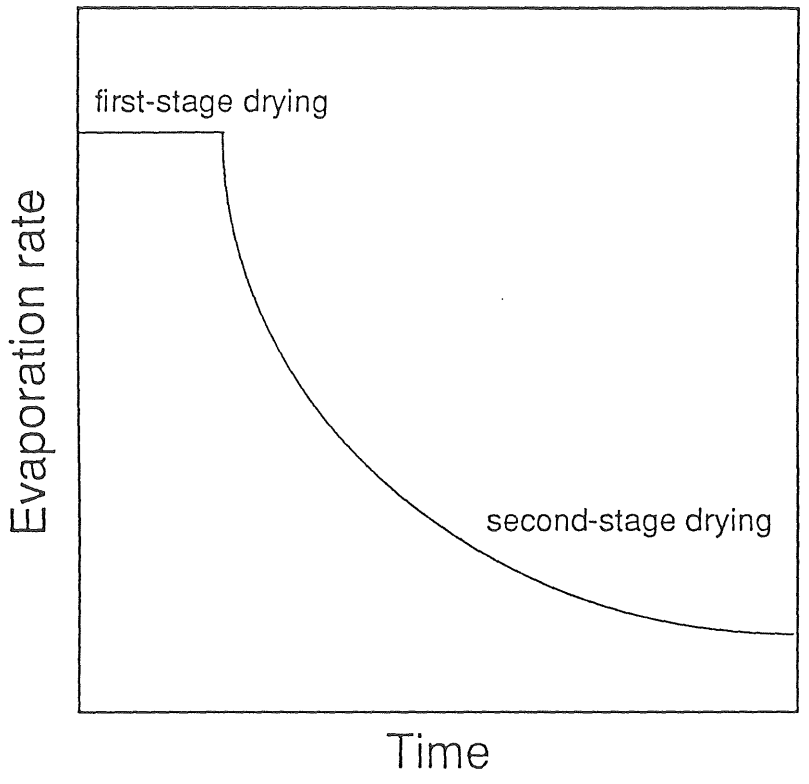

Figure 1 An illustration for the two stages of evaporation process (after Campbell [1985] but slightly modified).

Hillel [1971, pp. 192-193] explained the two stages as follows:

> "(1) an early, *constant-rate stage*, during which the evaporation rate is determined by external and soil-surface conditions (insofar as the latter modify the effective atmospheric evaporativity acting upon the soil), rather than by conductive properties of the profile; and (2) a *falling-rate stage*, during which the evaporation proceeds at a rate ever lower than the evaporativity and the actual rate is dictated by the ability of the soil profile to deliver moisture toward the evaporation zone."

As seen from the expression above, the first stage corresponds to a period where $q_s \simeq q_{sat}(T_s)$, and also the second stage to a period where $q_s < q_{sat}(T_s)$.

Hillel also explained the mechanism of the stage shift as follows:

> ". . . the end of the first, i.e., the beginning of the second, stage of drying. . . is sometimes accompanied by the downward movement into the profile of a drying front or a drying zone, so that actual evaporation take place at some depth and the water must move through the desiccated zone by vapor diffusion."

Campbell [1985, pp. 98-99] gave a similar but more sophisticated explanation as follows:

> "When the soil dries sufficiently that water cannot be supplied to the surface fast enough to meet the evaporative demand, the soil surface dries and the evaporation rate is reduced. This reduction is caused by the increased diffusion resistance of the dry soil which is between the wet soil and the atmosphere. As the depth of the dry layer increases, the evaporation rate decreased."

and

> "The depth of the dry layer which forms is determined by the rate at which liquid water can be supplied to the drying front. If liquid water supply is too

slow, the dry layer deepens, causing an increase in vapor diffusion resistance. This reduces evaporation rate until supply and demand are brought back into balance."

These explanations indicate an importance of the formation of the dry layer and the position of the zone where vaporization actually takes place, in understanding a restriction mechanism of evaporation.

Although expressions used to indicate the dry layer or the zone where evaporation takes place are different among researchers (see Table 3), the terms, *dry surface layer* (DSL) and *evaporation zone*, are used in the present study.

2.4.2 Relationship between the dry surface layer and evaporation zone

It appears that there had already been people who accept the importance of the formation of the DSL as the mechanism of the restriction of evaporation, a half of a century or more before. In the paper of Penman [1941], descriptions similar to the explanation by Hillel and Campbell are found. Budyko [1948] presented a model for the restriction of evaporation based on the thickness of the DSL. Hide [1954] also pointed out the importance of the formation of the DSL and the resistance to vapor transfer within the layer, in understanding the restriction mechanism of evaporation. However, their ideas were somewhat speculative without sufficient data.

It can be said that detailed investigations on the evaporation zone and the DSL began from the paper of Philip [1957]. Philip carried out an analytical investigation on the evaporation within the soil under quasi-steady-state conditions, based on the theory of non-isothermal water transport by liquid and vapor phase [Philip and de Vries, 1957]. His calculations indicated that the phase transformation of water took place in a narrow zone below the soil surface, and both inflection of water content profile and the peak of

Table 3 Some expressions for the evaporation zone and the dry surface layer (DSL), used in previous studies.

Reference	*evaporation zone*	*dry surface layer (DSL)*
English expressions		
Penman [1941]		dry layer
Hide [1954]		dry layer, static layer
Philip [1957]	evaporation site	
Benoit and Kirkham [1963]		surface air-dry zone, surface air-dry layer
Gardner and Hanks [1966]	evaporation zone	
Fuchs and Tanner [1966]		dry top layer, dry layer
van Hylckama [1966]		dry top layer
Fritton et.al. [1967, 1970]	evaporation zone, evaporation surface, vaporization surface	dry surface layer
Heller [1968]		bone dry front
Abramova [1969]	evaporating layer	
Hillel [1980]	evaporation zone	dried surface zone, desiccated zone, drying-front
Barnes and Allison [1983]	evaporating front, evaporating surface	dry surficial layer, dry surface layer, dry-soil layer
Menenti [1984]	evaporation front	
Mahfouf and Noilhan [1991]		dry superficial layer
O'Kane [1991]	evaporating surface	
van de Griend and Owe [1994]	evaporative front	dry top layer
Japanese expressions		
Kayane [1973]	*johatsu-men*	*kanso-so*, *kanso-doso*, *kanso-dojo-so*
Nomura and Inoue [1979]		*kansha-so* (Dry Sand Layer)
Iwata [1984]	*johatsu-men*	*kanso-so*
Kobayashi et al. [1986]		*kansha-so* (Dry Sand Layer), *kanso-hyoso* (Dry Surface Layer)
Kuzuha et al. [1988]	*johatsu-iki* (evaporating region)	*kanso-iki*
Ishihara [1989]	*johatsu-men* (evaporating front), *johatsu-iki*	
Fukuhara et al. [1990]		*kanso-iki*, *kanso-so*
Nakano [1991]		*kanso-so* (drying layer)
Hiyama et al. [1993]	*johatsu-men* (evaporating front)	*kanso-hyoso* (Dry Surface Layer)
Kondo [1994]		*kanso-hyoso*

vapor pressure profile were formed at the depth identical to that of the zone. Benoit and Kirkham [1963] found out from their column experiment the fact that evaporation rate decreased as the DSL develops, and pointed out that the DSL prevented water vapor from being transported freely into the atmosphere. From measurements of soil heat flux at several depths, Gardner and Hanks [1966] found that evaporation actually took place beneath the soil surface and the evaporation zone moved downward during soil drying. Laboratory experiments by Fritton et al. [1967] showed that the visually observed bottom-boundary of the DSL approximately corresponded to the inflection of water content profile. The correspondence between the bottom boundary of the DSL and the inflection of water content profile has been also reported by other researchers [e.g., Nomura and Inoue, 1979; Yamanaka et al., 1996].

Hanks et al. [1967] applied the theory of Philip and de Vries [1957] to the results of their laboratory experiments and showed that the liquid water transport from deeper soil layer was changed to the vapor flux at some depth below the soil surface. Fritton et al. [1967] also found that the peak of Cl^- concentration profile appeared just below the bottom boundary of the DSL. The liquid water flux transports Cl^- but vapor flux does not. Thus, the finding of Fritton et al. [1967] implies that a change of upward liquid water flux to vapor flux takes place at the bottom boundary of the DSL.

There are several investigations on the formation of DSL. Heller [1968] proposed a model which describes the development of the DSL. Fritton et al. [1970] showed that the isothermal diffusion equation for liquid water were not able to simulate the formation of the dry surface layer. In a numerical study of van Keulen and Hillel [1974], the possible influence of different diffusivity-water content relations on the formation of the DSL is discussed. They showed that the use of a *hooked* diffusivity function (which takes into account the increase in vapor diffusivity in the dry range) allowed the simulation of the formation of the DSL even though an isothermal condition was assumed. Campbell [1985] also pointed out the important role of vapor transport on the formation of the DSL.

As for the change of liquid water flux to vapor flux, there have been isotopic studies. Allison et al. [1983] obtained in their laboratory experiments the isotopic concentration profile which has a peak at some depth below the soil surface. Allison and Barnes [1983, 1985] reported that a similar shape of the profile was found under field conditions. They regarded the peak of the profile as a location where liquid water flux changed to vapor flux, based on a semi-empirical theory [Barnes and Allison, 1983, 1984] for the profile of stable isotopic compositions in soil water. Although the theory of Barnes and Allison was limited under specific conditions, it was later modified to be applicable for more general conditions [Barnes and Walker, 1989; Shurbaji and Phillips, 1995; Melayah et al., 1996a] and was verified under various conditions [Walker et al., 1988; Barnes and Allison, 1988; Barnes et al., 1989; Shimojima et al., 1990; Shurbaji et al., 1995; Melayah et al., 1996b].

The explanations by Hillel and Campbell seem to have been derived from the researches mentioned above. Besides these researches, numerous studies on the DSL and the evaporation zone have been presented until now [e.g., Kobayashi et al., 1986, 1987, 1989, 1991a, 1991b; Ishihara et al., 1989; Fukuhara et al., 1990, 1992, 1994; Sato et al., 1990; Hiyama et al., 1993; Takeda, 1993; Takano et al., 1997]. The results of these studies generally support the validity of the Hillel's and the Campbell's explanations.

2.4.3 Structure of the evaporation zone

The evaporation zone has been often treated as horizontal plane (i.e., having negligible thickness) located within the soil because of the visual clearness of the boundary between the DSL and a relatively moist underlayer, particularly in sandy soils. The z_e-based surface resistance approaches mentioned in the previous section are examples of those. In fact, analytical calculation of Philip [1957] showed that the thickness of evaporation zone was approximately several millimeters. Numerical computations of Kuzuha et al., [1988] also simulated the evaporation zone of a few millimeters thickness. Barnes and Allison [1988]

stated that the evaporation zone was narrow at least in moderately wet soils, based on their isotopic studies.

van Hylckama [1966], however, stated that the DSL was not always as visible to the eye and evaporation could occur throughout a considerable depth. Fuchs and Tanner [1967] also indicated that the evaporation zone cannot be treated as a plane, from a disagreement between observation and estimation by their energy balance model assuming the zero-thickness evaporation zone. Furthermore, direct measurements of humidity within the soil by Yamanaka et al. [1994] indicated that evaporation could transiently take place at the upper part of the DSL. Although wind tunnel experiments of Yamanaka et al. [1997] demonstrated the validity of the assumption of zero-thickness evaporation zone for steady-state atmospheric conditions, the experiments under varying atmospheric conditions showed that evaporation can take place within the DSL (not only at the bottom boundary) due to the change in radiation (or resulting change in soil temperature). Therefore, there is a possibility that the structure of evaporation zone and its relation to the DSL depend on the atmospheric conditions. Furthermore, in general the boundary between the DSL and the underlayer is not very clear in fine-textured soils so that it is expected that the structure of evaporation zone is also related to the soil type.

Chapter 3

Preliminary numerical experiment on the structure of the evaporation zone

3.1 High resolution model of water and heat flows

As seen in Section 2.4.3, the structure of the evaporation zone has not yet been elucidated in detail. One of the reasons for this is that an arrangement of measurement-devices or calculation-nodes was not sufficiently dense in the previous works. Particularly in field observations or laboratory experiments, it is actually impossible to measure water content or flux with spatial intervals of 1 mm or less. The method of numerical computation, however, allows investigation into this subject.

In order to clarify the microscopic structure of evaporation zone and to investigate its theoretical aspects, numerical experiments were conducted using a one-dimensional model of water and heat flow with very high resolution. Figure 2 shows the arrangement of calculation nodes of the model. The soil profile of 60-cm thickness was divided into 144 layers, and the thickness of each layer ranged from 0.5 mm (near the surface) to 10 cm (at

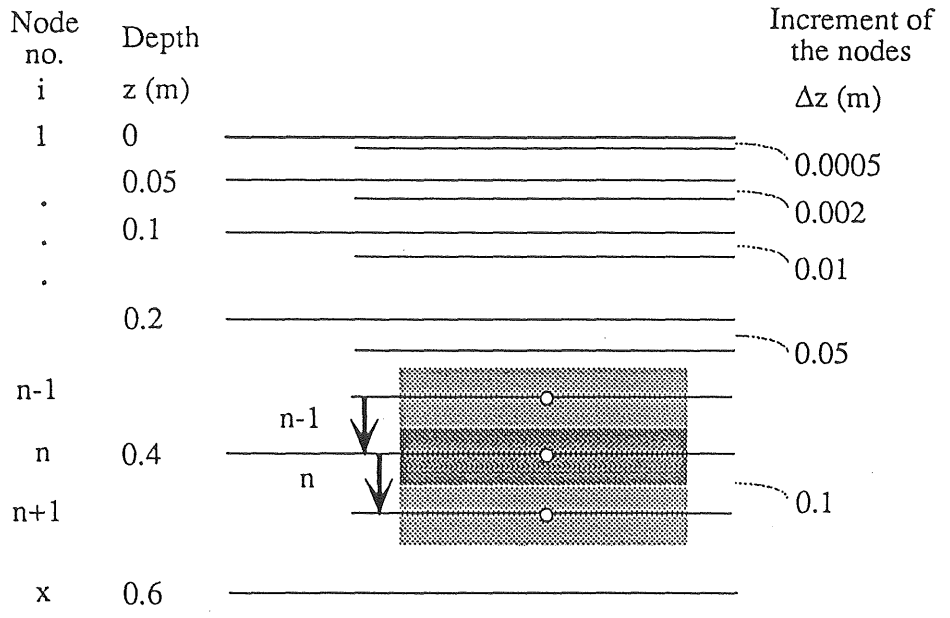

Figure 2 Arrangement of calculation nodes in the high resolution model.

deeper depth).

The model used was fundamentally based on the modified Philip and de Vries theory [Philip and de Vries, 1957; Sophocleous, 1979; Milly, 1982]. The basic equations of the model are summarized in Table 4. Although the liquid water flux can be divided into three components (i.e., component driven by matric-head gradient, that by temperature gradient and that by gravity), the component driven by the temperature gradient was not considered in Equation (3.3) since it is less important in dry soils (see Figs. 10 and 11 of Hanks et al. [1967] and see also Campbell [1985, pp. 102-103]). In Equation (3.4) the first term on the right-hand side represents the vapor water flux driven by temperature gradient, and the second term represents that driven by matric-head gradient. In Equation (3.5) the first term on the right-hand side represents the heat flow due to conduction; the second term indicates the transfer of latent heat by vapor movement. The sensible heat transfer by the liquid water flow was neglected in (3.5) because of its less significance in unsaturated soils [Shinjyo and Shirai, 1978]. Equation (3.6) describes the assumption that water in the liquid phase and that in vapor phase are in local thermodynamic equilibrium, and is almost identical to Equation (2.9).

Besides the two factors that were not adopted in the model as mentioned above, the following factors were also neglected: hysteresis effects [e.g., Hillel, 1980, pp. 128-132]; spatial variability of soil physical properties [e.g., Warrick and Nielsen, 1980, pp. 319-344]; effects of salt or osmotic potential [e.g., Qayyum and Kemper, 1962; Letey et al., 1969; Bresler and Laufer, 1974]; enhancement of vapor and heat transfers due to a steeper local temperature-gradient [e.g., Philip and de Vries, 1957; Westcot and Wierenga, 1974; Cass et al., 1984]; vapor transfer mechanisms besides molecular diffusion [e.g., Yamanaka et al., 1997, Section 2.1.3]; effects of irregular surfaces and shrinkage cracks [e.g., Hillel, 1980, pp. 135-137]; swelling of clayey soils [e.g., Nakano, 1991, pp. 149-168]; non-Darcy behavior of water movement [e.g., Iwata et al., 1994, pp. 324-330]; and others. These factors may be important under certain special conditions. Therefore, although this model assumes some-

Table 4 Basic equations in the high resolution model.

Equation	Number
Continuity equations	
$\frac{\partial \rho_l \theta}{\partial t} + \frac{\partial \rho_v(\theta_{sat}-\theta)}{\partial t} = -\frac{\partial (J_l+J_v)}{\partial z}$	(3.1)
$C\frac{\partial T}{\partial t} = -\frac{\partial (J_h)}{\partial z}$	(3.2)
Flux equations	
$J_l = -\rho_l K(\frac{\partial \psi}{\partial z} - 1)$	(3.3)
$J_v = -D_{ve} h \frac{d\rho_{vsat}}{dT}\frac{\partial T}{\partial z} - D_{ve}(\rho_v g/RT)\frac{\partial \psi}{\partial z}$	(3.4)
$J_h = -(\lambda + lD_{ve} h \frac{d\rho_{vsat}}{dT})\frac{\partial T}{\partial z} - lD_{ve}(\rho_v g/RT)\frac{\partial \psi}{\partial z}$	(3.5)
Vapor-liquid equilibrium equation	
$h = \exp(\psi g/RT)$	(3.6)
Soil hydraulic properties	
$\theta = \theta_r + \frac{\theta_{sat}-\theta_r}{[1+(-a\psi)^n]^m}$	(3.7)*
$K = K_{sat}\frac{\{1-(-a\psi)^{n-1}[1+(-a\psi)^n]^{-m}\}^2}{[1+(-a\psi)^n]^{m/2}}$	(3.8)*
Soil thermal properties	
$C = C_m(1-\theta_{sat}) + C_l\theta$	(3.9)
$\lambda = c_A + c_B\theta - (c_A - c_D)\exp[-(c_C\theta)^{c_E}]$	(3.10)†
Soil diffusive property	
$D_{ve} = 1.02 D_{va}(\theta_{sat}-\theta)^{4/3}$	(3.11)‡

ρ_l, the liquid water density; θ, the volumetric (liquid) water content; t, the time; ρ_v, the water vapor density; θ_{sat}, the saturated water content; J_l, the liquid water flux; J_v, the vapor water flux; z, the depth; C, the volumetric heat capacity; T, the temperature; J_h, the heat flux; K the unsaturated hydraulic conductivity; ψ the matric head; D_{ve}, the effective vapor diffusivity within soils; h, the relative humidity of soil-pore air; ρ_{vsat}, the saturation vapor density; g, the gravity acceleration; R, the gas constant for water vapor; θ_r, the residual water content; a, m, n, the empirical parameters for soil hydraulic properties ($m = 1 + 1/n$); K_{sat}, the saturated hydraulic conductivity; C_m, the specific heat for soil mineral; C_l, the specific heat for liquid water; c_A, c_B, c_C, c_D, c_E, the semi-empirical parameters for soil thermal conductivity; D_{va}, the vapor diffusivity in air.

* van Genuchten [1980]

† McInnes [1981]

‡ Millington [1959]

what ideal condition, it is worthwhile applying the model to obtain fundamental aspects of the processes of evaporation and soil moisture movement.

As the lower boundary conditions, constant temperature and no water flux were assumed. At the upper boundary, evaporation flux from the soil surface into the atmosphere (E) was given as the sink of water, and $R_n - H - lE$ was given as the source of heat, where R_n is the net radiation, H the sensible heat flux from the surface into the atmosphere, and l the latent heat for vaporization. The R_n was calculated by using Equation (2.6). The E and H can be expressed by the following bulk-type formulas, respectively:

$$E = \rho C_E u(h_s q_{sat}(T_s) - q_a) \tag{3.12}$$

$$H = \rho c_p C_H u(T_s - T_a), \tag{3.13}$$

where ρ is the density of the air, C_E the bulk transfer coefficient for vapor transfer, h_s the relative humidity at the soil surface, $q_{sat}(T_s)$ the saturation specific humidity at the surface temperature T_s, q_a the specific humidity of the air, c_p the specific heat of the air at constant pressure, C_H the bulk transfer coefficient for sensible heat transfer, and T_a is the air temperature. In Equations (3.12) and (3.13) atmospheric stability correction was not considered since it is not important to the subject of this study. The expression of (3.12) is followed by the bulk-α type parameterization schemes. As mentioned in Section 2.3.1 (A1), if values for a sufficiently thin surface layer are used, the defects of this scheme can be prevented.

The nonlinear partial differential equations (3.1) and (3.2) were solved by a Crank-Nicolson implicit method with Gauss elimination. A flowchart of the computation is given in Figure 3.

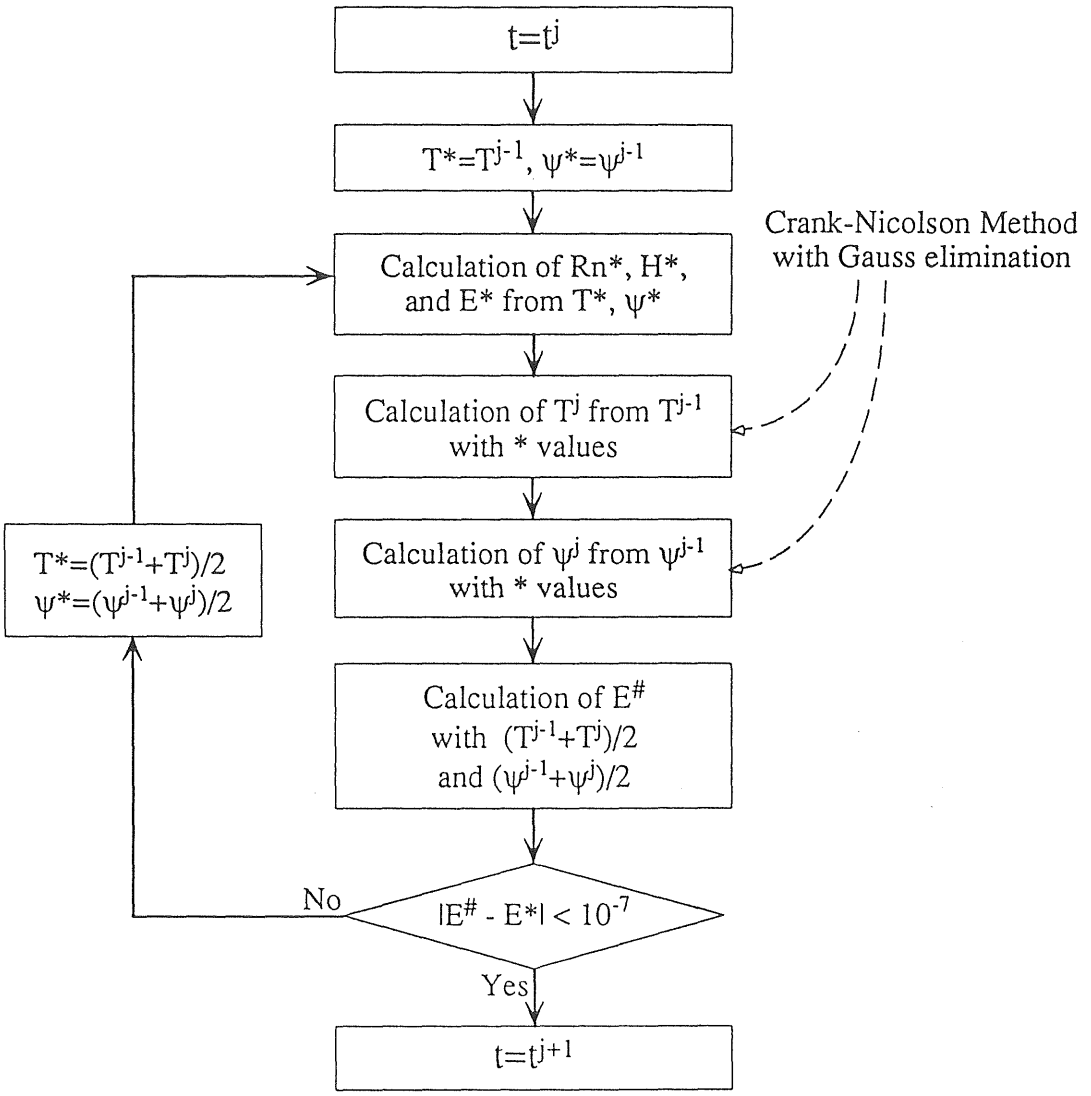

Figure 3 Flowchart of computation in the high resolution model. The *-values are referenced values at the period between two time steps.

3.2 Experimental design

3.2.1 Atmospheric conditions

In this study two sets of atmospheric conditions were assumed, namely, constant atmospheric conditions (Case 1) and diurnally varying atmospheric conditions (Case 2). Atmospheric conditions and parameters concerning soil surface properties assumed for the Case 1 are summarized in Table 5. For the Case 2, diurnal variations of downward short-wave radiation R_{sd} and air temperature T_a were given as follows:

$$R_{sd} = \max[800\cos(2\pi(t_{ls}+12)/24), 0] \tag{3.14}$$

$$T_a = 25 + 3\cos(2\pi(t_{ls}+10)/24), \tag{3.15}$$

where t_{ls} (hr) is the local standard time (LST).

3.2.2 Soil conditions

In the present study, three example soils were chosen as experimental soil materials. Parameters in Equations (3.7) and (3.8) for the three soils are listed in Table 6 and soil moisture characteristic curves described by Equation (3.7) for the soils were shown in Figure 4. Since empirical parameters in Equation (3.10) were not available for each soil, identical values were assumed for all soils (i.e., $c_A = 0.65; c_B = 1.38; c_C = 27; c_D = 0.47; c_E = 4$).

3.2.3 Initial conditions and experimental procedure

Constant temperature profile (25 °C) was given as initial conditions for the Case 1. Initial matric-head profile was assumed to be equilibrium profile for a water table, and was given by $\psi = z - z_w$ where z_w is the depth of the water table (= 0.6 m for sand; = 5.0 m for loam and clay). Numerical computations for the Case 1 were continued until the evaporation zone moved down to the depth of 2 cm below the soil surface.

Table 5 Values of atmospheric conditions and soil surface properties assumed in computation for the Case 1.

Variable	Value
Downward short-wave radiation (W/m^2)	800
Downward long-wave radiation (W/m^2)	300
Wind speed (m/s)	5
Air temperature (℃)	25
Specific humidity of atmosphere (kg/kg)	0.013
Surface albedo	0.4
Bulk transfer coefficient	0.00134

Table 6 Values of parameters for soil hydraulic properties (given as Equations (3.7) and (3.8)) of three experimental soils.

Soil	θ_{sat} (m^3/m^3)	θ_r (m^3/m^3)	a (1/m)	n (-)	K_{sat} (m/s)
Toyoura Sand*	0.412	0.0239	3.14	7.0	1.25×10^{-5}
Silt Loam G.E.3 †	0.396	0.131	0.423	2.06	5.73×10^{-7}
Beit Netofa Clay †	0.446	0.0	0.152	1.17	9.49×10^{-9}

* fitted to the data of Hiyama et al. [1993]

† data from van Genuchten [1980]

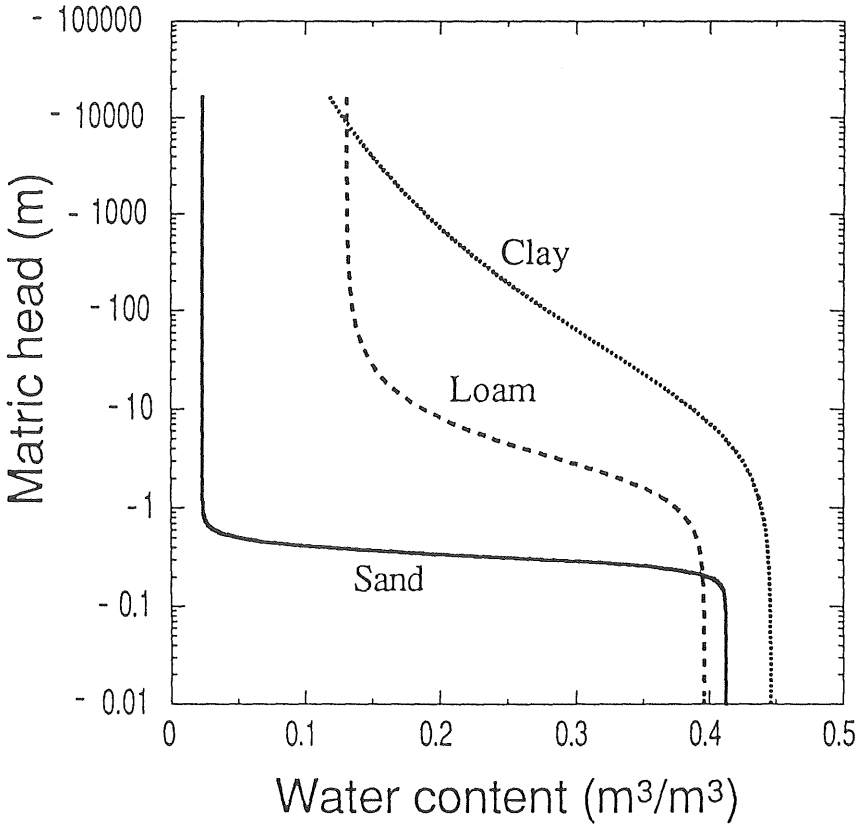

Figure 4 Soil moisture characteristic curves for three experimental soils given by Equation (3.7) with parameters in Table 6.

Initial conditions for the Case 2 were given by the computational results for the Case 1. Computations for the Case 2 were started from noon ($t_{ls} = 12$), and results for the 24-hour period of the next day will be presented.

3.3 Computational results for constant atmospheric conditions (Case 1)

Computational results for Toyoura sand under constant atmospheric conditions (Case 1) are shown in Figure 5. The evaporation rate at each calculation node (E_{node}) was evaluated by the following equation:

$$E_{node} = \frac{\partial J_v}{\partial z} + \frac{\partial \rho_v(\theta_{sat} - \theta)}{\partial t}, \tag{3.16}$$

where J_v is the vapor flux, z the depth, ρ_v the density of water vapor, θ_{sat} the saturated (volumetric) water content, θ the volumetric water content, and t (second) is the time. The figure indicates an inflection of water content profile, and also indicates that the upward liquid water flux is converted to the vapor flux at the depth of the inflection point. In addition, it can be seen that the E_{node} has a large value only at the depth of the inflection.

A very good agreement was found between these computational results and observation results of Yamanaka et al., [1996] (Figure 6). This agreement demonstrates the validity of the model used. From a comparison between the observed and computed results, an inflection in water content profile appears to correspond to the visually determined bottom boundary of the DSL. It is remarkable that the evaporation zone was located at the inflection of water content profile (i.e., the bottom boundary of the DSL) and that the evaporation zone was extremely thin (less than 0.5 mm thickness).

The features that appeared in the results for the sand were also seen in the computed results for silt loam G.E.3. On the other hand, Figure 7 for Beit Nefota clay indicates that the evaporation zone was thicker than that in sand. A comparison between Figures

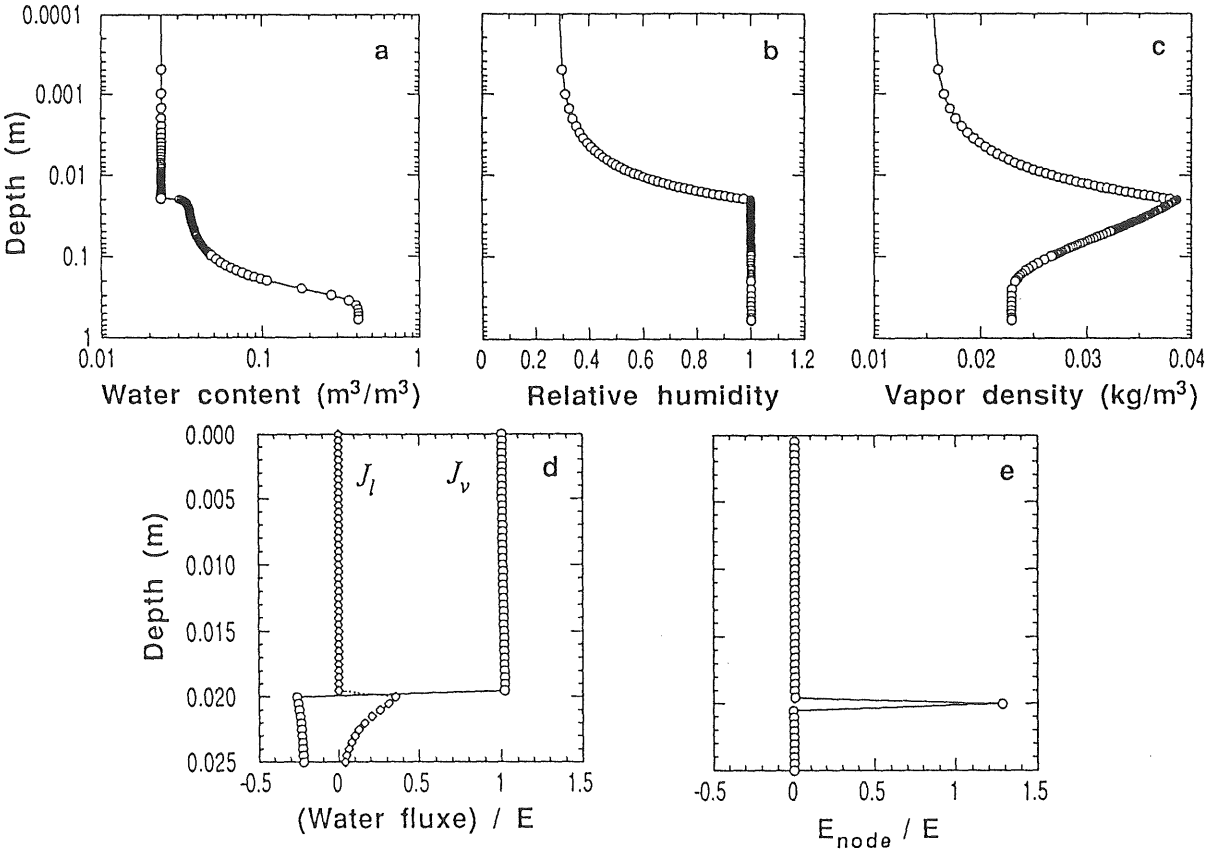

Figure 5 Computational results for the sand (Case 1). J_l and J_v are the water fluxes in liquid and vapor phases, respectively; E and E_{node} are the evaporation rates at the soil surface and at each calculation node, respectively. Note that scales of vertical axis are different between the top and bottom columns.

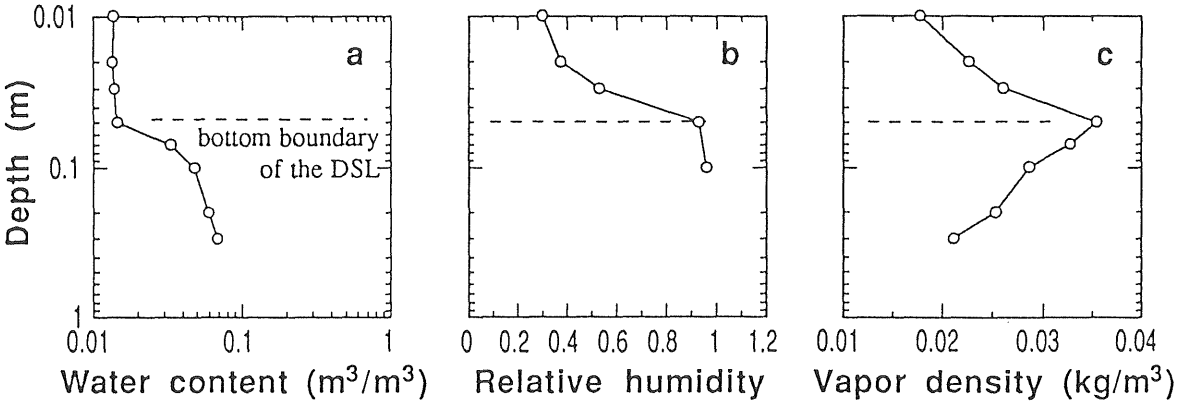

Figure 6 An example of field observation results (after Yamanaka et al., 1996). Dashed line represents the depth of the bottom boundary of the DSL.

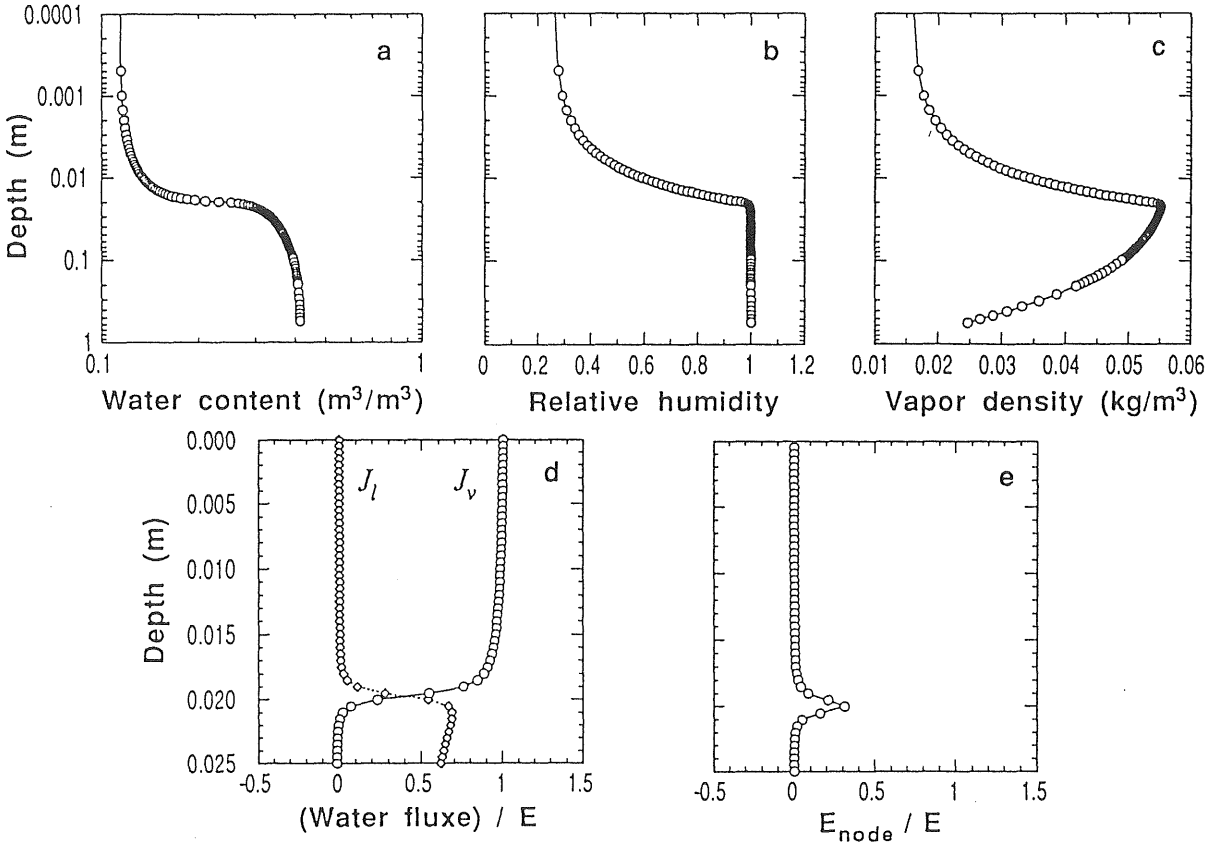

Figure 7 Computational results for the clay (Case 1). Notations in the figures are same as Figure 5.

5 and 7 clarifies that the decrease of liquid water flux toward the soil surface around evaporation zone was gentler in the clay than in the sand. On the other hand, there is another point of difference between the clay and the other soils. The vapor flux slightly increased toward soil surface at the upper region of the DSL where no liquid water transport from deeper soil layers exists. While the evaporation at each calculation node is negligibly small, accumulated evaporation over the upper region of the DSL is certainly not negligible. The soil moisture characteristic curve of the clay (see Figure 4) shows that the clay can retain abundant liquid water at a low matric head level where liquid water transport is difficult. The evaporation at the upper region of the DSL in the clay may be due to its retention properties.

3.4 Computational results for diurnally varying atmospheric conditions (Case 2)

Figure 8 shows computational results for the loam under diurnally varying atmospheric conditions (Case 2). The location of the evaporation zone diurnally varies to balance the liquid water supply from deeper layer and the diurnally varying evaporative demand. During the nighttime (5 and 20 LST), a part of the vapor that evaporated at the bottom boundary of the DSL condenses within the DSL. Although the peak of vapor density profile correspond not to the bottom boundary of the DSL but to the peak of temperature profile in the nighttime so that some divergence of vapor flux (i.e., evaporation) can occur not only at the bottom boundary of the DSL but also at the temperature peak, the value of E_{node} at the temperature peak is considerably smaller than that at the bottom boundary of the DSL. The relatively thick evaporation zone just after sunrise (7 LST) was probably resulted from the condensation within the DSL during the nighttime. Evaporation within the DSL, however, does not continue very long, and the profile at mid-afternoon (15 LST)

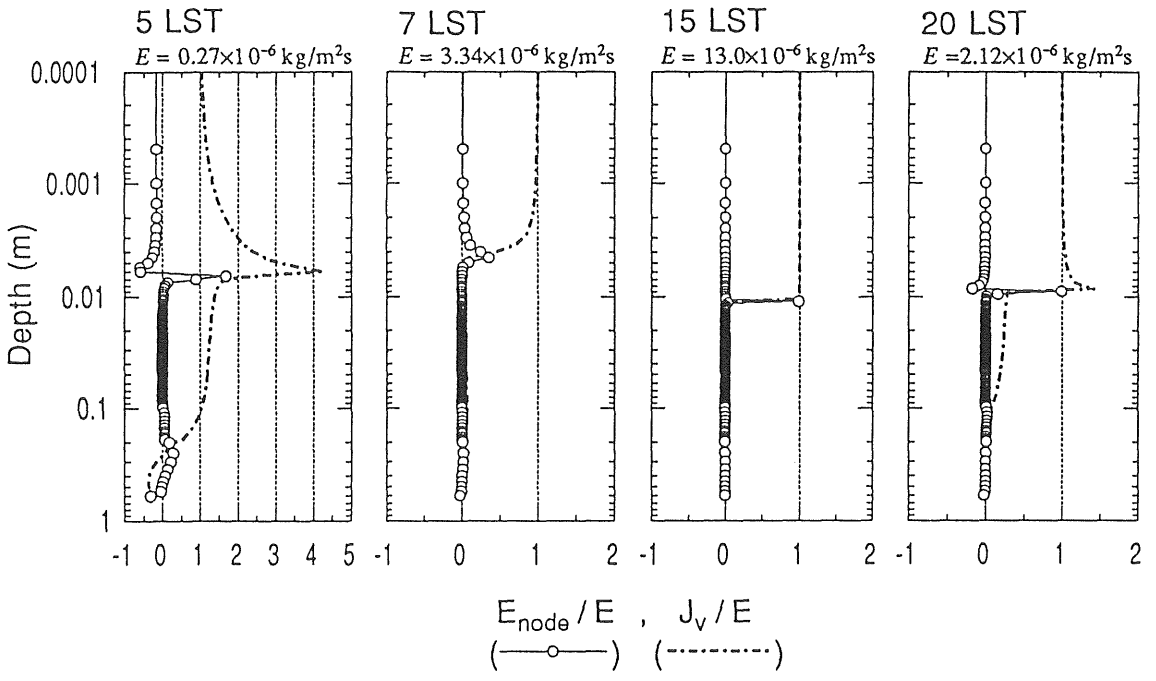

Figure 8 Computational results for the loam (Case 2); time evolution of vertical profiles of E_{node} and J_v (both normalized by E).

is very similar to that obtained under the constant atmospheric conditions (see Figure 5 but for the sand).

On the other hand, diurnal variation of the location of the evaporation zone was not remarkable for the clay (Figure 9). During the nighttime, condensation takes place within the DSL as well as in the case of loam, although there are some condensation from the atmosphere in the case of clay. The most interesting feature is that the evaporation zone can be separated into two sub-zones (i.e., bottom boundary of the DSL and upper region of the DSL). The upper evaporation zone moves downward with time and merges into the lower evaporation zone. As a result, in mid-afternoon the two evaporation zones become a single zone and then the structure of the evaporation zone is similar to that under the constant atmospheric conditions. Amounts of condensation and re-evaporation appear to be larger in the clay than in the loam.

3.5 Summary

Numerical experiments by using a high resolution model of water and heat flows produced the following results:

(1) Under constant atmospheric conditions, the evaporation zone was mainly located at the bottom boundary of the DSL and was considerably thin. However, the thickness of the evaporation zone at the bottom boundary of the DSL depended on the soil types. In addition, in fine-textured soils evaporation took place also at the upper region of the DSL, even though there was no liquid water supply.

(2) Under diurnally varying radiation conditions, even in coarse-textured soils, soil water transiently evaporated within the DSL through a condensation/re-evaporation process with diurnal variation in solar radiation. Amounts of condensation and re-evaporation were larger in fine-textured soils than in coarse-textured soils.

It should be noted that the results obtained by the model largely depend on the math-

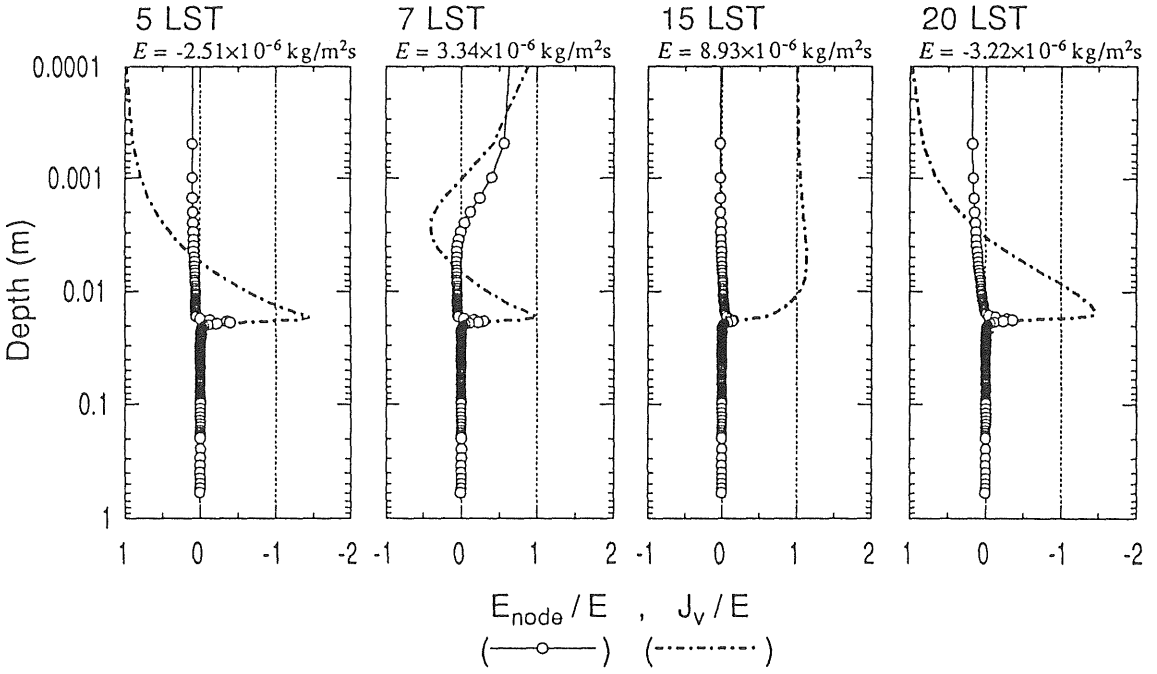

Figure 9 Computational results for the clay (Case 2). Notations in the figures are same as Figure 8.

ematical representation of hydraulic properties (i.e., Equations (3.7) and (3.8)). It has been pointed out that Equation (3.7) cannot well approximate data obtained at low water content region [e.g., Nimmo, 1991; Ross et al., 1991; Yamanaka et al., 1995a]. Therefore, more detailed observational studies for various types of soils should be done for verifying this numerical results.

Chapter 4

Data

4.1 Field observation site

Micro-meteorological and soil-hydrological observations were carried out at three sites: the fallow site, the sand dune site, and the playa site (Table 7). The observation sites are all representative bare lands which commonly exist in the world, and different types of the soil.

Results of detailed soil analysis are summarized in Table 8. Particle size composition was determined by the pipette method [Day, 1965]. Particle size limits and classification of soil texture were determined by the method of International Society of Soil Science [e.g., Nakano et al., 1995]. Particle density was measured by the pycnometer method [Blake, 1965].

General descriptions of topography, climate, and others at each site will be shown below.

4.1.1 Fallow site

Observation was performed at a pre-seeding radish field (60 m × 50 m), which was located at the lacustrine lowland of *Lake Kasumigaura*, during the period of July 21 - 30,

Table 7 Summary of the field observation sites.

Site	Soil texture	Location
Fallow	Sandy loam	Ibaraki, Japan (35°58'N, 140°27'E)
Sand dune	Sand	Tottori, Japan (35°32'N, 134°14'E)
Playa (dried lake)	Silty clay	Kalgoorlie, Australia (30°32'S, 121°25'E)

Table 8 Results of soil analysis for the three observation sites.

Site Depth (m)	Soil texture	Particle size composition (%)			Particle density (Mg/m^3)	Porosity (%)	Bulk density (Mg/m^3)
		Sand	Silt	Clay			
Fallow							
0-0.05	Sandy loam	80.7	9.5	9.8	2.74	61.7	1.05
0.05-0.10	Sandy loam	72.5	17.7	9.8	2.74	62.6	1.03
0.10-0.15	Sandy loam	70.5	20.2	9.3	2.74	62.2	1.04
0.25-0.30	Sandy loam	71.5	19.7	8.8	2.75	47.8	1.44
0.45-0.50	Sandy loam	73.0	19.2	7.8	2.76	52.8	1.31
Sand dune							
0-0.05	Sand	96.2	2.0	1.8	2.68	43.8	1.50
0.05-0.10	Sand	95.7	3.0	1.3	2.68	44.4	1.49
0.10-0.15	Sand	95.2	3.0	1.8	2.67	44.4	1.49
0.25-0.30	Sand	94.7	3.5	1.8	2.68	44.1	1.50
0.45-0.50	Sand	96.7	2.0	1.3	2.69	44.8	1.48
Playa							
0-0.05	Silty clay loam	20.8	57.3	21.9	2.69	62.4	1.01
0.05-0.10	Silty clay	16.8	56.8	26.4	2.71	58.2	1.13
0.10-0.15	Light clay	15.8	41.7	42.5	2.50	56.9	1.08
0.25-0.30	Heavy clay	13.2	26.2	60.6	2.53	46.5	1.36
0.45-0.50	Heavy clay	12.2	31.6	56.1	2.55	46.3	1.37

1996. Although the field was surrounded by fields of various types of crops (e.g., paddy, water melon, corn), the area including the surrounding fields was almost flat. The soil of the field is classified as Coarse-textured Brown Lowland Soils (*Shiba* series), which have no humus horizon and small humic content (< 5%) [Ibaraki Pref., 1987]. Soil texture of the soil is sandy loam (see Table 8). The surface of the field was tilled one week before the beginning of the observation period to remove weeds which were sparsely growing.

Climatic conditions, and rainfall records before and during the observation period at and around this site are shown in Figure 10. The data presented in the figure were all obtained at Sawara station, Japan Meteorological Agency (35°55′ N, 140°30′ E). Average annual precipitation is 1375 mm [Choshi Local Meteorological Observatory, 1980].

4.1.2 Sand dune site

Field observation was carried out in a coastal dune, *Tottori Sand Dune*, during the period of Aug. 11 - 19, 1996. Most parts of the dune were bare condition, while pine forests distributed at the part of the inland side margin of the dune. Because this sand dune was very hilly, a relatively flat section (500 m × 500 m) in the dune was selected as the observation site. The central point of the selected section was at the distance of approximately 450 m from the coast and 250 m from the pine forests. The soil at the site is classified as Sand-dune Regosols, which have no formation of A-horizon and extremely small humic content [Tottori Pref., 1975]. Soil texture of the soil is sand (see Table 8).

Climatic conditions, and rainfall records before and during the observation period at and around this site are shown in Figure 11. The data presented in the figure were all obtained at Tottori station, Japan Meteorological Agency (35°29′ N, 134°14′ E). Average annual precipitation is 1949.5 mm [Japan Meteorological Agency, 1991].

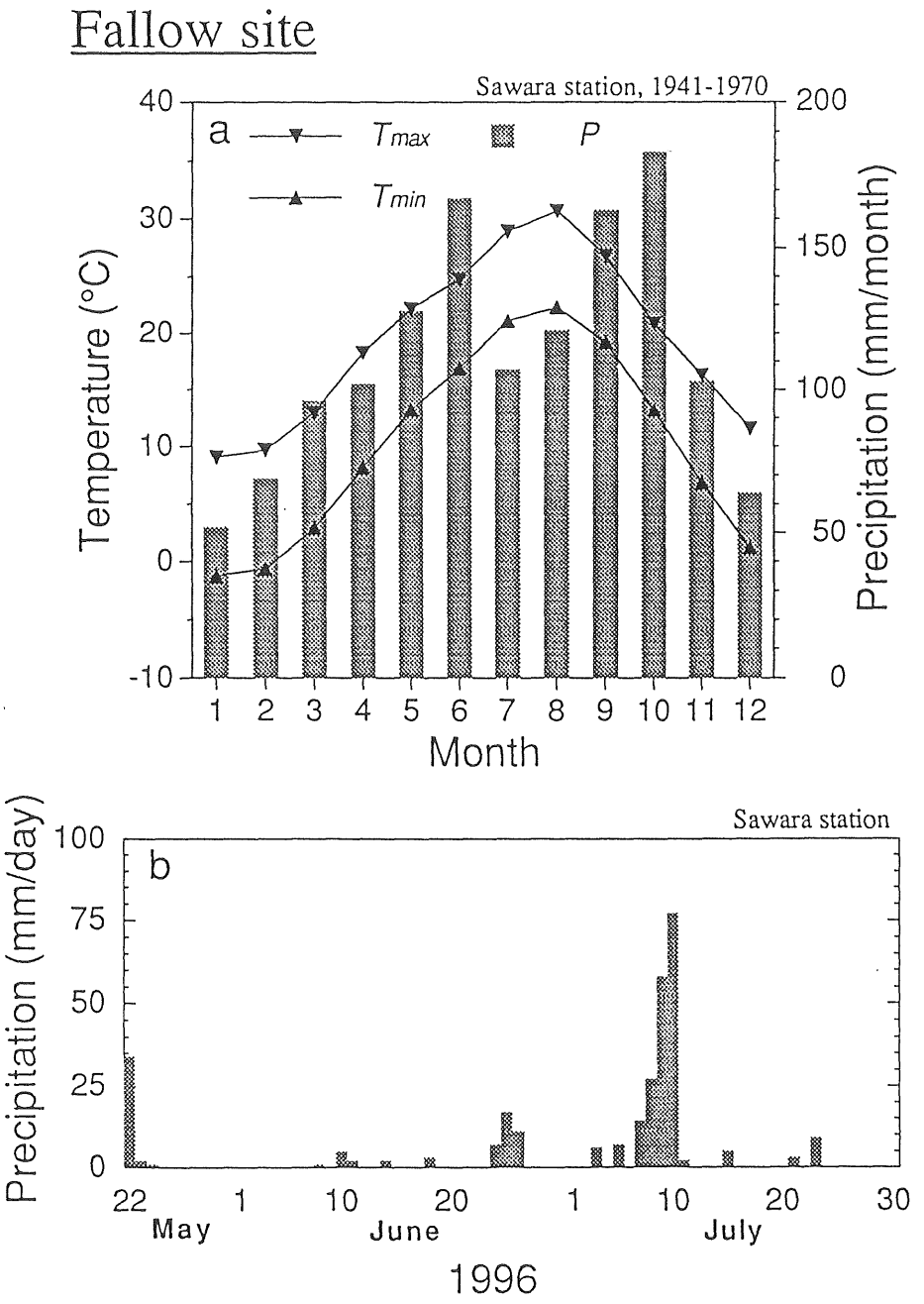

Figure 10 Climatic conditions and rainfall records at the fallow site; (a) annual variations in monthly averaged daily maximum temperature (T_{max}) and minimum temperature (T_{min}), and monthly precipitation (P) (source: Choshi Local Meteorological Observatory, 1980), and (b) rainfall records before and during the observation period.

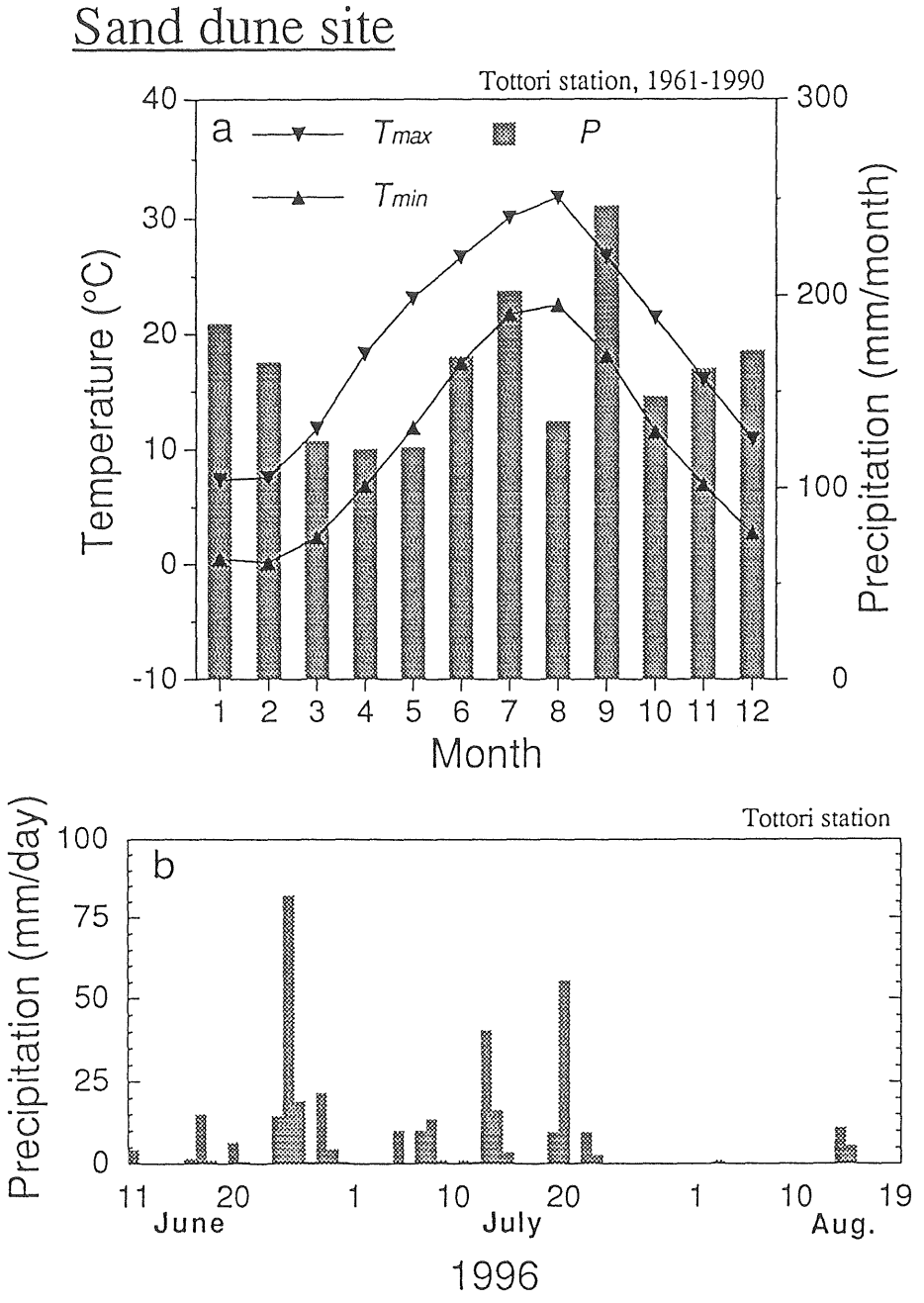

Figure 11 Climatic conditions and rainfall records at the sand dune site; (a) annual variations in monthly averaged daily maximum temperature (T_{max}) and minimum temperature (T_{min}), and monthly precipitation (P) (source: Japan Meteorological Agency, 1991), and (b) rainfall records before and during the observation period.

4.1.3 Playa site

Field measurements were conducted at a dried-up playa-lake, *Arrow Lake* (1 km × 1 km), during the period of Mar. 7 - 12, 1996. The lake was surrounded by low woods of casuarina and eucalyptus with scattered saltbushes. At the playa floor, vegetation scarcely existed because of its hyper saline conditions. Although the surface was almost flat, there were many cracks of approximately 2 cm deep. The soil at the site is classified as Massive Sesquioxidic Soils (*red earths*), in which horizons are often weakly developed [Hubble et al., 1983]. Soil texture of the soil ranges from silty clay loam to heavy clay (see Table 8). As a typical feature of Massive Sesquioxidic Soils [Hubble et al., 1983], Table 8 indicates that clay content of the soil gradually increases with depth.

Climatic conditions, and rainfall records before and during the observation period at and around this site are shown in Figure 12. The data presented in the figure were all obtained at Kalgoorlie-Boulder station, Bureau of Meteorology, Australia (30°47′ S, 121°27′ E). Average annual precipitation is 259.9 mm [Bureau of Meteorology, Australia, 1994].

4.2 Measurements

Measurement components and their methods are summarized in Table 9. On an intensive observation day (IOD) selected arbitrary during the observation period for each site, sampling frequencies of surface water content and thickness of the DSL were increased, and isotopic composition of surface soil water was added to the list of measurements (see Table 9b). Furthermore, soil-profile investigation was carried out on an arbitrary day (see Table 9c). Measured values of micro-meteorological elements were averaged every hour.

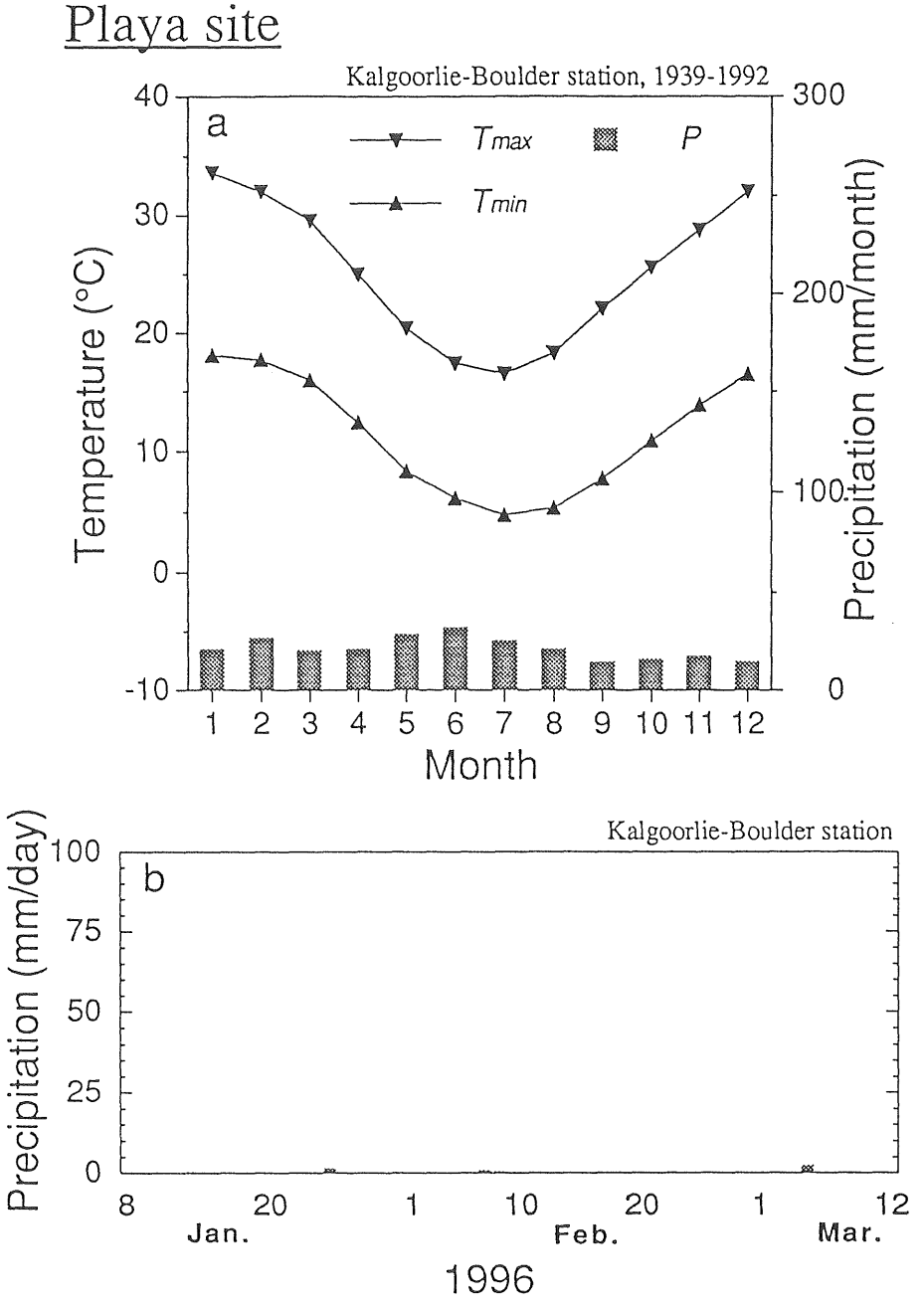

Figure 12 Climatic conditions and rainfall records at the playa site; (a) annual variations in monthly averaged daily maximum temperature (T_{max}) and minimum temperature (T_{min}), and monthly precipitation (P) (source: Bureau of Meteorology, Australia, 1994), and (b) rainfall records before and during the observation period.

Table 9 List of observation components.

a) General components

Component	Instrument (or method)	Sampling point			Sampling interval
		Fallow	Sand dune	Playa	
Wind speed	3-cup anemometer	0.23, 0.31, 0.53, 0.73, 2.01 m height	0.25, 0.34, 0.56, 0.75, 2.03 m height	0.27, 0.51, 0.78, 1.30, 2.07 m height	30 sec
Air temperature	Ventilated Pt thermometer*	0.135, 0.30 m height	0.10, 0.27 m height	0.24, 1.76 m height	5 min
Air humidity	Ventilated capacitance humidity sensor	0.135, 0.30 m height	0.10, 0.27 m height	0.24, 1.76 m height	5 min
Upward / downward total radiation	Total radiometer	1.10 m height	1.10 m height	1.10 m height	5 min
Upward / downward short-wave radiation	Albedometer	1.10 m height	1.10 m height	1.10 m height	5 min
Soil-surface temperature	Infrared-radiation thermometer	1.75 m height	1.75 m height	1.75 m height	5 min
Soil heat flux	Heat flux plate	0.1 m depth	0.1 m depth	0.1 m depth	5 min
Soil temperature	Pt thermometer*	0.01, 0.03, 0.05, 0.1, 0.3, 0.5 m depth	0.01, 0.03, 0.05, 0.1, 0.3, 0.5 m depth	0.01, 0.03, 0.05, 0.1, 0.3, 0.5 m depth	5 min
Pore-air humidity in the soil	Capacitance humidity sensor	0.01, 0.03, 0.05, 0.1, 0.3, 0.5 m depth	0.01, 0.03, 0.05, 0.1, 0.3, 0.5 m depth	0.01, 0.03, 0.05, 0.1, 0.3, 0.5 m depth	5 min
Water content of surface soil	Soil core sampling + oven drying	0-1, 0-5 cm depth	0-1, 0-5 cm depth	0-5 cm depth	24 hr (at noon)
Thickness of the DSL	Observation by eyes	-	-	-	24 hr (at noon)

* Pt thermometer = Platinum resistance thermometer

Table 9 (continued)

b) Additional components during intensive observation day (IOD)

Component	Method	Sampling point			Sampling interval
		Fallow (Jul. 27, 1996)	Sand dune (Aug. 17, 1996)	Playa (Mar. 9, 1996)	
Water content of surface soil	Soil core sampling + oven drying	0-1, 0-5 cm depth	0-1, 0-5 cm depth	0-5 cm depth	4 hr
Thickness of the DSL	Observation by eyes	-	-	-	4 hr
Isotopic composition of surface soil water	Soil water sampling + mass spectrometry	0-1 cm depth*	0-1 cm depth*	0-1 cm depth#	4 hr

c) Additional components on soil-profile investigation

Component	Method	Sampling point		
		Fallow (Jul. 29, 1996)	Sand dune (Aug. 13, 1996)	Playa (Mar. 10, 1996)
Water content of soil	Soil core sampling + oven drying	0-1, 1-3, 3-5, 5-6, 6-7, 7-8, 8-9, 9-10, 10-15, 25-30, 45-50 cm depth	0-1, 1-2, 2-3, 3-4, 4-5, 5-10, 10-15, 25-30, 45-50 cm depth	0-2, 2-5, 5-10, 10-15, 25-30, 45-50 cm depth
Isotopic composition of soil water	Soil water sampling + mass spectrometry	0-1, 1-3, 3-5, 5-6, 6-7, 7-8, 8-9, 9-10, 10-15, 25-30, 45-50 cm depth*	0-1, 1-2, 2-3, 3-4, 4-5, 5-10, 10-15, 25-30, 45-50 cm depth*	0-2, 2-5, 5-10, 10-15, 25-30, 45-50 cm depth#

* extracting soil-water by ordinary temperature distillation method

extracting soil-water by azeotropic distillation method

4.2.1 Micrometeorological elements

Horizontal location of the micrometeorological observation tower, where anemometers, ventilated thermometers and humidity sensors were installed, was decided to make use of advantage of a longer fetch by considering the dominant wind direction. Vertical arrangement of instruments on the tower were also decided by considering the fetch requirement for each observation site.

All anemometers, thermometers, and humidity sensors were calibrated using the wind tunnel of the National Research Institute for Earth Science and Disaster Prevention. In addition, to reduce further instrumental errors between two ventilated thermometers or two ventilated humidity sensors, comparative measurements (with ventilation) under field conditions were carried out and then one set of ventilated thermometer/humidity sensor was calibrated by referring the outputs from another set of thermometer/humidity sensor. Net radiometer and albedometer were also calibrated by comparing the outputs of them to those from standard instruments in the experimental field of the Environmental Research Center of the University of Tsukuba. These calibration procedures were performed before and after the observation periods. The root mean square differences (RMSD) between the calibrated values from each instrument and the referenced values from standard instrument are 0.03-0.07 m/s for anemometers, 0.011-0.026 °C for thermometers, 0.31-0.65 % for humidity sensors, 0.055 °C for ventilated thermometers, 0.30 % for ventilated humidity sensors, 12.66 W/m^2 for radiometer, and 4.42 W/m^2 for albedometer.

4.2.2 Soil water content

Soil water content was determined by soil sampling and oven dry method (at 110 °C). Soils were sampled by soil core samplers (100 cc) at 0-5, 5-10, 10-15, 25-30 and 45-50 cm depths and were sampled by using a small shovel (sampling volume: 100 cc) at the other depths.

Volumetric water content θ was evaluated by the following relationship:

$$\theta = w\frac{\rho_b}{\rho_l} \tag{4.1}$$

where w is the gravimetric water content ($\equiv M_w/M_s$, M_w the mass of liquid water, M_s the mass of soil particles), ρ_b the dry bulk density of the soil (averaged over several samples that obtained at the same depth), and ρ_l the density of liquid water. In the evaluation of water content in the shallow depth zone, where the soil was sampled by using a shovel, the value of bulk density for 0-5 or 5-10 cm depth was used. Soil sampling was performed at horizontally different two points, and then the values were arithmetically averaged. The RMSD of measured water content between the two samples were 0.39 % at the fallow site, 0.30 % at the sand dune site, and 1.35 % at the playa site. The large value of RMSD at the playa site may be due to a large variability in soil water distribution.

4.2.3 Thickness of the DSL

The thickness of the DSL was measured with a caliper square by excavating the soil surface. The bottom boundary of the DSL is visually distinguishable from the contrast of color between the DSL and the underlying soil layer [e.g., Fritton et al., 1967; Matsuda et al., 1977]. Measurement of the thickness of the DSL was carried out at horizontally different ten points, and then its arithmetic mean and standard deviation were calculated.

4.2.4 Stable isotopic analysis of soil water

Soil sampling for stable isotopic analysis was made using a small shovel, and sample soils were shield up in double polyethylene bags to prevent the change in isotopic composition due to evaporation or mixing of vapor from the air. Sample waters were extracted from the soil by the ordinary temperature distillation (OTD) method [Yamanaka and Shimada, 1997] at the fallow site and at the sand dune site, and by the azeotropic distillation method

[Revesz and Woods, 1990] at the playa site.

For deuterium analysis, extracted water samples were deoxidized by zinc reduction method [e.g., Coleman et al., 1982; Kendall and Coplen, 1985], and D/H ratio was determined with MAT 252 (Finnigan MAT) mass spectrometer of the Institute of Geoscience, University of Tsukuba. For oxygen-18 analysis, CO_2 equilibration method [e.g., Epstein and Mayeda, 1953] was used for the preparation of samples and $^{18}O/^{16}O$ ratio was determined with Delta S (Finnigan MAT) mass spectrometer of the Institute of Geoscience, University of Tsukuba. The isotopic compositions are expressed in the standard δ-notation as per mil deviations from the internationally accepted V-SMOW (Vienna Standard Mean Ocean Water; Craig [1961], Gonfiantini [1978]).

The reproducibility in sample preparation and analysis by the mass spectrometer is ± 1 $^{\circ}/_{\circ\circ}$ in δD and ± 0.1 $^{\circ}/_{\circ\circ}$ in δ^{18}O. The error caused by water extraction from the soil (including that caused by sample preparation and mass spectrometer analysis) is ± 2.5 $^{\circ}/_{\circ\circ}$ for δD and ± 0.47 $^{\circ}/_{\circ\circ}$ for δ^{18}O by the OTD method [Yamanaka and Shimada, 1997], and is ± 2 $^{\circ}/_{\circ\circ}$ for δD and ± 0.2 $^{\circ}/_{\circ\circ}$ for δ^{18}O by the azeotropic distillation method [Revesz and Woods, 1990].

Although Yamanaka and Shimada [1997] stated that the accuracy of the OTD method obtained for a sand might change for different types of soils, Table 10 indicates the almost same magnitudes of the accuracy both in δD and δ^{18}O for sandy loam of the fallow site. On the other hand, interlaboratory comparison by Walker et al. [1994] indicates that errors in the azeotropic distillation method larger than those shown by Revesz and Woods [1990] could be introduced by any cause in the operation of distillation procedure. Thus, the accuracy of the azeotropic distillation method in the present study may be somewhat worse than that listed above.

Table 10 Comparison of δ values between water extracted by centrifugation method and that by ordinary temperature distillation (OTD) method. Samples A and B were collected at the fallow site, but at different depth.

Sample	C[a]	OTD[b]	Diff.[c]	Ref. err.[d]
δD (‰)				
A	-76.8	-73.5	3.3	±2.5
B	-93.4	-90.5	2.9	±2.5
$\delta^{18}O$ (‰)				
A	-9.32	-9.00	0.32	±0.47
B	-10.67	-10.88	-0.21	±0.47

[a] δ value of water extracted by centrifugation

[b] δ value of water extracted by OTD

[c] Difference of δ values between water extracted by centrifugation and that by OTD

[d] Referenced value of error introduced by OTD (from Yamanaka and Shimada [1997])

4.2.5 Chemical compositions of soil water

Only at the playa site, measurements of electric conductivity (E. C.), cation and anion concentrations of soil water were performed because it was expected that there was salt accumulation.

Sample water was prepared by adding 100 g distilled water to 20 g moist soil and by shaking those sufficiently. Electric conductivity of the sample water was measured by an E. C. meter (SC-82, Yokogawa). Concentrations of dissolved substances (Na^+, K^+, Ca^{2+}, Mg^{2+}, SO_4^{2-}, NO_3^-) were determined by Capillary Electophoresis System (Quanta 4000, Waters Co.), and HCO_3^- content was determined by tiltration method of H_2SO_4.

Ion concentrations were calculated as milliequivalents per unit volume of soil matrix (X), expressed as meq/m^3(soil), by using the following relationship [Ronen et al., 1996] (but slightly modified):

$$X = \chi \frac{M_{dw} + M_{ws} w/(1+w)}{\rho_b M_{ws}[1 - w/(1+w)]}, \tag{4.2}$$

where χ is the (measured) concentration in the sample water (meq/l), M_{dw} and M_{ws} are the the weight of distilled water added to soil sample (100 g) and that of wet soil sample (20g), respectively. It should be noted that the value X represents the total concentration of a specific ion, found in both the solid and liquid phase of the soil.

Chapter 5

General aspects of micro-meteorological and soil hydrological characteristics

In this chapter, general aspects of observed micrometeorological and soil hydrological elements will be described as a basic information for analyses presented in later chapters. Also, it would be important as examples of the chorographical descriptions for micrometeorology and soil hydrology, even though the observation period in each site is very short for complete description.

5.1 Fallow site

Observed results of micrometeorological elements are shown in Figure 13. Figure 14 shows (a) the inter-diurnal variations in surface water content and the thickness of the DSL, and (b) the diurnal variation patterns of those.

At the early stage of the observation period, soil moisture condition was relatively wet due to antecedent rainfalls (see Figure 10b), and downward short-wave radiation (solar

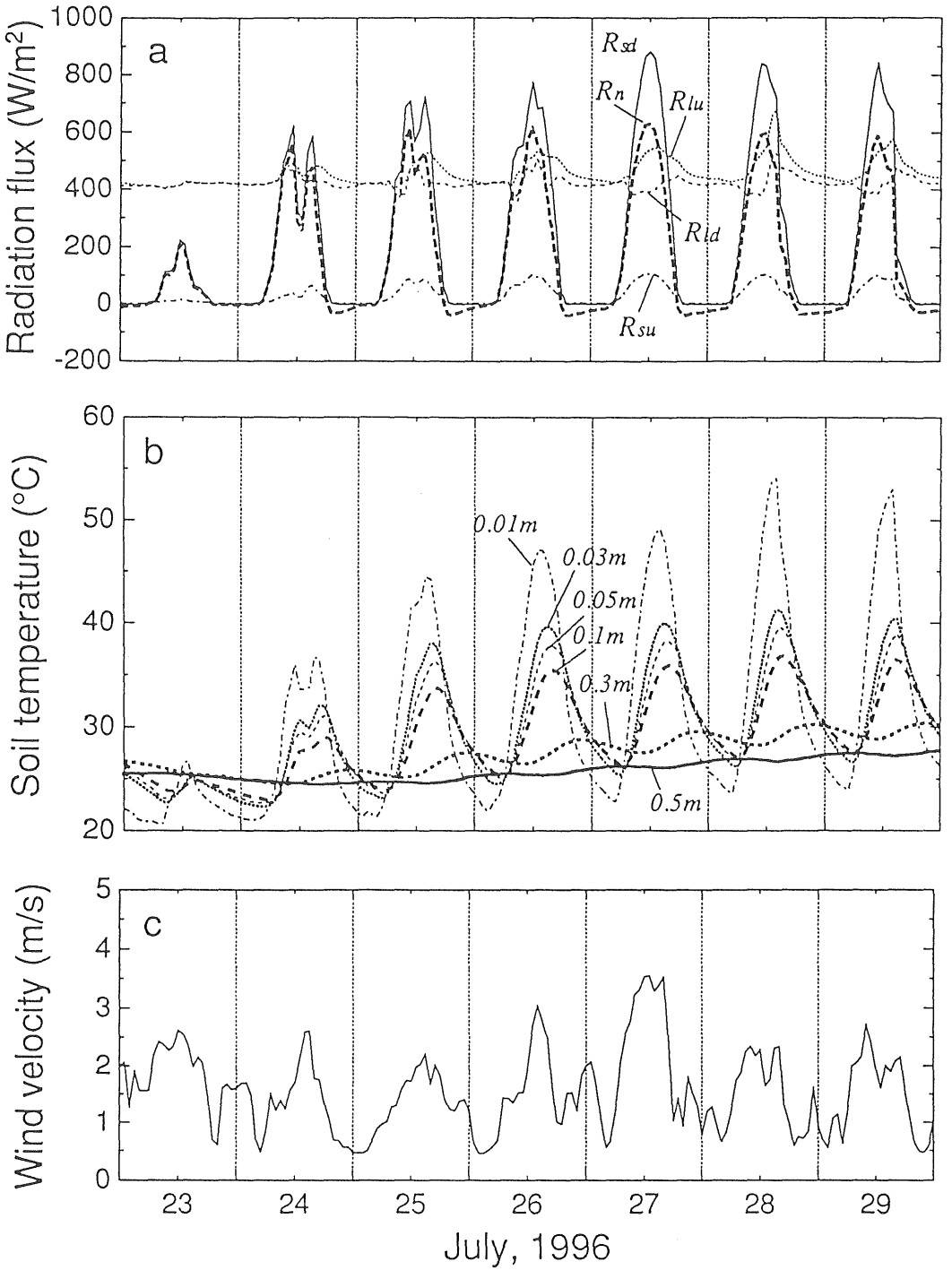

Figure 13-1 Observation results of micrometeorological elements for the fallow site; (a) radiation balance components (R_n, the net radiation; R_{sd}, the downward short-wave radiation; R_{su}, upward short-wave radiation; R_{ld} downward long-wave radiation; R_{lu}, upward long-wave radiation), (b) soil temperature at different depths, and (c) wind velocity at the height of 0.53 m.

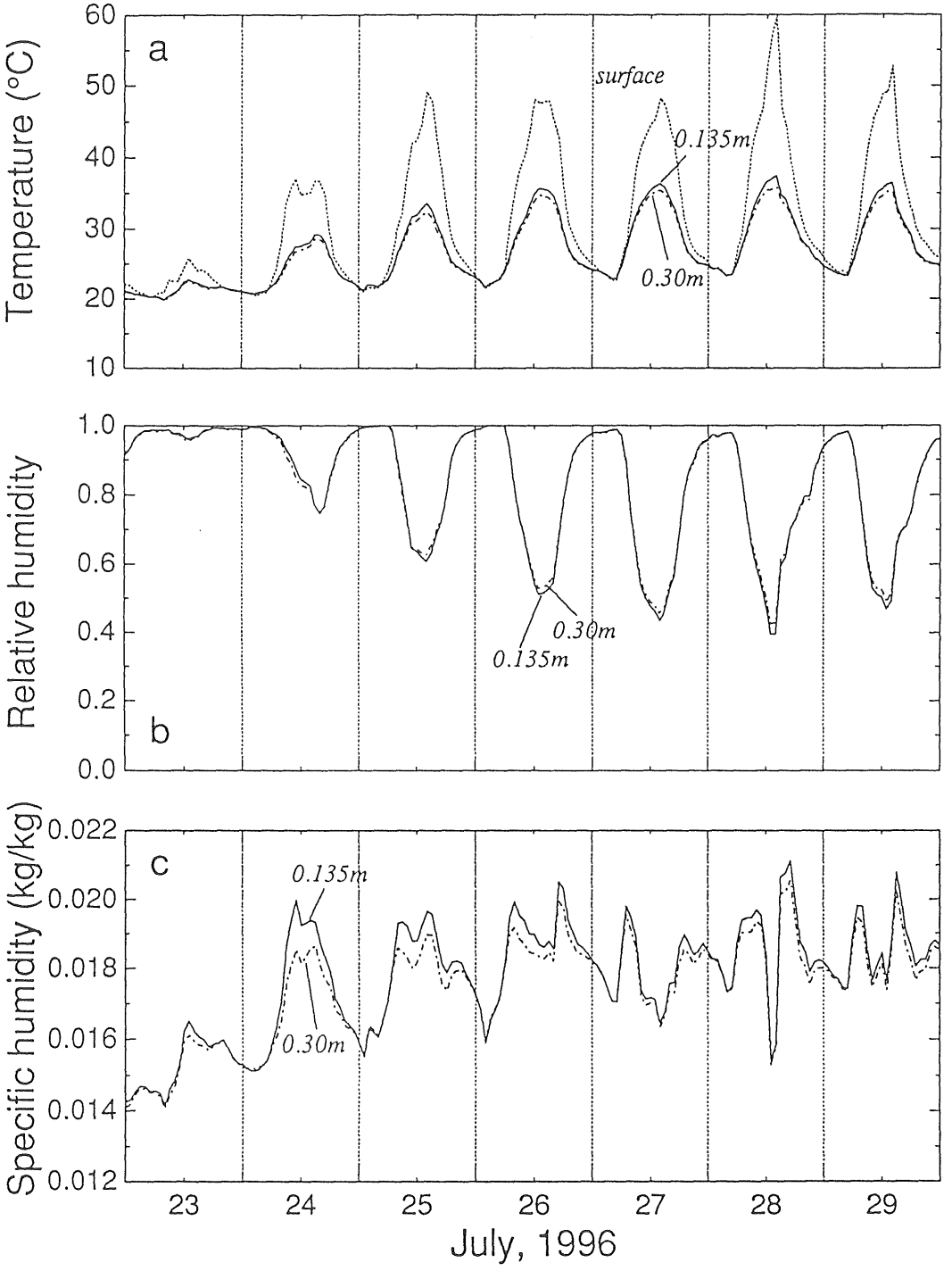

Figure 13-2 Observation results of micrometeorological elements for the fallow site; (a) temperature, (b) relative humidity, and (c) specific humidity, at two levels (0.135 and 0.30 m) in the atmosphere. Soil surface temperature is added in the top column of the figure.

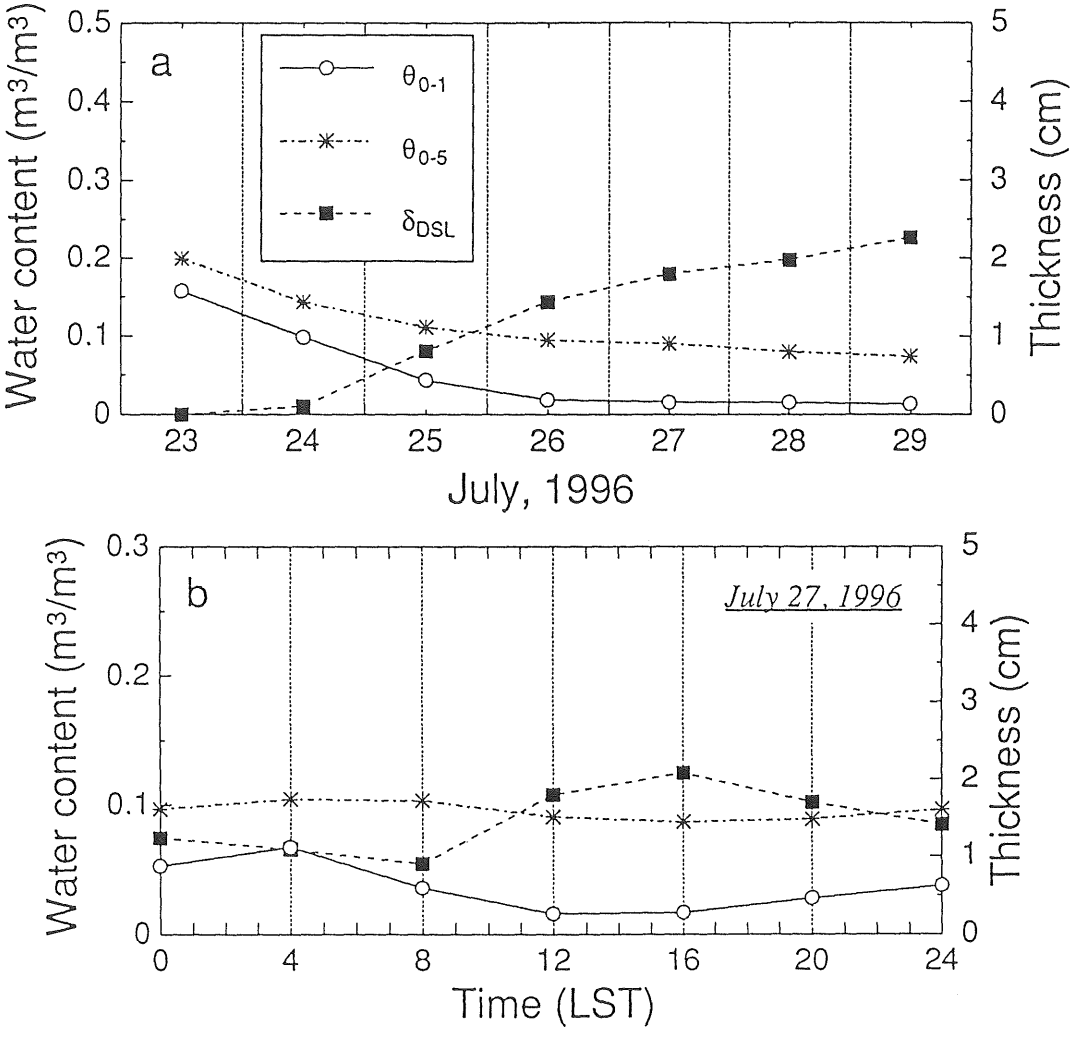

Figure 14 Temporal variations of the surface water content and the thickness of the DSL (δ_{DSL}) for the fallow site; (a) inter-diurnal variation, and (b) diurnal variation. θ_{0-1} and θ_{0-5} denote water content of the surface soil layers of 1 cm and 5 cm, respectively.

radiation) was considerably small because of the effect of cloud (Figure 13-1a). Upward and downward long-wave radiations were almost the same. After June 25, downward short-wave radiation remained quite large owing to successive clear conditions of sky. Then upward short-wave and long-wave radiation fluxes increased gradually. The increase of short-wave radiation is due to an increase of surface albedo accompanying with soil drying (see Figure 14), and the increase of long-wave radiation was caused by an increase of surface temperature (see Figure 13-2a). On the other hand, downward long-wave radiation did not show any obvious increase. The reason for this may be that the effect of the increase of the atmospheric temperature was canceled by the effect of the decrease of cloud amount. Inter-diurnal variation in net radiation was not as large as that in downward short-wave radiation due to an increase in the upward radiation fluxes.

Figure 15 shows (a) the inter-diurnal evolution of the diurnal course of surface albedo and (b) the relationship between surface albedo and volumetric water content of surface soil of 1-cm or 5-cm thickness obtained at noon. Figure 15b indicates that the inter-diurnal increase of surface albedo (Figure 15a) is related to the decrease of surface soil moisture. The figure also indicates a step-like change in surface albedo. The value of surface albedo is approximately 0.075 when θ_{0-1} is larger than 9 % (or $\theta_{0-5} > 14\%$), and is approximately 0.125 when θ_{0-1} is smaller than 4 % (or $\theta_{0-5} < 11\%$). On the other hand, Figure 15a indicates that the surface albedo varies with time in a day. As pointed out by Nkedirim [1972], Idso et al. [1975] and Nakagawa [1982], this variation is expected to be partly due to the change in the solar zenith angle. However, an asymmetric diurnal variation pattern was observed on July 24 and 25. This may be due to the effect of diurnal change in surface moisture.

Figure 13-1b indicates increases both in the daily average value and in the amplitude of the diurnal fluctuation of soil temperature. The diurnal range of soil temperature at 1 cm depth reached to 30.2 °C. Nevertheless, soil temperature hardly varied diurnally and inter-diurnally at the depth of 0.5 m. Temperature gradient increased during soil drying

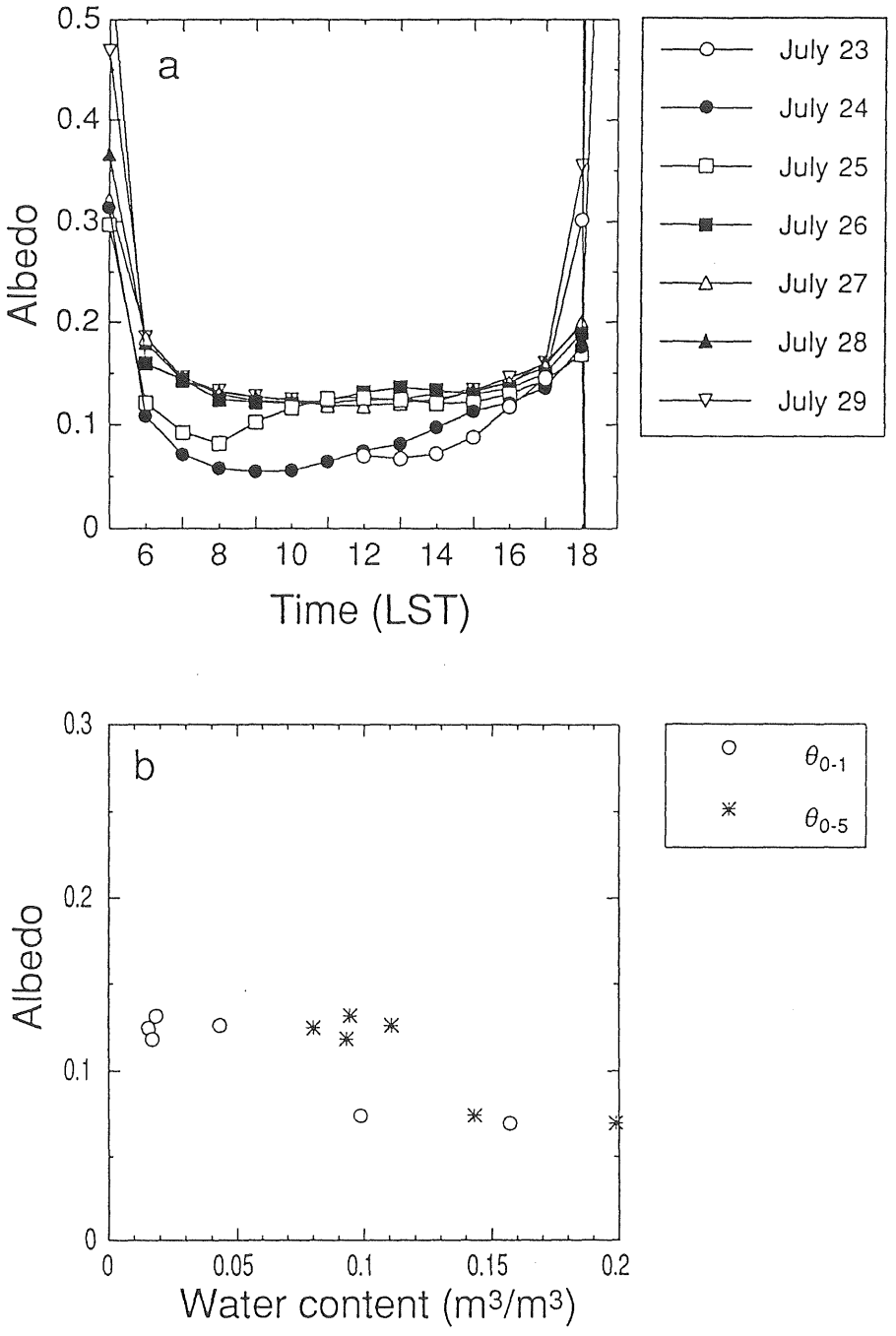

Figure 15 Results of albedo measurements for the fallow site; (a) diurnal and inter-diurnal variation of the surface albedo, and (b) relationship between the surface albedo and the surface water content.

particularly at the shallower zone, and reached to 8°C/cm at its maximum.

In Figure 13-1c, diurnal variation in wind velocity can be recognized. The wind velocity is large at daytime and small at nighttime.

Figure 13-2a indicates a variation in air temperature similar to that in soil temperature. However, the diurnal range of air temperature is considerably smaller than that of soil temperature, and is 12.6 °C at the maximum at 0.30 m height. A considerably large difference was observed between air temperature at 0.135 m height and radiometically determined surface temperature, while the temperature difference between the height of 0.135 and 0.30 m was very slight.

Very clear diurnal variation in relative humidity can be seen in Figure 13-2b. The daytime values of relative humidity showed a tendency to decrease inter-diurnally, while nighttime values were almost unity and hardly varied.

Inter-diurnal variation in specific humidity generally showed a tendency to increase slightly (Figure 13-2c). The reason for this tendency may be that the observation site was surrounded by the land which can be more effective as vapor sources (e.g., cultivated field, lake). On the other hand, the diurnal variation pattern of specific humidity appears to change every day. The variation pattern on July 24 has a single maximum at around noon while that on later days has two maxima in the forenoon and the late afternoon. There are too few data to determine whether the variation pattern with two maxima was caused by a lack of vapor supply from the soil surface in the mid-afternoon and the decay of convective mixing in the late afternoon, or by advection from surrounding area and wind direction change.

In Figure 14a, water contents both of 0-1 cm (θ_{0-1}) and 0-5 cm (θ_{0-5}) soil-layers decrease gradually. The thickness of the DSL was almost zero during two days just after a rainfall; then the thickness increased gradually and reached to approximately 2 cm on July 28 after five days since the rainfall. The diurnal variation of water content could be seen in both θ_{0-1} and θ_{0-5} (see Figure 14b), while the diurnal range was considerably larger in θ_{0-1}

(5.05 %) than in θ_{0-5} (1.5 %). The phase of diurnal fluctuation of θ_{0-5} appears to lag behind that of θ_{0-1}. The diurnal variation in the thickness of the DSL was similar to that reported by Nomura and Inoue [1979] and Kobayashi et al. [1991a, b]. Diurnal range of the thickness of the DSL was 1.17 cm.

Figure 16a shows the three-phase distribution of the soil. In the figure, the effect due to tillage is appeared in the changes in volumetric solid content and slightly in water content at around the depth of 20 cm. Except for this effect, soil water content gradually decreases toward shallower depth, while there is an inflection of water content profile at around 2 cm depth. Figure 16b shows the vertical profile of soil water content at shallower zone. The figure indicates an agreement between the depth of the inflection point and the depth of the bottom boundary of the DSL. Observation results similar to this have been obtained by Nomura and Inoue [1979], Kobayashi et al. [1991a] and Yamanaka et al. [1996]. The water content of the bottom boundary of the DSL was between 2 and 7 %. This fact and Figure 15b suggest that the decrease in surface albedo occurs with the formation of the DSL.

5.2 Sand dune site

Results of micrometeorological measurements are shown in Figure 17. Figure 18 shows (a) the inter-diurnal variations in surface water content and the thickness of the DSL, and (b) the diurnal variation patterns of those.

As seen from the rainfall records (Figure 11b), during the period before the rainfall event on Aug. 14-15, soil moisture conditions was extremely dry. Downward short-wave radiation was very large throughout the observation period except for Aug. 14 and 15 (Figure 17-1a). Upward short-wave and long-wave radiations abruptly decreased after the rainfall, and then increased gradually. In contrast, downward long-wave radiation hardly varied. Upward long-wave radiation was larger than downward long-wave radiation except

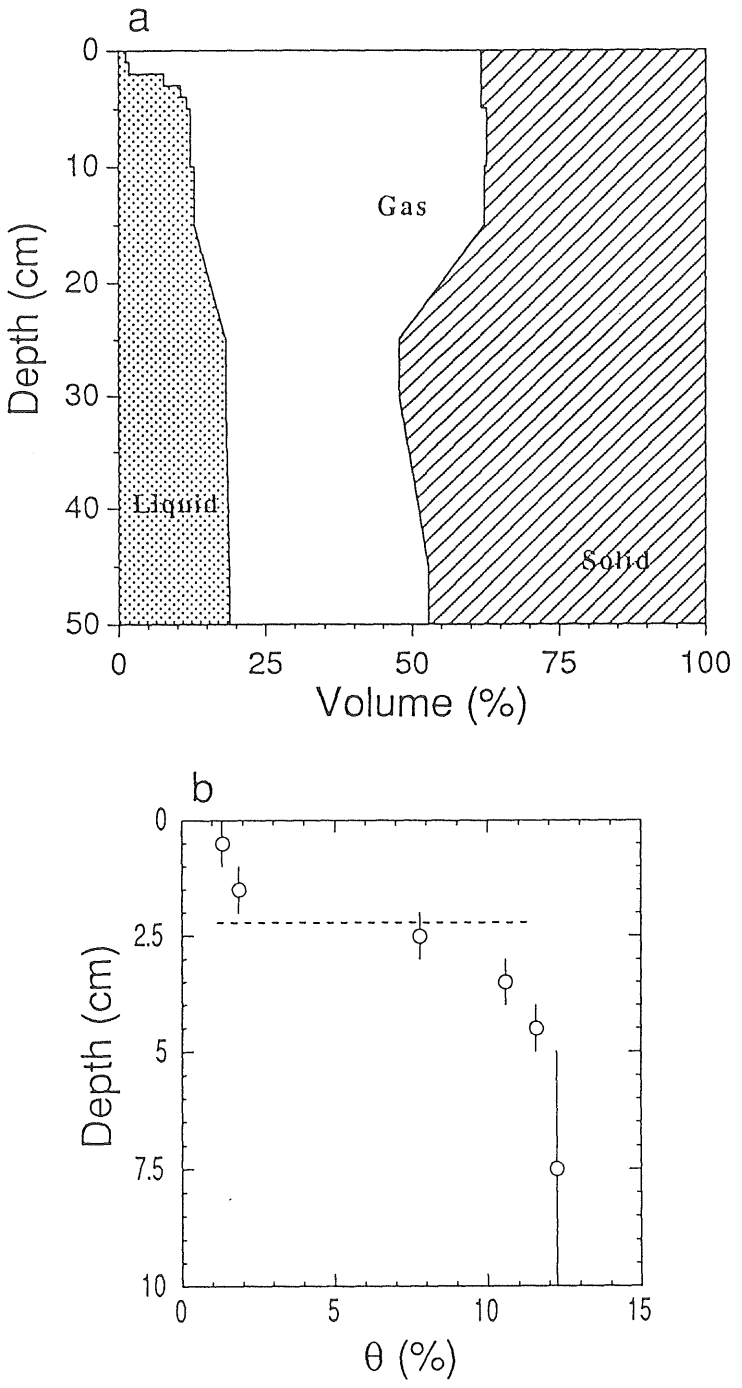

Figure 16 Soil hydrological characteristics for the fallow site; (a) three phase distribution of the soil, and (b) water content profile. Vertical bars indicate the thickness of sampled soil cores. Dashed line in the bottom figure denotes the depth of the bottom boundary of the DSL.

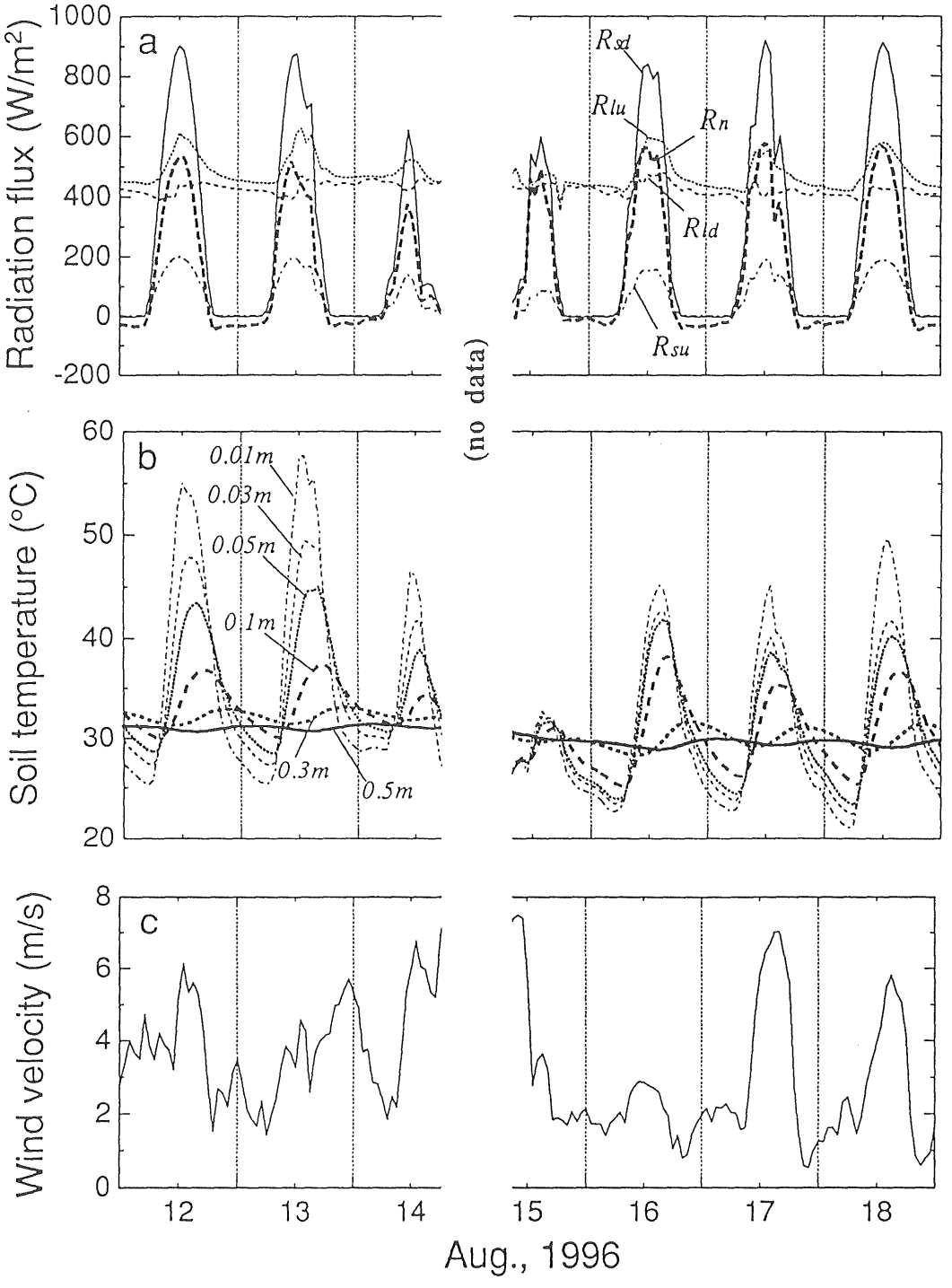

Figure 17-1 Observation results of micrometeorological elements for the sand dune site; (a) radiation balance components (R_n, the net radiation; R_{sd}, the downward short-wave radiation; R_{su}, upward short-wave radiation; R_{ld} downward long-wave radiation; R_{lu}, upward long-wave radiation), (b) soil temperature at different depths, and (c) wind velocity at the height of 0.34 m.

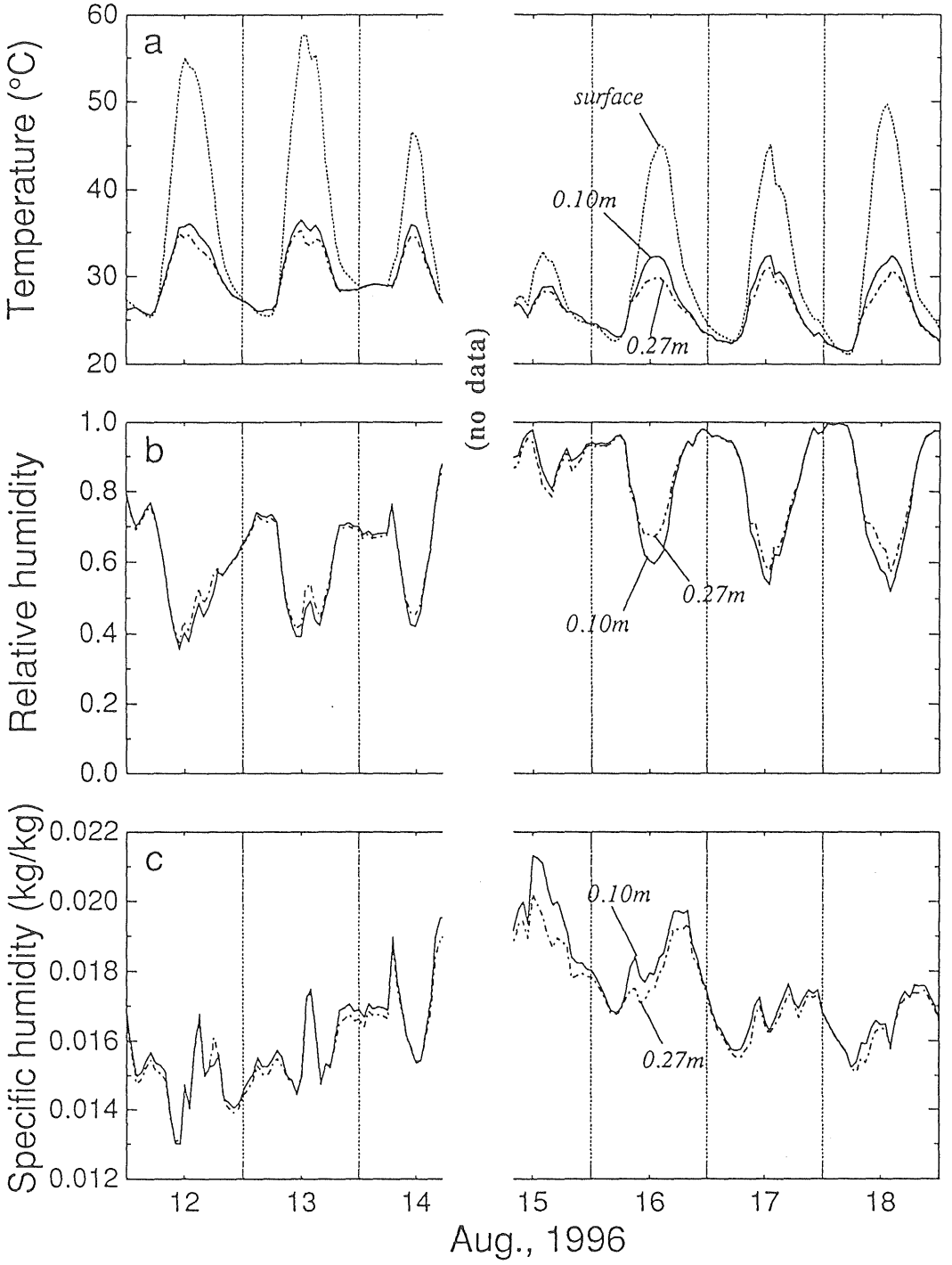

Figure 17-2 Observation results of micrometeorological elements for the sand dune site; (a) temperature, (b) relative humidity, and (c) specific humidity, at two levels (0.10 and 0.27 m) in the atmosphere. Soil surface temperature is added in the top column of the figure.

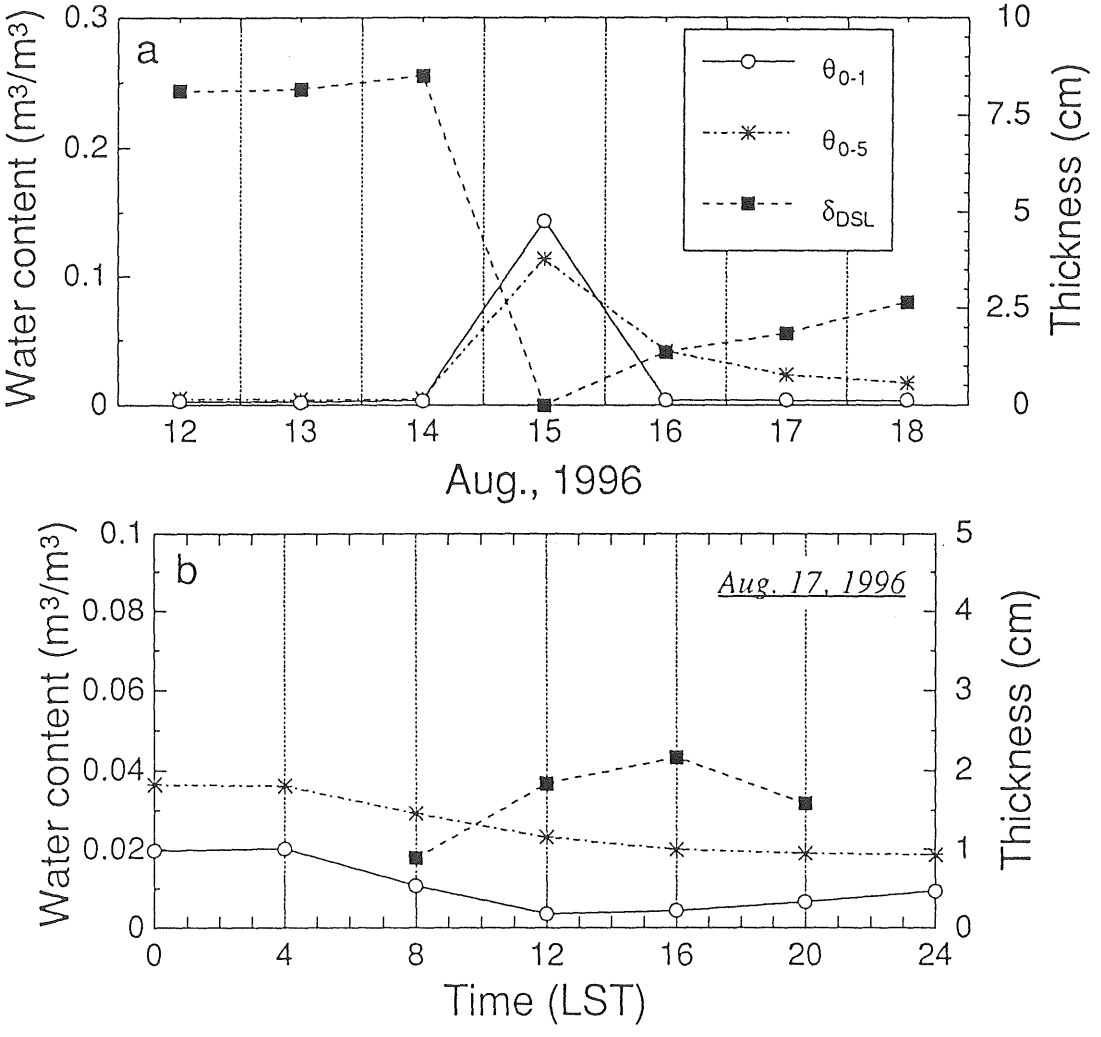

Figure 18 Temporal variations of the surface water content and the thickness of the DSL (δ_{DSL}) for the sand dune site; (a) inter-diurnal variation, and (b) diurnal variation. $\theta_{0\text{-}1}$ and $\theta_{0\text{-}5}$ denote water content of the surface soil layers of 1 cm and 5 cm, respectively.

for the period just after the rainfall.

Figure 19 shows (a) the inter-diurnal evolution of the diurnal course of surface albedo and (b) the relationship between surface albedo and volumetric water content of surface soil of 1-cm or 5-cm thickness both obtained at noon. Inter-diurnal increase in surface albedo accompanied the decrease in surface water content (Figure 19b), in a similar way at the fallow site. However, unlike the case of the fallow site the surface albedo abruptly changed at very low water content (< 0.5 %) in relation between albedo and θ_{0-1}, and gradually changed in relation between albedo and θ_{0-5}. Although the diurnal variation due to the changes in solar zenith angle and in surface moisture can be seen in Figure 19a, the effect of the zenith angle appears to be slightly larger than that for the fallow site.

The diurnal range of soil temperature at 1 cm depth reached to 32.4 °C (see Figure 17-1b). In contrast, soil temperature at 0.5 m depth hardly varied diurnally and inter-diurnally as was found in the fallow site. Temperature gradient at the shallower zone reached to 4.5 °C/cm at the maximum.

The diurnal variation in wind velocity, which is similar to that at the fallow site, can be seen in Figure 17-1c, particularly on days after the rainfall .

The variations in air temperature, relative humidity, and specific humidity were similar to those at the fallow site (see Figures 13-2 and 17-2). However, the nighttime values of relative humidity on the days before the rainfall were considerably smaller than unity while those at the fallow site were almost unity throughout the observation period. This may be due to the severe dry conditions of the soil at the sand dune site in the period or to the smaller effect of advection from the surrounding area because of the large extent of the sand dune. Diurnal range of air temperature at 0.27 m height was 8.3 °C at the maximum, which is smaller than that at the fallow site.

While θ_{0-5} gradually decreased after the rainfall on Aug. 14-15, θ_{0-1} rapidly decreased to very low level (< 0.5 %) and then maintained almost constant value (Figure 18a). The thickness of the DSL was quite large (approximately 8 cm) during three days before the

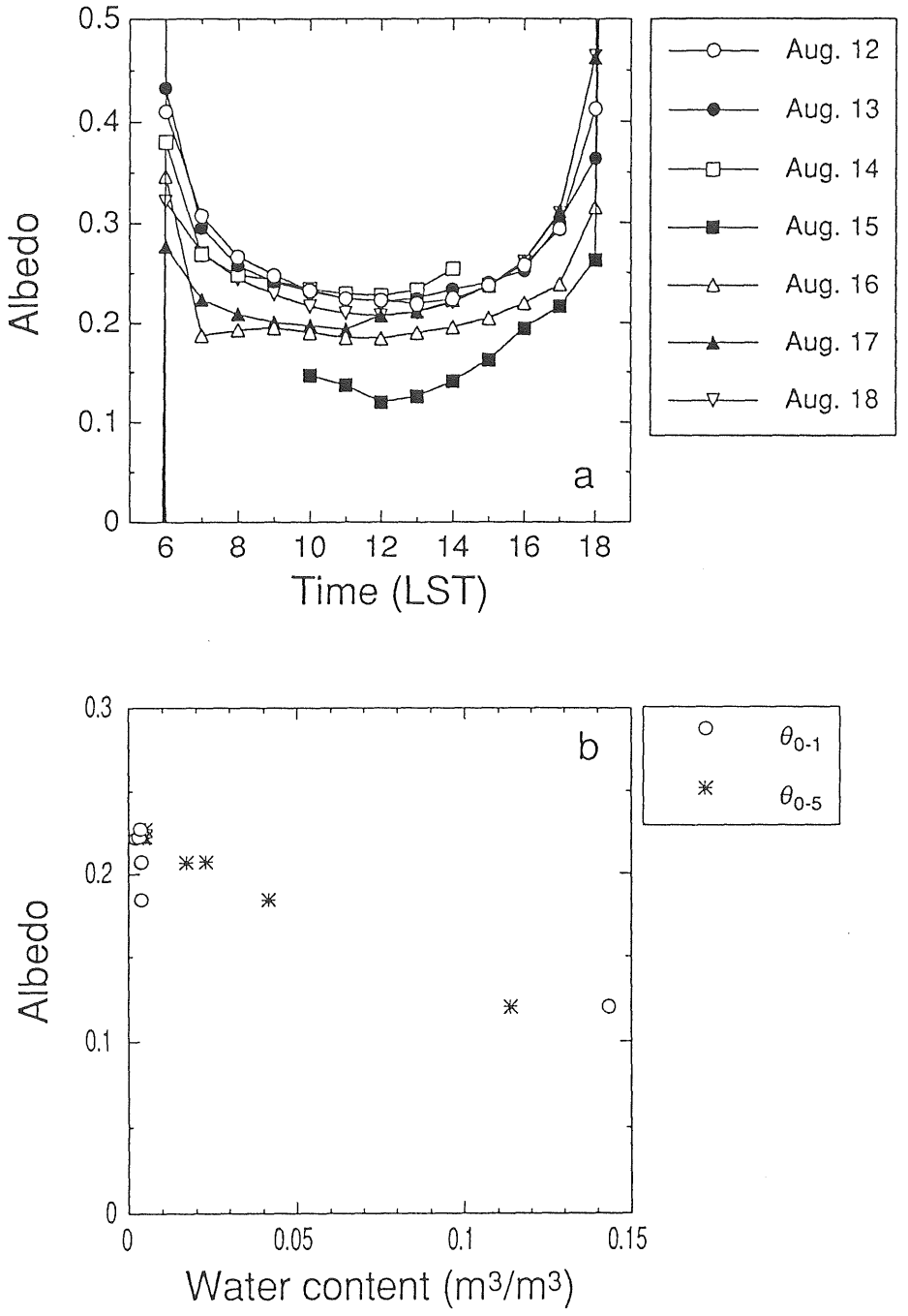

Figure 19 Results of albedo measurements for the sand dune site; (a) diurnal and inter-diurnal variation of the surface albedo, and (b) relationship between the surface albedo and the surface water content.

rainfall. Then the DSL disappeared with the onset of the rainfall and gradually redeveloped after the rainfall. The diurnal variation of water content could be seen in both θ_{0-1} and θ_{0-5} (Figure 18b). However the diurnal range was smaller in θ_{0-1} (1.57 %) than in θ_{0-5} (2.24 %), contrary to the case found at the fallow site. Diurnal range of the thickness of the DSL was 1.27 cm (although it was not possible to determine the thickness in the nighttime because of an unclear bottom boundary of the DSL).

Figure 20a shows the three-phase distribution of the soil. The figure indicates that the volumetric solid content is almost constant throughout the whole soil layer from the soil surface to the 50 cm depth. Soil water content was fairly small, and gradually decreases toward shallower depth. Nevertheless an inflection of water content profile can be seen at around 8 cm depth. Figure 20b indicates an agreement between the depth of the inflection point and the depth of the bottom boundary of the DSL. The water content of the bottom boundary of the DSL was between 1.0 and 1.8 %.

5.3 Playa site

Results of micrometeorological measurements at the playa site are shown in Figure 21. Figure 22 shows (a) the inter-diurnal variations in surface water content and the thickness of the DSL, and (b) the diurnal variation patterns of those.

Soil moisture conditions were also extremely dry in the observation period at the playa site. As seen in the variation of downward short-wave radiation, it was cloudy day on Mar. 11 while it was almost fine on the previous two days (Figure 21-1a).

Figure 23 shows (a) the inter-diurnal evolution of the diurnal course of surface albedo and (b) the relationship between surface albedo and volumetric water content of surface soil of 1-cm or 5-cm thickness obtained at noon. While significant inter-diurnal variation in surface albedo can not be seen since there were no change in soil moisture conditions, diurnal variation in surface albedo due to change in solar zenith angle exists (Figure 23a).

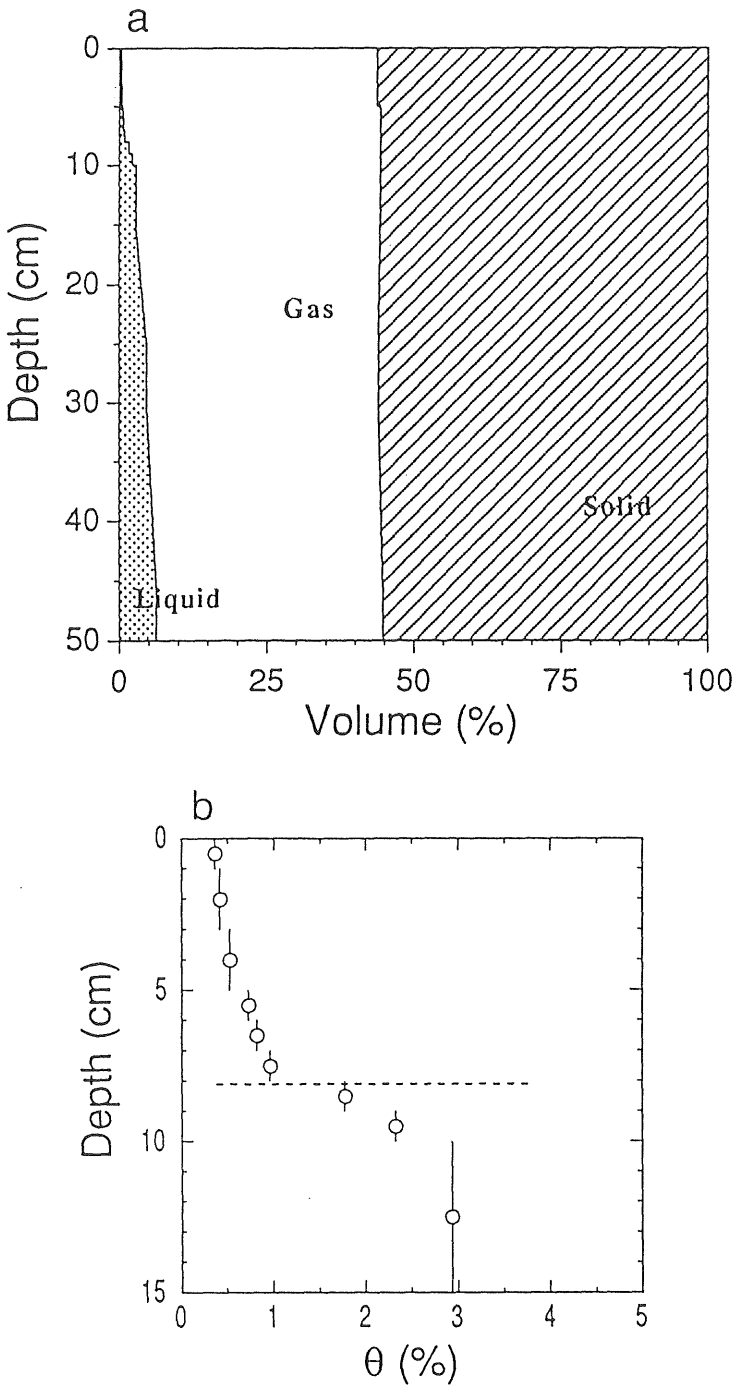

Figure 20 Soil hydrological characteristics for the sand dune site; (a) three phase distribution of the soil, and (b) water content profile. Vertical bars indicate the thickness of sampled soil cores. Dashed line in the bottom figure denotes the depth of the bottom boundary of the DSL.

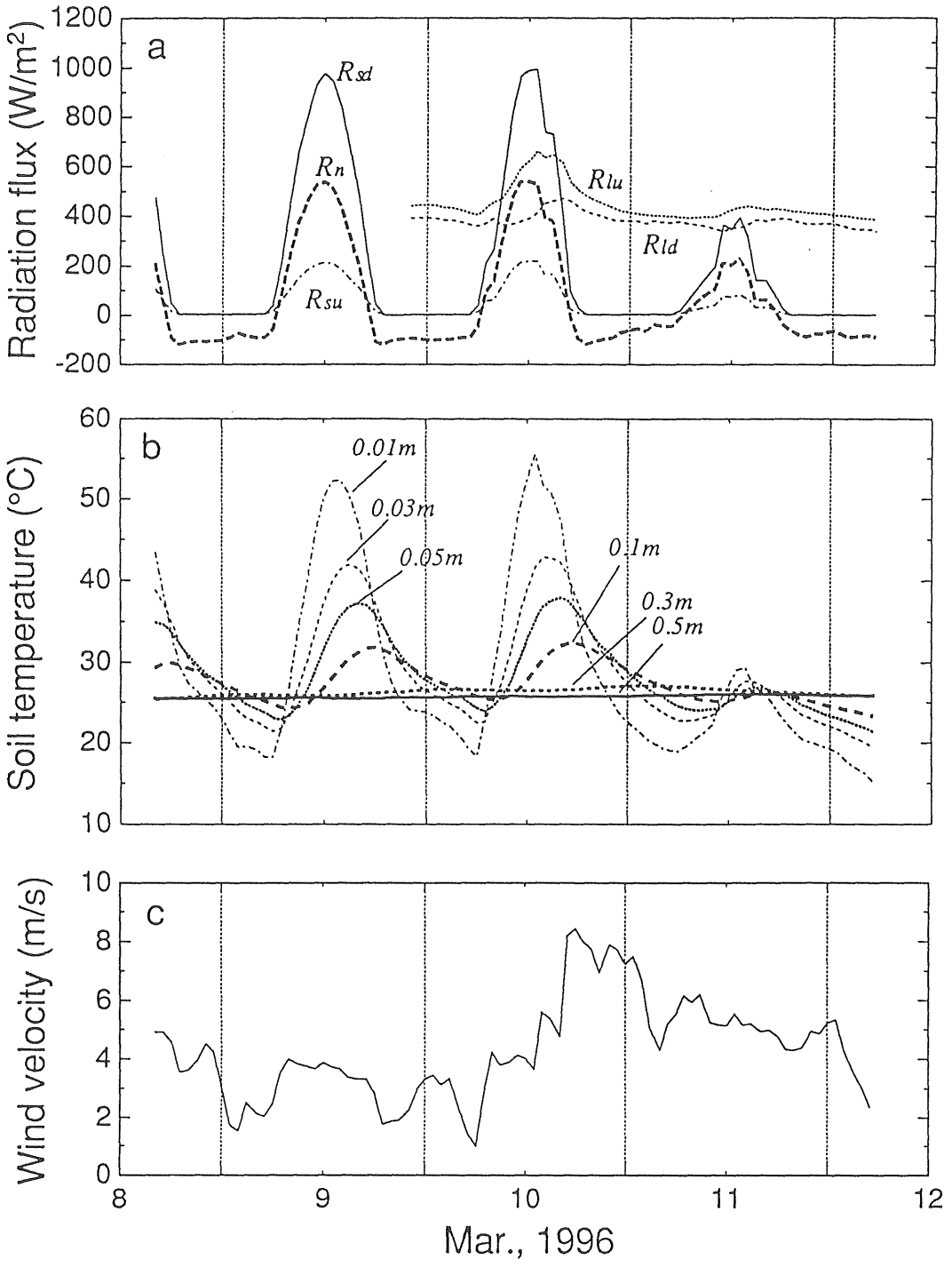

Figure 21-1 Observation results of micrometeorological elements for the playa site; (a) radiation balance components (R_n, the net radiation; R_{sd}, the downward short-wave radiation; R_{su}, upward short-wave radiation; R_{ld} downward long-wave radiation; R_{lu}, upward long-wave radiation), (b) soil temperature at different depths, and (c) wind velocity at the height of 2.07 m.

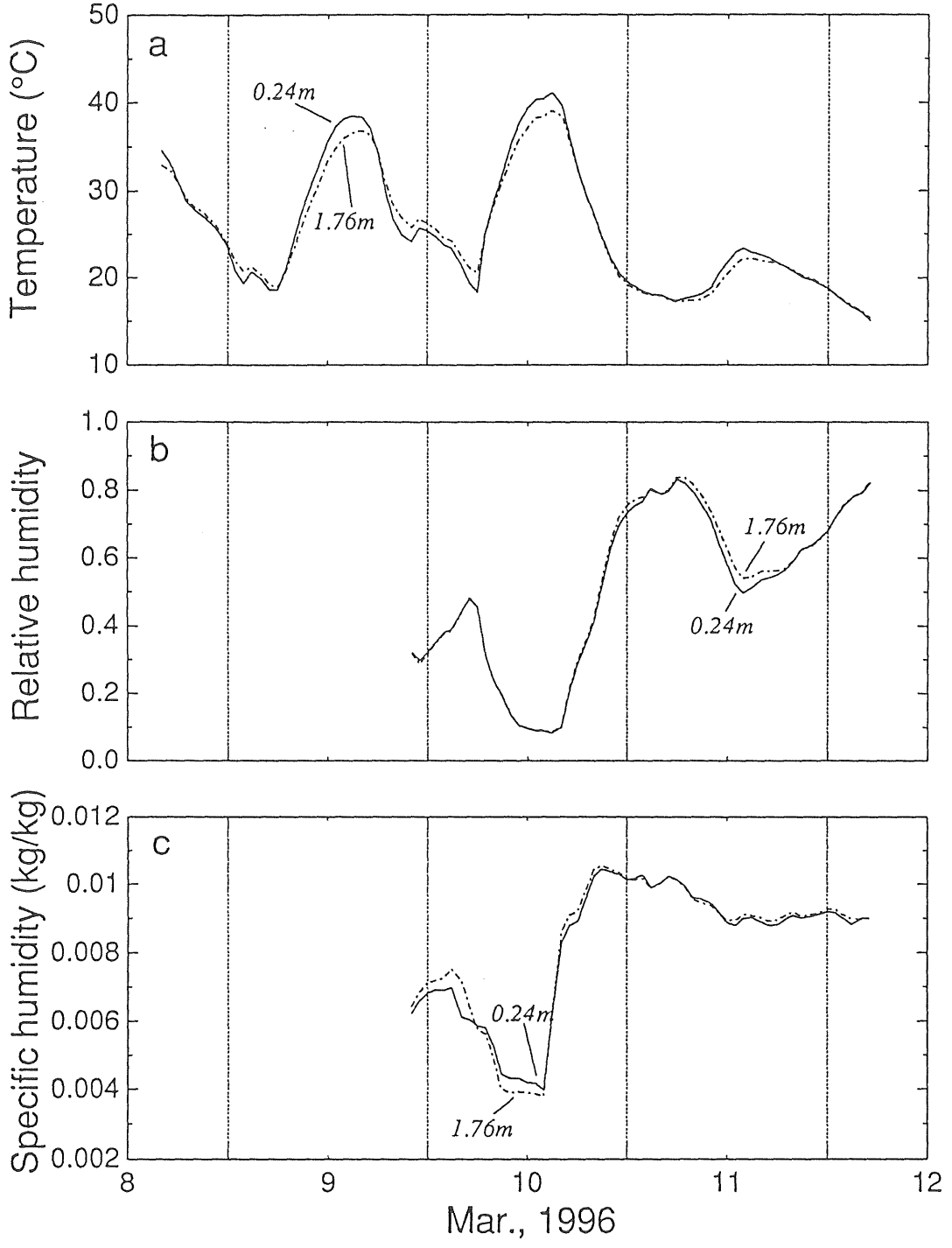

Figure 21-2 Observation results of micrometeorological elements for the playa site; (a) temperature, (b) relative humidity, and (c) specific humidity, at two levels (0.24 and 1.76 m) in the atmosphere. Soil surface temperature is added in the top column of the figure.

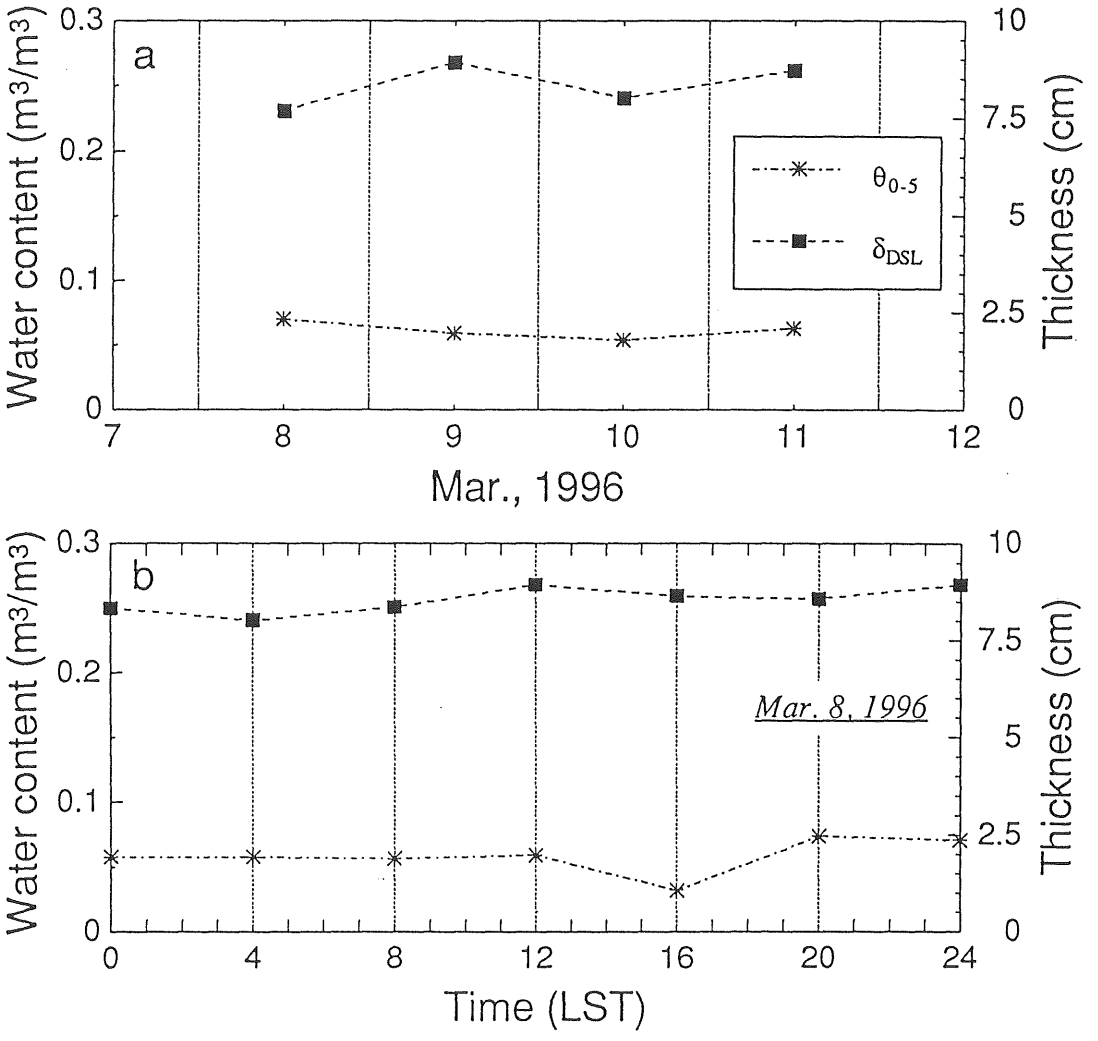

Figure 22 Temporal variations of the surface water content and the thickness of the DSL (δ_{DSL}) for the playa site; (a) inter-diurnal variation, and (b) diurnal variation. $\theta_{0\text{-}5}$ denote water content of the surface soil layers of 5 cm.

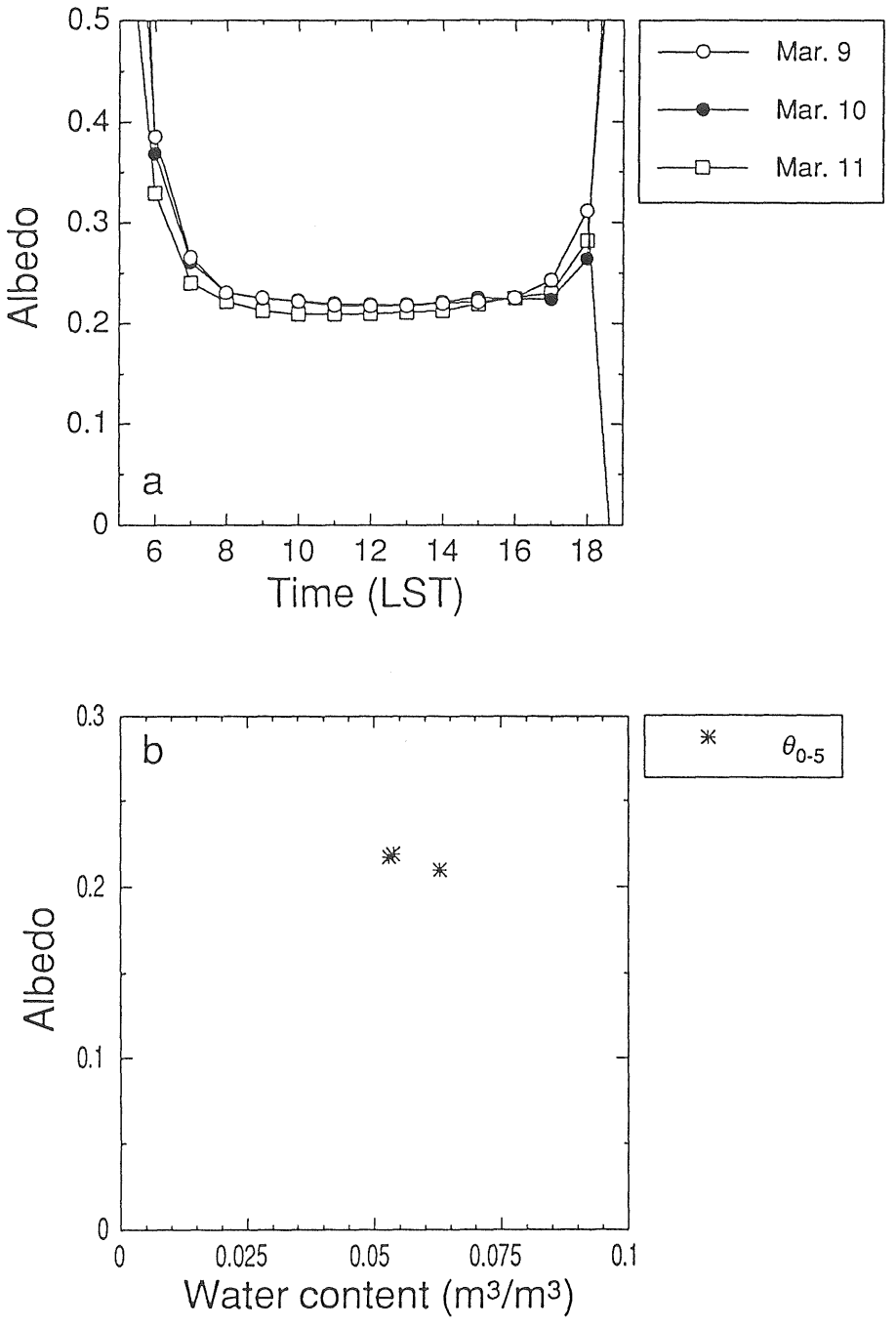

Figure 23 Results of albedo measurements for the playa site; (a) diurnal and inter-diurnal variation of the surface albedo, and (b) relationship between the surface albedo and the surface water content.

The value of surface albedo at noon was larger than that under dry soil condition at the fallow site, and was almost equal to that at the sand dune site.

The diurnal range of soil temperature at 1 cm depth reached to 37.2 °C (see Figure 21-1b), which is larger than that at the other two sites. In contrast, soil temperature at 0.3 and 0.5 m depth hardly varied diurnally and inter-diurnally. Therefore, it can be said that the dumping depth [Sellers, 1965, p. 136] for the playa site is smaller than that for the fallow site and the sand dune site. Temperature gradient at the shallower zone reached to 7.0 °C/cm at the maximum.

The diurnal variation in wind velocity can be seen on Mar. 9, while it is not clear on next two days due to the effect of passing of cyclone low (Figure 21-1c).

Diurnal range of air temperature at the height of 1.76 m reached to 18.6 °C, which is much larger than that for the other two sites. The nighttime values of relative humidity on Mar. 9-10 were considerably smaller than unity as well as that found in the earlier period at the sand dune site. An abrupt increase in relative humidity at the night on Mar. 10 is probably due to the effect of cyclone low. Noticeable is that the values of specific humidity is considerably smaller than those for the other two sites. (Note that the scale of vertical axis of Figure 21-2c differs from that of Figures 13-2c and 17-2c.) The reason for this may be that the playa site is located far from the ocean. Small values of R_{ld} (Figure 21-1a) relative to that at the other sites may be due to this low vapor content of the atmosphere.

In Figure 22a, significant inter-diurnal variations can not be seen in both θ_{0-5} and the thickness of the DSL because of no antecedent rainfall. The thickness of the DSL was quite large (approximately 8 cm). The diurnal variations were also not significant in both θ_{0-5} and the thickness of the DSL on Mar. 9. At the playa site, irregular rather than regular inter-diurnal and diurnal variations in water content are observed. The reason for this may be high spatial variability of soil moisture (see Section 4.2.2).

Figure 24a shows the three-phase distribution of the soil. The figure indicates that the solid volume is smaller in shallower zone than in deeper zone. Soil water content in deeper

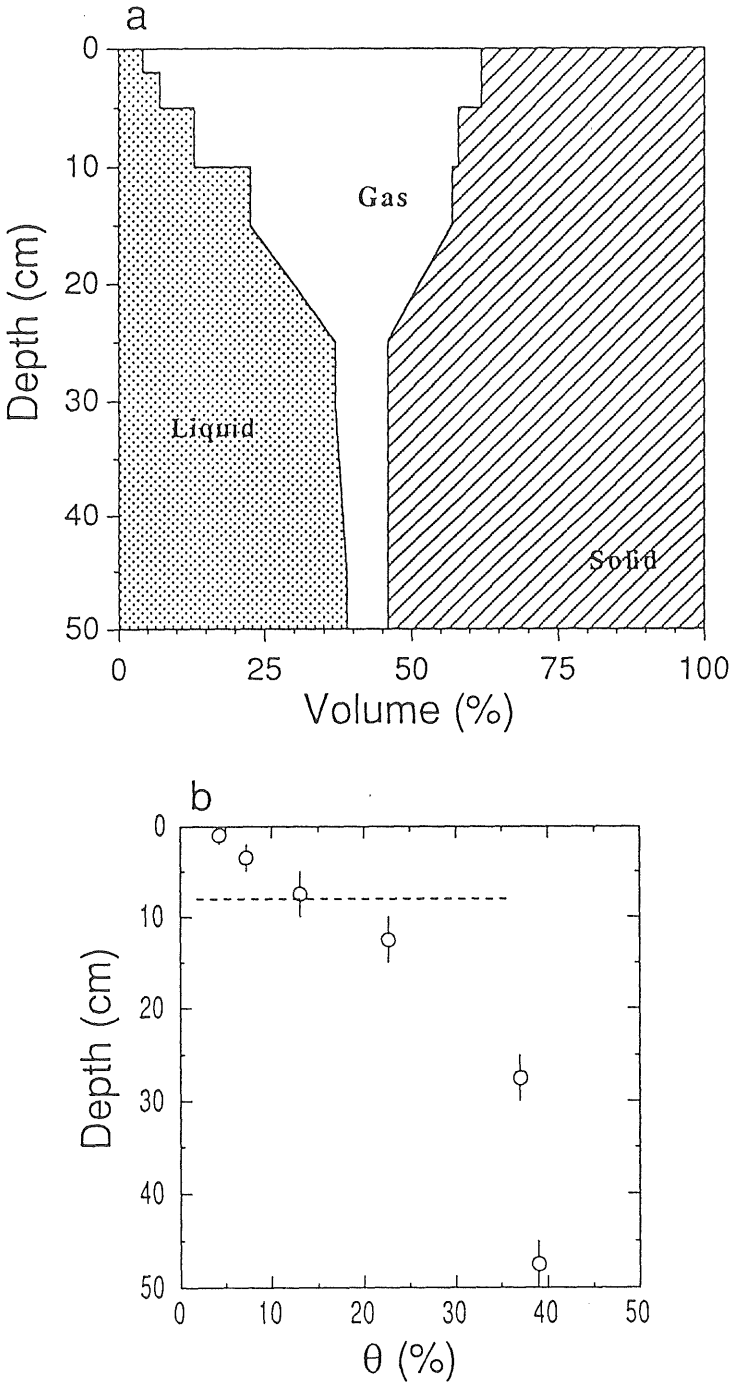

Figure 24 Soil hydrological characteristics for the playa site; (a) three phase distribution of the soil, and (b) water content profile. Vertical bars indicate the thickness of sampled soil cores. Dashed line in the bottom figure denotes the depth of the bottom boundary of the DSL.

zone is close to the saturation value, and gradually decreases toward shallower depth.

Figure 24b shows the water content profile and the position of the bottom boundary of the DSL. In the figure, there is no significant inflection in water content profile at around the bottom boundary of the DSL, and water content within the DSL is not constant and largely decreases toward the surface. The water content of the bottom boundary of the DSL was approximately 13 %.

Figure 25 shows vertical profiles of (a) electric conductivity of sample waters which were prepared by adding 100 g distilled water to 20 g moist sample soil, (b) cation and anion concentrations per unit volume of soil. The figures clearly indicates a salt accumulation at the shallow depth, and that the specie of the salt is mainly NaCl. As mentioned in Section 4.2.5, concentrations in Figure 25 represent not the concentrations of ions in soil water but the total concentrations in the solid and vapor phase within the soil. Based on the solubility of NaCl, it would be reasonable to assume that the soil water is in saturation conditions in the zone shallower than the depth of 5 cm.

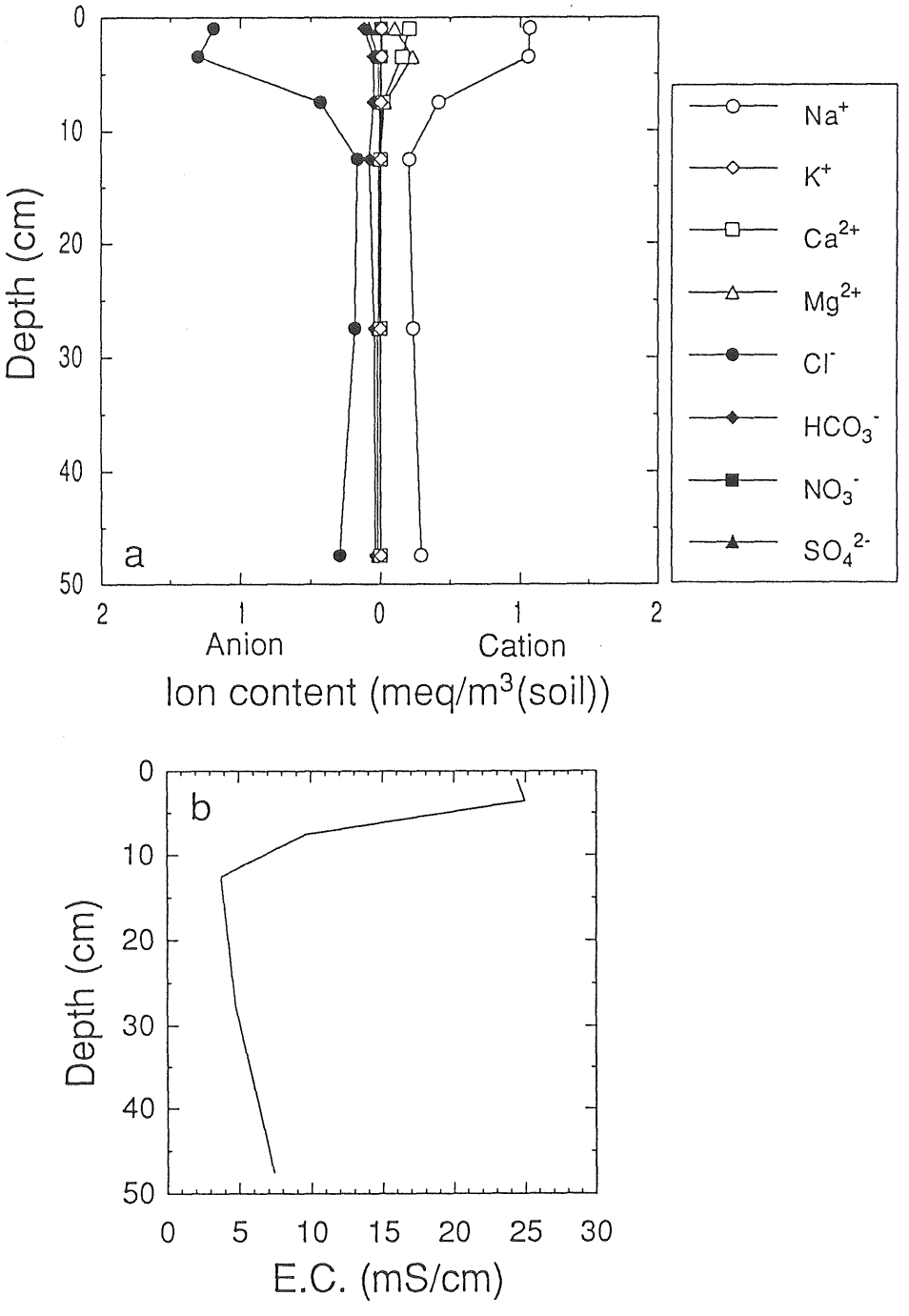

Figure 25 Vertical profiles of (a) ion content in the soil, and (b) electric conductivity (E.C.) of the sample water for the playa site.

Chapter 6

Surface energy balance and the restriction of evaporation

6.1 Determination of surface energy balance and surface resistance

6.1.1 Energy balance components

Energy balance components were determined based on hourly averaged data. Net radiation (R_n) was directly determined by outputs from radiometer. Soil heat flux (G) was determined by combination of heat flux plate measurement and calorimetry of soil between the soil surface and the plate. Briefly, G was determined by the following equation:

$$G = G_{plate} + S_{s-p}, \tag{6.1}$$

where G_{plate} is the outputs from heat flux plate (installed at the depth of 10 cm in the present study), and S_{s-p} the change rate of heat storage in soil layer between the soil surface and the plate. The values of S_{s-p} were determined on the basis of the temporal change in soil temperatures measured at five depths (i.e., 0, 1, 3, 5, and 10 cm) and the

heat capacity of the soil. In the procedure of calculating the soil heat capacity, variation in soil water content was considered using measured water content of surface soil of 5-cm thickness. This method allows the soil heat flux to be evaluated correctly when evaporation takes place above the heat flux plate.

Sensible (H) and latent (LE) heat fluxes were determined by Bowen ratio /energy balance method, as follows:

$$H = \frac{Bo}{1+Bo}(R_n - G) \tag{6.2}$$

$$LE = \frac{1}{1+Bo}(Rn - G) \tag{6.3}$$

$$Bo = \frac{c_p(T_2 - T_1)}{l(q_2 - q_1)} \tag{6.4}$$

where Bo is the Bowen ratio, c_p the specific feat of the air, l the latent heat for vaporization, and subscripts 1 and 2 denote the two measurement heights of temperature (T) and specific humidity (q).

In order to check the validity of flux determination, H and LE were also evaluated by the profile method [e.g., Brutsaert, 1982, pp. 197-198]. Comparisons between fluxes evaluated by the Bowen ratio /energy balance method and by the profile method showed sufficient accuracy of the flux determination (Table 11).

For the playa site, since humidity measurements were not available in some cases due to an accident of instruments, H was determined by profile method and LE was evaluated as the residual of surface energy balance during that period.

6.1.2 Surface resistance

Surface resistance (r_s) has been used as a parameter representing the effect of soil drying on the restriction of evaporation (see Section 2.3.1 (A3)). Although there is slight inconsistency in its definition [van de Griend and Owe, 1994, Yamanaka et al., 1997], it is meaningful to investigate its behavior for evaluating the effect of soil drying on the

Table 11 Statistics for the comparison between fluxes derived by the Bowen ratio /energy balance method (F_b) and those determined by the profile method (F_p).

	Regression constants for $F_p = aF_b + b$		Correlation coefficient	MAD $\langle \mid F_p - F_b \mid \rangle$	RMSD $\sqrt{\langle (F_p - F_b)^2 \rangle}$
	a	b	r	(W/m^2)	(W/m^2)
Fallow					
H	0.815	17.880	0.917	23.0	37.3
LE	1.072	21.922	0.859	44.7	65.6
Sand dune					
H	0.789	8.847	0.917	23.4	44.3
LE	0.959	17.439	0.786	36.9	56.9
Playa					
H	0.768	-2.010	0.962	18.4	30.1
LE	0.774	-5.415	0.837	12.0	20.7

MAD: mean absolute difference, RMSD: root mean square difference

restriction of evaporation.

Surface resistance is usually used in the form of Equation (2.12). Solving the equation for r_s gives the following equation:

$$r_s = \frac{\rho(q_{sat}(T_s) - h_a q_{sat}(T_a))}{E} + r_{av}, \tag{6.5}$$

where ρ is the density of the air, $q_{sat}()$ the saturation specific humidity, T_s the surface temperature, T_a the air temperature, h_a the relative humidity of the air, and r_{av} is the aerodynamic resistance to vapor transfer in the atmosphere. If one obtains measured values of T_s, T_a, h_a, E and r_{av}, surface resistance can be evaluated by Equation (6.5).

According to Monin-Obukhov similarity theory [e.g., Brutsaert, 1982], the aerodynamic resistance r_{av} in the atmospheric surface layer (ASL) is given as

$$r_{av} = \frac{1}{a_v k u_*}[\ln(\frac{z_a - d_0}{z_{0v}}) - \Psi_{sv}(\zeta)], \tag{6.6}$$

in which the friction velocity u_* is defined as

$$u_* = \frac{ku}{\ln(\frac{z_a - d_0}{z_{0m}}) - \Psi_{sm}(\zeta)}. \tag{6.7}$$

In the above, a_v $(= 1.0)$ is the ratio of the eddy diffusivity for water vapor to the eddy viscosity under neutral conditions, k $(= 0.4)$ the von Kármán's constant, z_a the height of the measurement of specific humidity and wind velocity in the ASL, and u is the wind velocity at the height of z_a. In addition, d_0 is the zero-plane displacement height ($d_0 = 0$, for bare soil), z_{0v} the water vapor roughness length, z_{0m} the momentum roughness length, $\Psi_{sv}(\zeta)$ the stability correction function for water vapor transfer, and $\Psi_{sm}(\zeta)$ the stability correction function for momentum transfer. Although there are many stability correction functions, the most common type [e.g., Brutsaert, 1982, pp. 68-71] is adopted in the present study.

The roughness lengths for vapor and momentum transfer are usually determined based on flow properties (e.g., friction velocity u_* and kinematic viscosity ν) and surface properties

(e.g. surface roughness length z_0). It is assumed that the parameters z_{0v} and z_{0m} are functions of the roughness Reynolds number z_{0+} ($\equiv u_* z_0/\nu$) as follows [for z_{0v} , Brutsaert, 1975; Brutsaert and Chan, 1978; for z_{0m}, Brutsaert, 1982; Hiyama et al., 1995]:

- for a rough regime ($z_{0+} > 2$)

$$z_{0v} = 7.4 z_0 \exp(-7.3 k a_v z_{0+}^{1/4} Sc^{1/2}) \tag{6.8}$$

and

$$z_{0m} = z_0 \tag{6.9}$$

- for a smooth regime ($z_{0+} < 0.13$)

$$z_{0v} = (30\nu/u_*) \exp(-13.6 k a_v Sc^{2/3}) \tag{6.10}$$

and

$$z_{0m} = 0.135\nu/u_* \tag{6.11}$$

- for a transitional regime ($0.13 \leq z_{0+} \leq 2$)

$$z_{0v} = \beta_0 z_{0v,r} + (1 - \beta_0) z_{0v,s} \tag{6.12}$$

and

$$\begin{aligned} z_{0m} &= z_0(0.799 + 0.224A - 2.06 \times 10^{-3} A^2 \\ &\quad - 4.90 \times 10^{-2} A^3 + 9.56 \times 10^{-3} A^4), \end{aligned} \tag{6.13}$$

where Sc ($\equiv \nu/D_{av}$) is the Schmidt number (= 0.595 in the lower atmosphere), D_{av} the molecular diffusivity of water vapor in the air, $z_{0v,r}$ and $z_{0v,s}$ are the values obtained by Equations (6.8) and (6.10), respectively, β_0 (= $(u_*/100 - 2)/18$) is a weighting factor, and $A = \ln(z_{0+})$.

Wind profiles under neutral atmospheric stability conditions (in the present study, $|R_i| < 0.05$; R_i is the Richardson number) allow to determine the values of z_{0m} and u_*. Values

of z_0 were determined from these z_{0m} and u_* values by an iteration procedure with above equations (see Sugita et al. [1995] for detailed procedure) for each observation sites. Statistics of z_0 evaluated at three sites is given in Table 12. In the present study, log-mean value was adopted since the frequency distribution of z_0 was not normal distribution and median of z_0 approximated to the log-mean value rather than arithmetic mean value.

6.2 Variations of surface energy balance during soil drying

Temporal variations in energy balance components at the three observation sites are shown in Figure 26. The figure for the fallow site clearly indicates inter-diurnal decrease in LE and increase in H during soil drying. The changes in these fluxes seem to accompany the decrease in soil water content or development of the DSL (see Figure 14). Nevertheless, G does not appear to be affected by soil drying. The inter-diurnal constancy of the amplitude of G may be due to the cancellation of the effect of decrease in thermal inertia of soil on G by the effect of increase in amplitude of soil surface temperature (see Section 2.2). Inter-diurnal variations in LE and H as seen at the fallow site are also illustrated in the figure for the sand dune site. Although similar variations are not clear at the playa site, the figure for the playa site may illustrates a variation in later stage of soil drying.

Noticeable is that the figures indicate a change in the diurnal variation pattern of fluxes as well as the inter-diurnal change in the peak value or the amplitude of those. As a typical example, the diurnal variation patterns of surface energy balance at the fallow site under wet and dry soil conditions are shown in Figure 27. The figure for the wet soil condition indicates that both LE and H vary keeping pace with the variation in R_n. On the other hand, for the dry condition the peak of LE shifts to earlier time and that of H moves to later time nevertheless the peak of R_n is positioned in the noon.

Table 12 Statistics of surface roughness length (z_0) evaluated at three observation sites.

Observation site	Mean (S.D.)	Median	Log-Mean
Fallow	6.99×10^{-3} (4.40×10^{-3})	6.22×10^{-3}	5.44×10^{-3}
Sand dune	1.65×10^{-4} (1.75×10^{-3})	1.15×10^{-4}	1.18×10^{-4}
Playa	1.51×10^{-4} (1.89×10^{-3})	9.59×10^{-5}	9.75×10^{-5}

(Unit: m)

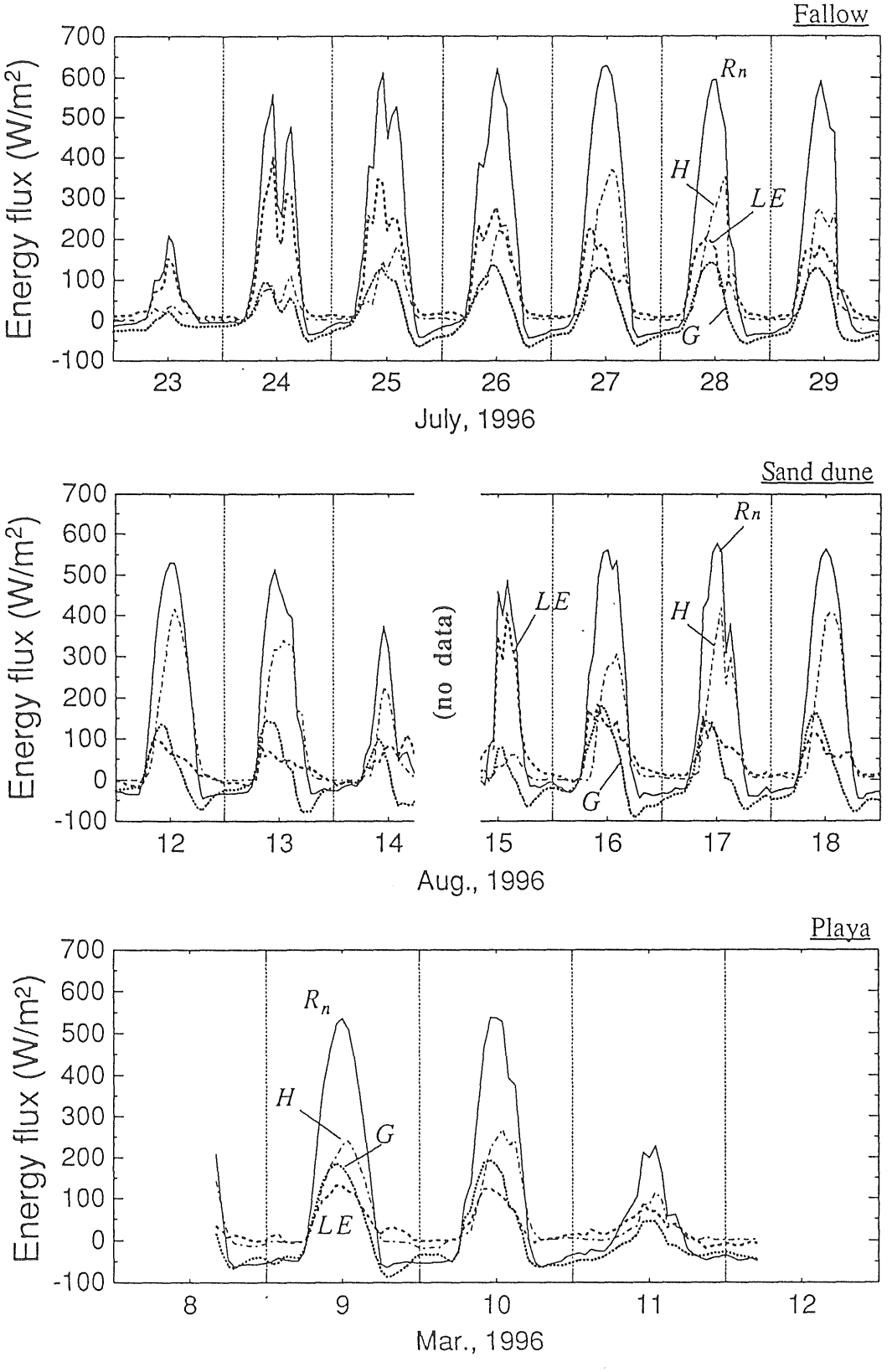

Figure 26 Temporal variations of surface energy balance components (R_n, the net radiation; LE, the latent heat flux; H, the sensible heat flux; G, the soil heat flux) for the three sites.

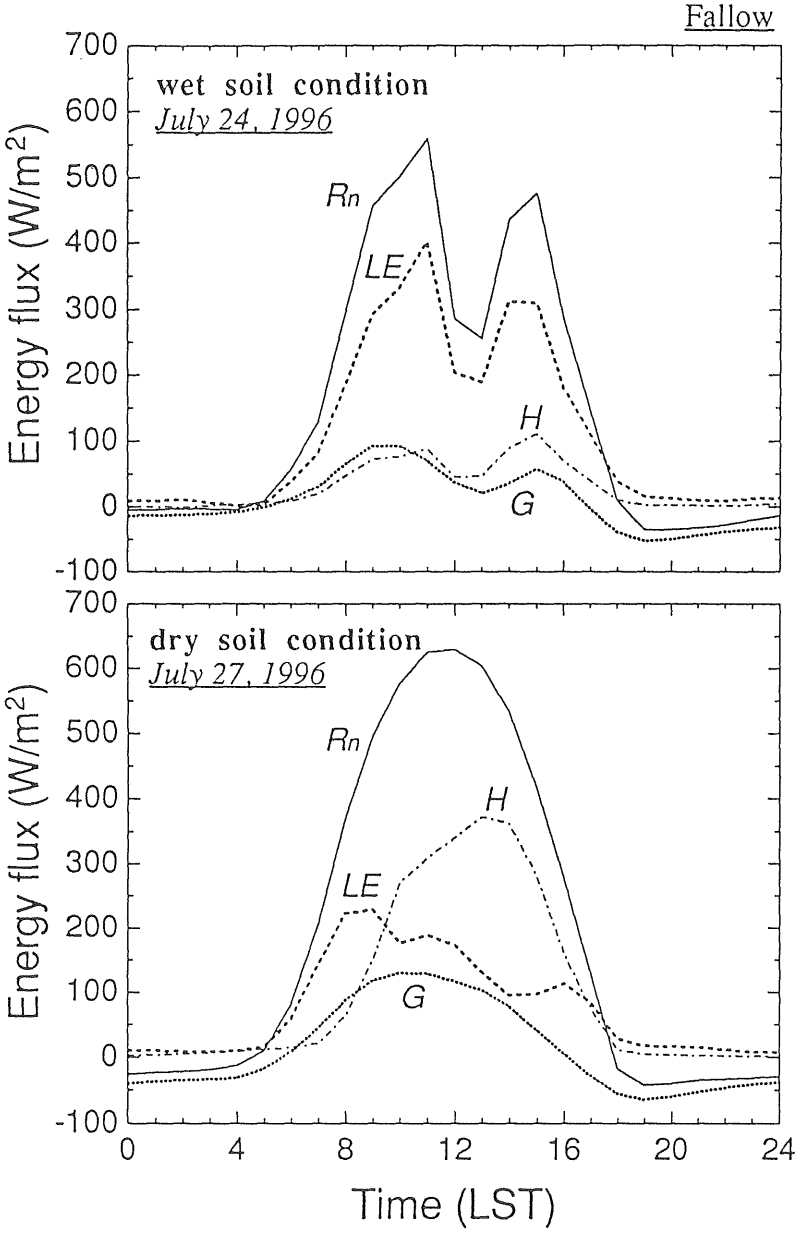

Figure 27 An example of the diurnal variation patterns of energy balance components under wet and dry soil conditions (fallow site).

In order to examine more quantitatively the pattern shift of diurnal variations in LE and H, Bowen ratios in the forenoon and in the afternoon will be compared. Figure 28 shows the inter-diurnal variations in the forenoon-averaged Bowen ratio (Bo_{fore}) and the afternoon-averaged Bowen ratio (Bo_{after}) for the three observation sites. For convenience' sake, Bo_{fore} was evaluated based on the data from 7 to 12 LST and $Bo_{after}$was evaluated based on the data from 12 to 17 LST in the present analysis. The figure indicates a tendency of increase in both Bo_{fore} and Bo_{after} during soil drying although there are some fluctuations probably due to the variation of atmospheric conditions. The increase in Bo_{fore} is, however, not as large as that in Bo_{after}. This indicates that the effect of soil drying on surface energy partitioning is smaller in the forenoon than in the afternoon.

Figure 29 shows the relationship between Bo_{after} and Bo_{fore} for the three observation sites. The figure indicates an almost linear relationship for each site, and that the ratio Bo_{after}/Bo_{fore} is the largest at the sand dune site and is the smallest at the playa site. Thus, it can be said that the pattern shift of diurnal variations in LE and H depends on the soil type, although there may be some effects of atmospheric conditions on the pattern shift.

6.3 Diurnal variation of surface resistance

Many studies concerning surface energy balance at vegetation covers have reported that the soil drying can not affect the diurnal variation in energy partitioning of available energy into latent and sensible heat fluxes, while it can affect the inter-diurnal variation in those fluxes [Shuttleworth et al, 1989; Gurney and Hsu, 1990; Sugita and Brutsaert, 1991; Nichols and Cuenca, 1993; Hiyama et al, 1995; Brutsaert and Chen, 1996]. However, the temporal variation of surface energy balance at bare soil surfaces, which was mentioned in previous section, suggests that the soil drying can affect the energy partitioning not only in inter-diurnal time scale but also in diurnal scale.

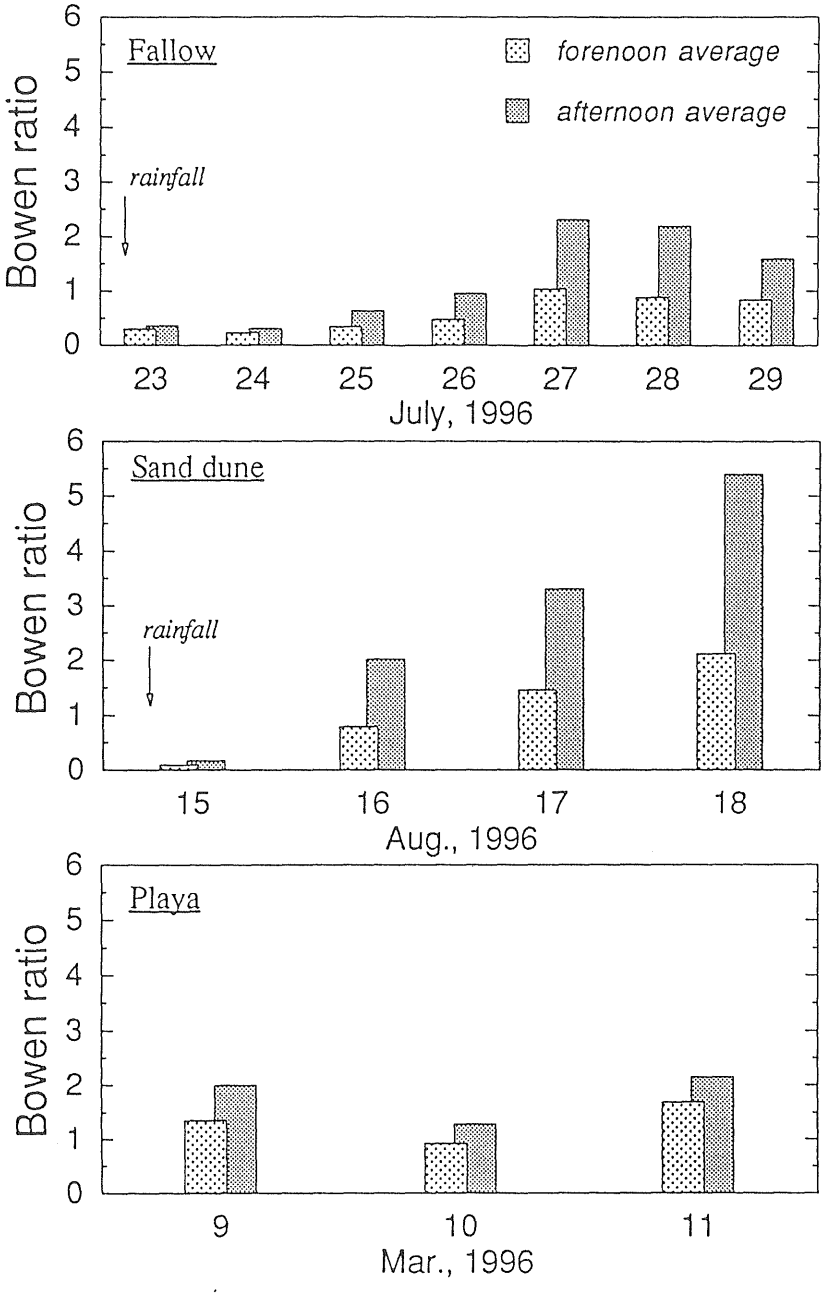

Figure 28 Inter-diurnal variations of forenoon-averaged and afternoon-averaged Bowen ratios (Bo_{fore} and Bo_{after}) for the three sites.

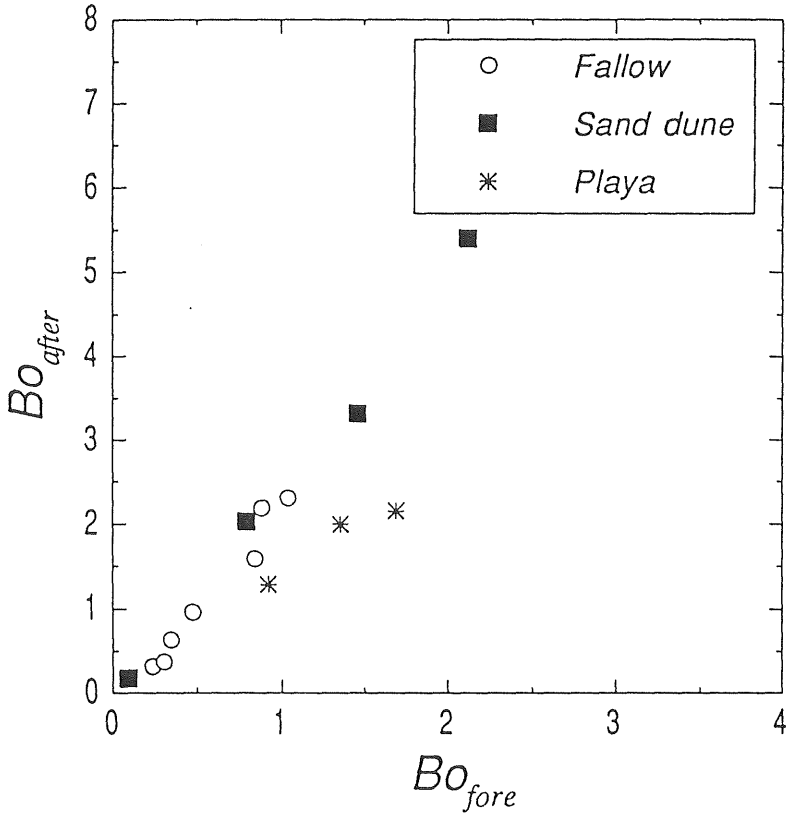

Figure 29 Relationships between forenoon-averaged and afternoon-averaged Bowen ratios for the three sites.

Figure 30 shows an example of temporal variations in actual and potential rates of evaporation. In the figure, an important point is that the difference between actual and potential rates of evaporation became remarkable from July 25. This means that the restriction of evaporation starts with the formation of the DSL (see Figure 14). Another important point in Figure 30 is that the actual rate of evaporation in the early forenoon is equal to the potential rate through the observation period. This suggests that there is no restriction of evaporation in the early forenoon even though the soil drying progresses.

Figure 31 shows diurnal variations in surface resistance for the three observation sites. The figure indicates that surface resistance is considerably small and its diurnal variation is not remarkable when the DSL disappears (July 23 for the fallow site, Aug. 15 for the sand dune site). Also, the figure clearly indicates that the values of surface resistance in the afternoon increase as the soil dries. Nevertheless, the values in the early morning are very small and less variable throughout the observation period at each site. At the playa site, the values of surface resistance in the early forenoon are relatively large and diurnal variation in surface resistance is smaller than that for the other sites. Variations in Bowen ratio and its dependency upon soil types mentioned in previous section could be introduced by these characteristics in diurnal behavior of surface resistance.

The diurnal variations of surface resistance were supposedly caused by the diurnal fluctuations of soil moisture conditions (i.e., drying during the daytime due to evaporation and succeeding rewetting during the nighttime due to water supply from deeper layers). Figures 14b and 18b indicate a high variability of surface soil moisture for the fallow and the sand dune sites, respectively, and Figure 22b indicates a low variability for the playa site.

Figure 32 indicates a complication in the relationship between surface resistance (r_s) and average water content of surface soil layer (θ). In the figure, two types of data are shown. The Noon data were collected at noon (LST) everyday through the observation period, and the IOD data were collected every 4 hours on an intensive observation day.

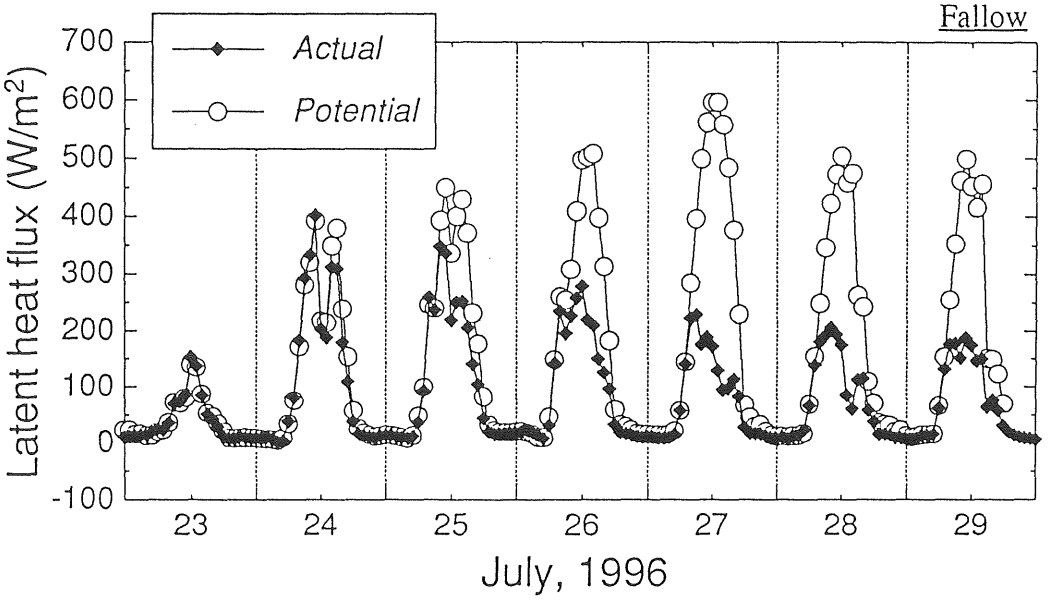

Figure 30 An example of the temporal variations in actual evaporation determined by Bowen ratio /energy balance method and potential evaporation derived by Penman equation (fallow site).

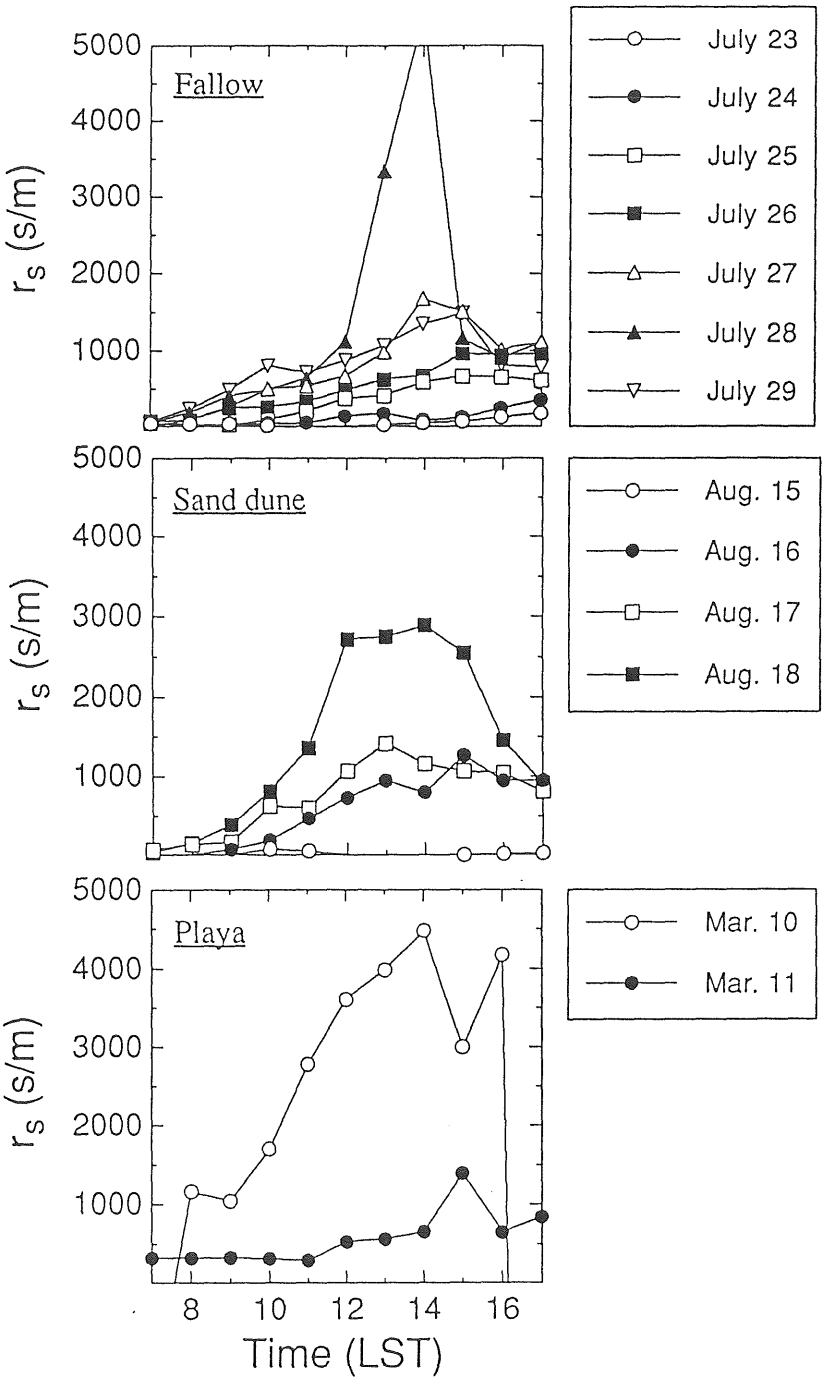

Figure 31 Diurnal and inter-diurnal variations in surface resistance (r_s) for the three sites.

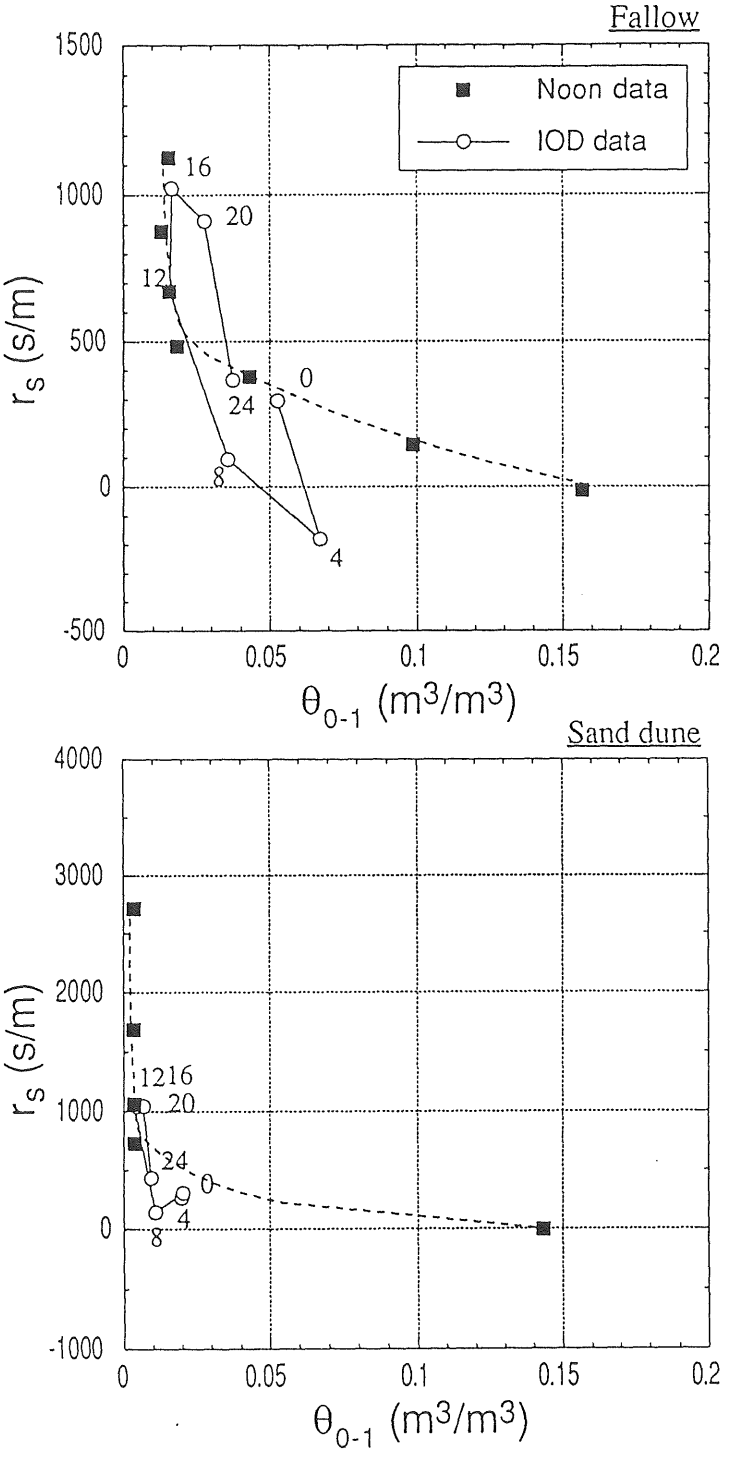

Figure 32 Relationship between surface resistance (r_s) and surface water content (θ_{0-1}) for the fallow and the sand dune sites.

For the noon data, the figure suggests that the surface resistance can be represented as a function of surface water content alone. However, it indicates clearly a hysteresis loop in the r_s-θ relationship for the IOD data. In other words, the relationship can change in the course of a day. While it should be noted that the accuracy of surface resistance determination during the nighttime is relatively low due to small magnitude of latent heat flux, the surface resistance at 08 LST of the IOD data when the accuracy problem is not an issue is significantly smaller than that expected from the noon data.

Similar hysteresis in the r_s-θ relationship was also found in the data of Camillo and Gurney [1986] and Daamen and Simmonds [1996]. Nevertheless, the surface resistance has been parameterized based on surface water content alone in many studies (see Table 2). For simulating diurnal variations in evaporation or surface energy balance accurately, diurnal behavior of surface resistance and its relation to water content should be investigated further.

6.4 Summary

Analyses of surface energy balance and surface resistance were carried out based on the micrometeorological field measurements. Results of the analyses are as follows:

(1) Soil drying affected surface energy balance, particularly in energy partitioning of available energy into latent heat and sensible heat fluxes, both in inter-diurnal and diurnal time scale. Soil drying induced a decrease in latent heat flux and an increase in sensible heat flux inter-diurnally, and also introduced a change in diurnal variation variation patterns of the fluxes.

(2) Surface resistance increased with the decrease in water content of surface soil layer. However, the relation of surface resistance to the surface water content differed between in inter-diurnal and diurnal time scales.

(3) The restriction of evaporation drying soil during began with the formation of the

DSL, and was enhanced with the DSL development.

Chapter 7

Transport and phase transition of surface soil moisture

7.1 Vertical profile of stable isotopic composition of soil water

Many works on the stable isotopic composition of water in the unsaturated zone have reported that the vertical profile of isotopic ratio has its peak at a short distance below the soil surface, and that the isotopic ratio decreases rapidly towards the surface in the zone above the peak point of the profile. Barnes and Allison [1983] presented an explanation that water moves upward by liquid phase in the zone below the peak point of the isotopic ratio profile and water is transported by vapor diffusion in the zone above the peak. If this is the case, vertical profile of isotopic compositions of soil water should allow classification of a soil profile into the liquid water transport region and the vapor transport region. This explanation was verified later by theoretical and semi-theoretical works (see Section 2.4.2). In addition, Shurbaji and Phillips [1995] indicated that the gradual change of upward water flux from liquid phase to vapor phase made the peak shape of isotope profiles gentle.

Figure 33 shows the vertical profiles of isotopic ratio and water content for the three observation sites. In the figure, position of the bottom boundary of the DSL, which was visually observed, is included as dashed lines. For the fallow and the sand dune sites, a sharp peak can be found at around the bottom boundary of the DSL in both δD and δ^{18}O profiles. This suggests that the form of the upward water flux abruptly changes from liquid phase to vapor phase at the bottom boundary of the DSL. In other words, the evaporation of soil water takes place at the bottom boundary of the DSL. The clear change in the vertical gradient of water content formed at the bottom boundary of the DSL also supports this idea.

On the other hand, the figure for the playa site indicates that the profiles of δD and δ^{18}O have a gentler peak, and that the region which has high δ-value tends to extend upward from the bottom boundary of the DSL. In addition, clear change in water content gradient at the bottom boundary of the DSL can not be seen in the profile. This suggests that the phase of water flux changes gradually, and that the liquid- and vapor-water transports coexist in the lower part of the DSL in the case of the playa site.

Figure 34 shows the δ-diagram presentations of the data shown in Figure 33. The figure indicates that the data points are almost plotted around two lines (except some data of deeper depths) for each observation site. One line is fitted to the data above the peak of the profile (i.e., in the vapor transport region; Line 1), and the other is to the data below the peak (i.e., in the liquid water transport region; Line 2). Such features also predicted by the theory of Barnes and Allison [1983] (see Appendix A). According to their theory, the difference in the slopes between the two lines reflects the difference in formation mechanisms of isotopic compositions of soil water, and a degree of the difference in the slopes depends on the isotopic compositions both of originated soil water (i.e., antecedent precipitation) and of atmospheric water vapor. The smaller δ values for the data in the vapor water transport region and the gentle slope of the Line 1 are not introduced by mixing of atmospheric water vapor into the DSL, but introduced by preferential isotopic exchange between liquid and

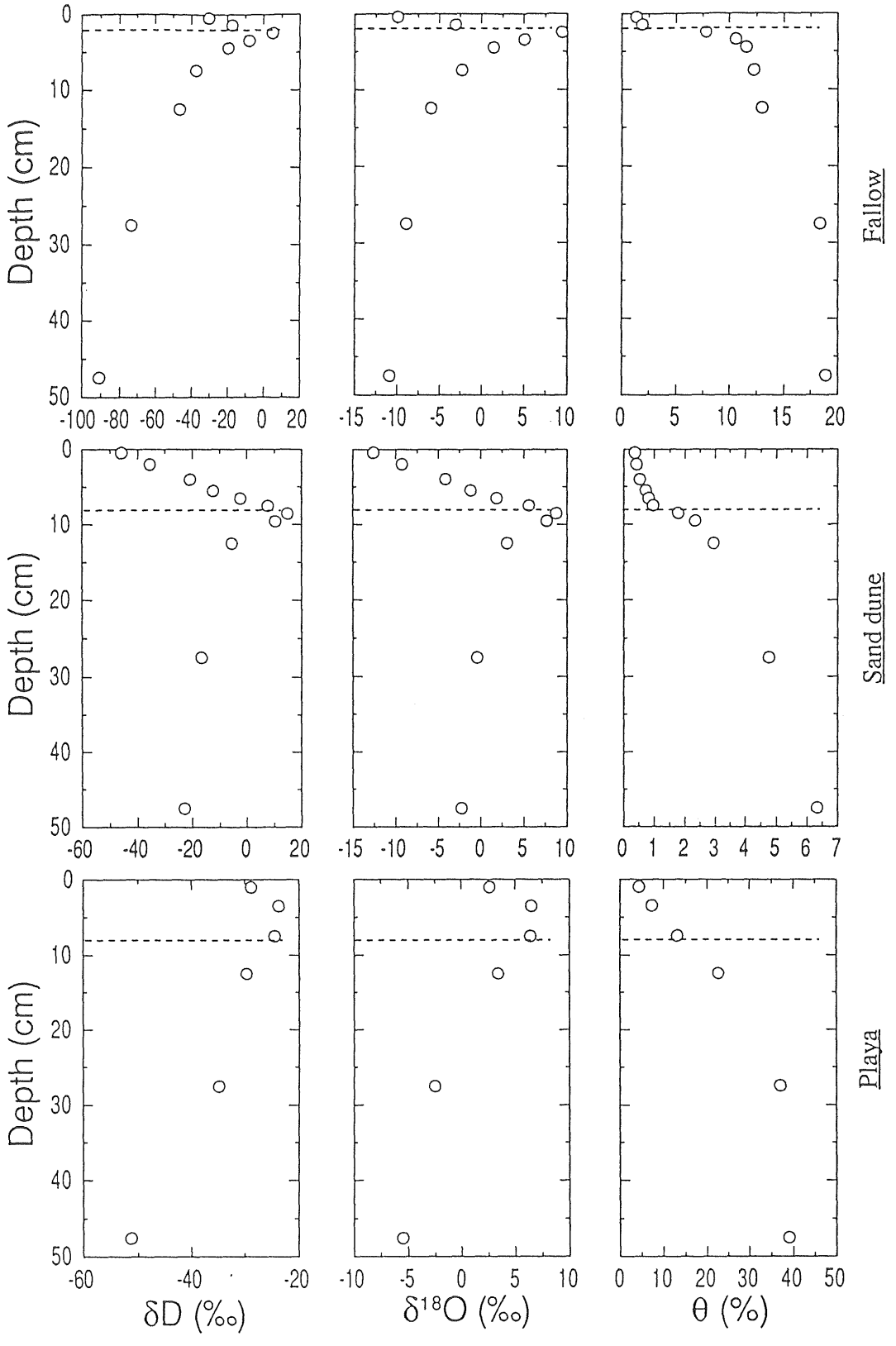

Figure 33 Vertical profiles of isotopic compositions (δD, $\delta^{18}O$) and soil water content for the three sites. Dashed line indicates the depth of the bottom boundary of the DSL.

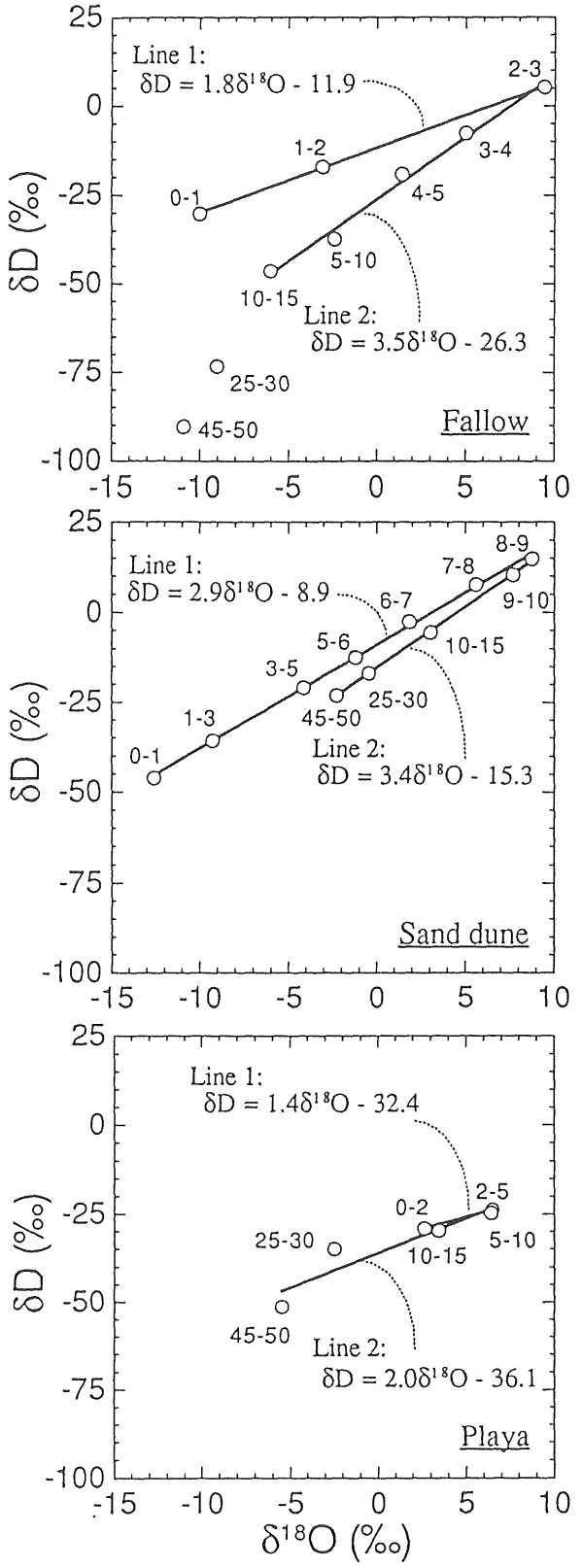

Figure 34 δ-diagram of the soil water from different depths for the three sites. Regression lines are added with dividing two types of data (i.e., data above and below the peak). Number beside each plot denotes the depth zone of the sampled soil.

vapor phase of soil water in the vapor transport region.

On the other hand, isotopic compositions of surface soil water indicated a small diurnal variation that δ values decreased in the daytime and increased in the nighttime (Figure 35). The diurnal variation of δ values of surface soil water suggests that some isotopic exchange between the liquid and vapor phases of water occur in the vapor transport region with diurnal cycle. Therefore, it can be thought that there are phase transitions of water in the vapor transport region, while whether the phase transition is evaporation or condensation can not be specified.

Figure 36 indicates that the data shown in Figure 35 distribute around Line 1 which appears in Figure 34. Thus, it would be reasonable to assume that the diurnal variation of δ values of surface soil water is caused by a variation in the depth of the peak point of the profile, that is, the boundary between the liquid water transport region and vapor transport region (which corresponds to the bottom boundary of the DSL except for the playa site).

7.2 Water balance of the surface soil layer

Water balance of the surface soil layer is expressed as

$$W = J_b - E \tag{7.1}$$

where W is the change rate of water storage in the surface soil layer, J_b the water flux across the bottom boundary of the layer, and E is the water flux across the soil surface (i.e. evaporation rate). Given the measured values of W and E, the value of J_b can be evaluated.

Figure 37 shows the diurnal variations in water fluxes evaluated by means of the above procedures for the data obtained on the intensive observation day. The values of W was determined by water content measurements with 4-hour intervals, and evaporation rate

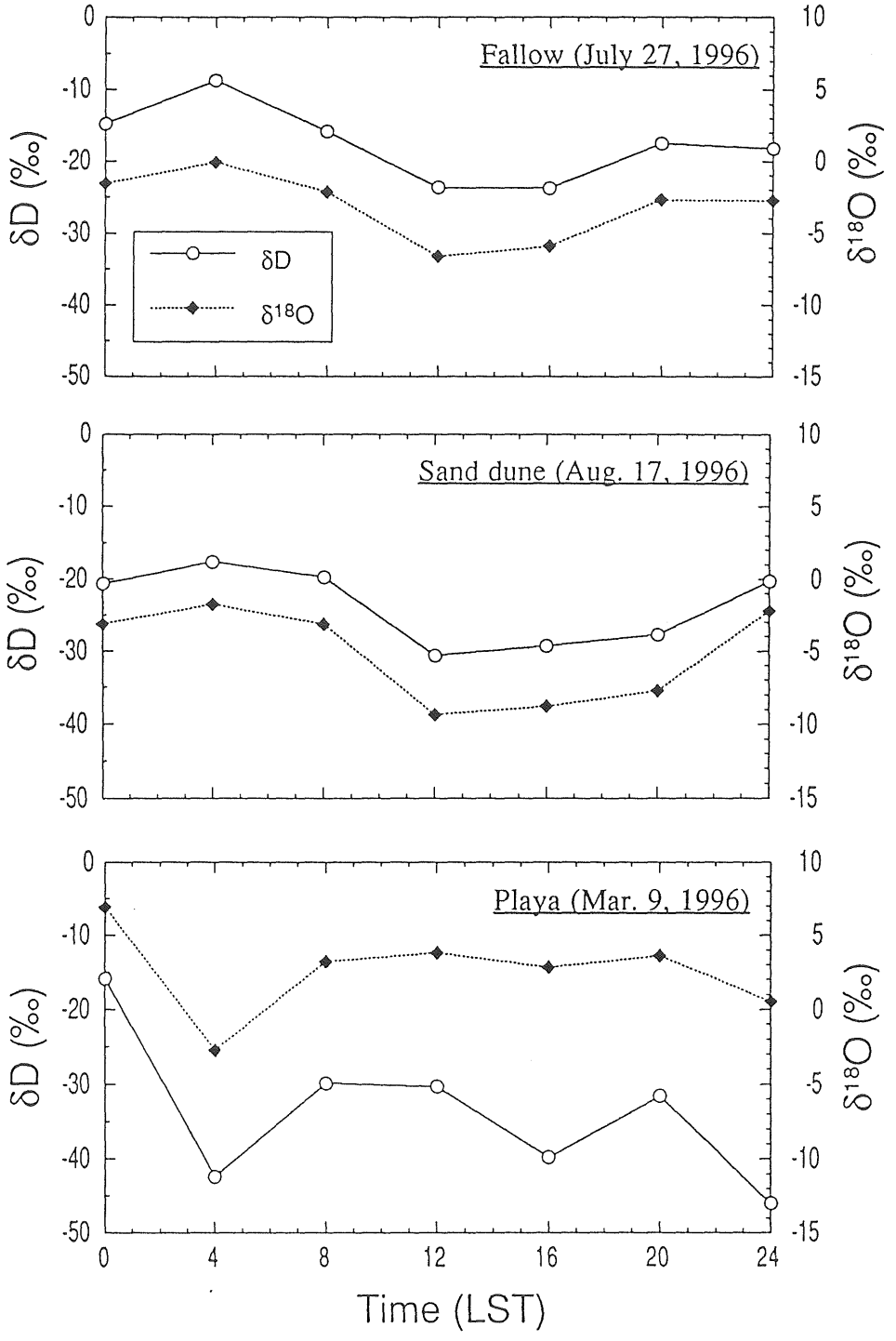

Figure 35 Diurnal variations of isotopic compositions of water in the surface soil of 1 cm (2 cm for the playa site) for the three sites.

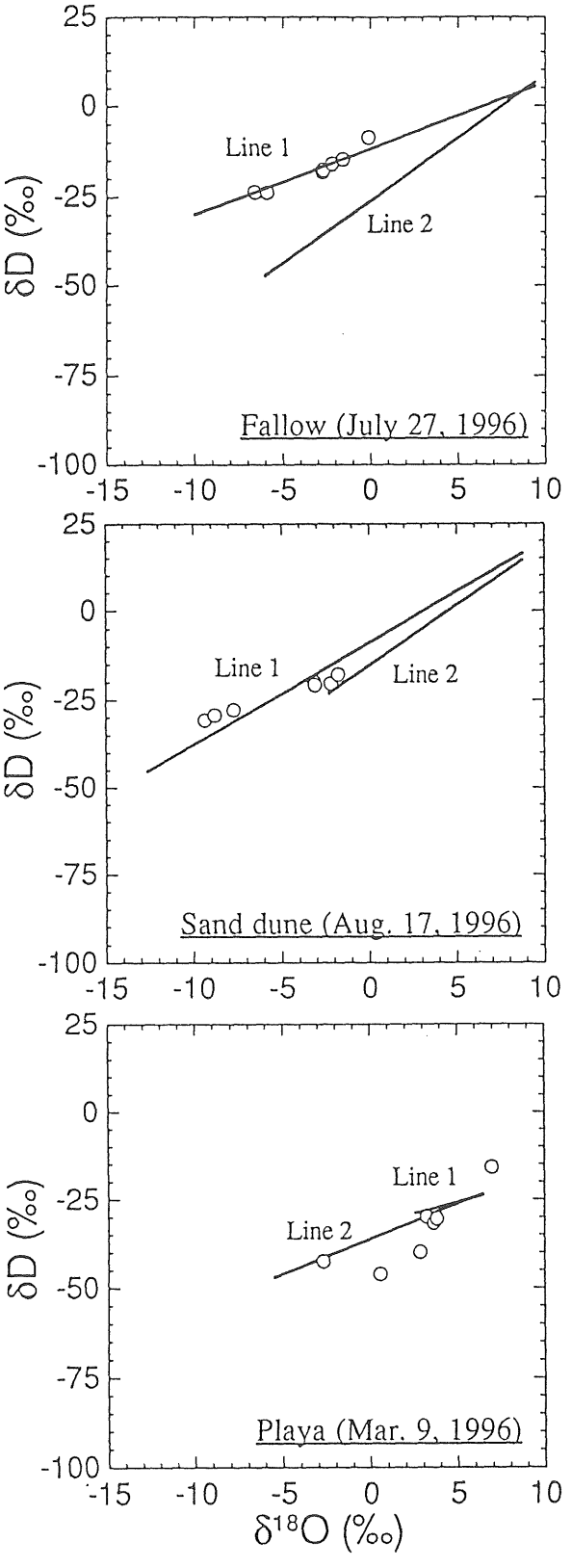

Figure 36 δ-diagram of the surface soil water sampled at different time of the day. Lines are identical to that shown in Figure 34.

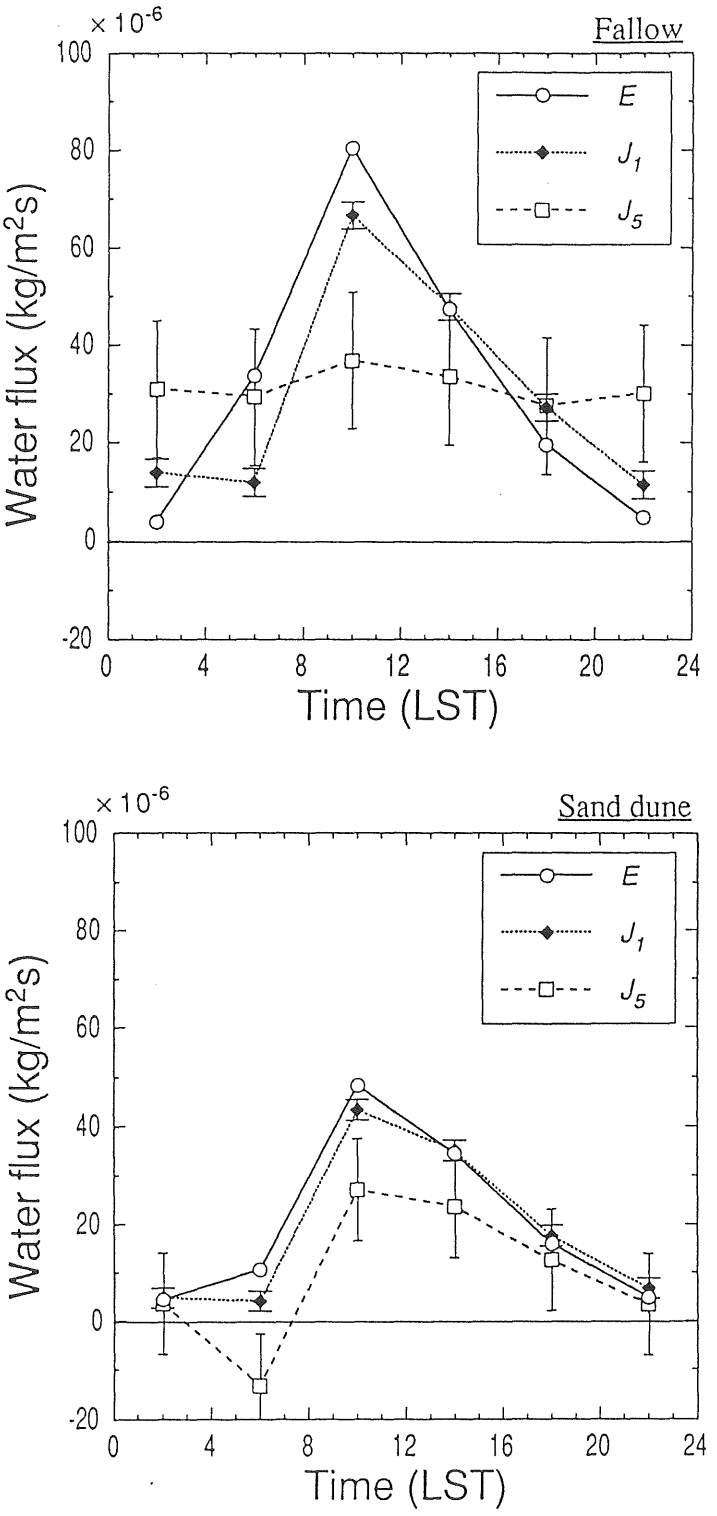

Figure 37 Diurnal variations of water fluxes derived from water balance in the surface soil for the fallow and the sand dune sites. Error bar indicates an uncertainty of the flux evaluation due to errors in water content measurement.

obtained from the energy balance was also averaged over 4 hours to produce E for the same time period. The values of J_1 and J_5 were evaluated by taking the surface soil layers of 1-cm and 5-cm thickness, respectively. Error bars in the figure represent an evaluation error of water flux introduced by uncertainties in water content measurements.

In the figures both for the fallow site and the sand dune site, J_1 is smaller than E in the forenoon, and is larger than E in the late afternoon and the nighttime. Based on the interpretation on the isotopic investigation mentioned in the previous section and the fact that the observed thickness of the DSL on the corresponding days (July 27 for the fallow site and Aug. 17 for the sand dune site) was larger than 1 cm, J_1 can be assumed in vapor phase. Thus, the figures suggest that (net) evaporation takes place not only at the bottom boundary of the DSL but also within the DSL in the forenoon, and that condensation of vapor traveling up from the bottom boundary of the DSL takes place within the DSL in the late afternoon and the nighttime.

Table 13 summarizes the ratio J_1/E at each time period. The ratio has values of approximately 0.37 in the early morning, and ranges from 1.1 to 3.6 in the late afternoon and the nighttime for both the fallow site and sand dune site. This means that the amount of evaporation occurring within the surface soil layer of 1-cm thickness occupies more than 60 % of total evaporation in the early morning, and that about 50 % of vapor traveling up from the bottom boundary of the DSL condenses within the DSL in the late afternoon and the nighttime.

On the other hand, diurnal variations in J_5 are different between for the fallow site and for the sand dune site (Figure 37). For the fallow site, J_5 tends to be almost constant throughout the day. In contrast, J_5 for the sand dune site diurnally varies and is considerably small during the nighttime. Although the soil dryness slightly differs between the fallow site and the sand dune site, the difference in the J_5 variations may reflects that the ability of supplying water from deeper soil layers to the soil surface for fine-textured soil is larger than that for coarse-textured soil.

Table 13 Ratio of water flux at the depth of 1 cm (J_1) to the evaporation flux at the surface (E) for each time period.

Site	Time period (LST)					
	0 - 4	4 - 8	8 - 12	12 - 16	16 - 20	20 - 24
Fallow	3.60	0.35	0.83	1.01	1.40	2.43
Sand dune	1.08	0.38	0.90	1.02	1.10	1.40

Figure 38 shows the variation in water storage changes of the layers of 0-1 cm and of 0-5 cm depth. The figure indicates that the amplitude of W_{0-1} is considerably larger than that of W_{0-5}. This may be related the lack of liquid water transport from deeper soil layers into the DSL. On the other hand, the figure indicates that the amplitude of W_{0-1} is larger for the fallow site than that for the sand dune site. In other words, the amount of evaporation or condensation within the DSL is larger for the fallow site, although the J_1/E hardly differed between the two sites. The relationship between the storage capacity of water in the DSL and soil properties will be discussed later.

7.3 Behavior of water vapor within the soil

Figure 39 shows the temporal variations of pore-air humidity within the soil. In general, pore-air humidity within the wet soil is always close to unity [Campbell, 1985]. Results of numerical experiment presented in Chapter 3 indicated that relative humidity in the soil was almost unity until a lack of liquid water supply from deeper layers took place. The figure for the sand dune site indicates that the relative humidity in the DSL decreases at the daytime, and that the humidity in the zone below the DSL is almost unity and does not vary. This suggests that the liquid water transport from deeper soil layers ceased at the bottom boundary of the DSL.

The figure for the playa site also indicates the low values of relative humidity in the DSL just like the case for the sand dune site. The diurnal variation of humidity, however, differs from that for the sand dune site, and humidity increases at the daytime. The low values of humidity in the DSL may be due to the lack of or insufficient liquid water supply into the DSL, and the daytime increase of humidity may be introduced by the evaporation due to non-negligible liquid water supply from deeper layers. In other words, liquid water transport in the DSL is not enough but non-negligible at the playa site.

It should be noted that the reduction of soil air humidity may be partly due to the

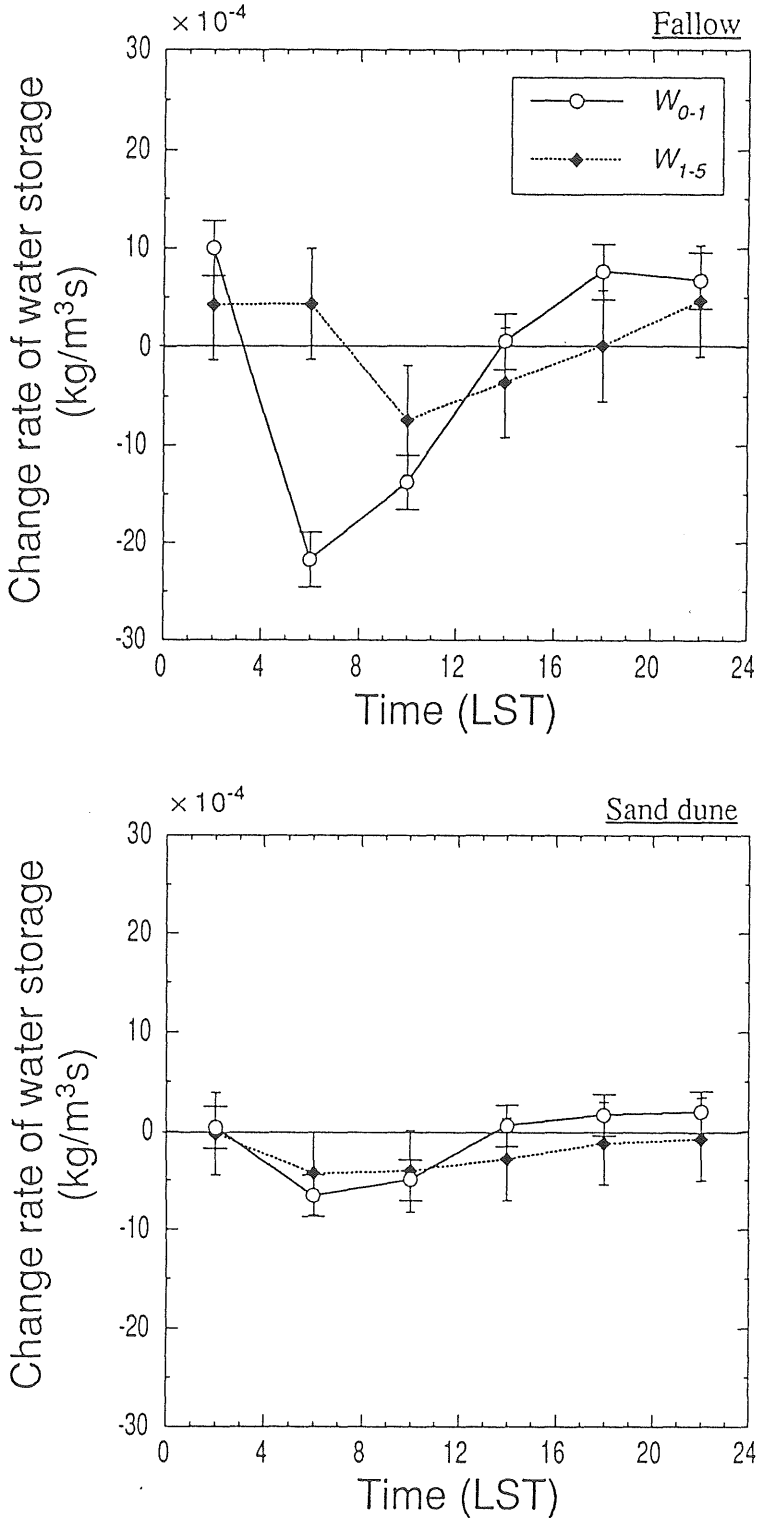

Figure 38 Diurnal variation of the change rate of the water storage in the surface soil for the fallow and the sand dune sites. Error bar indicates an uncertainty of the rate evaluation due to errors in water content measurement.

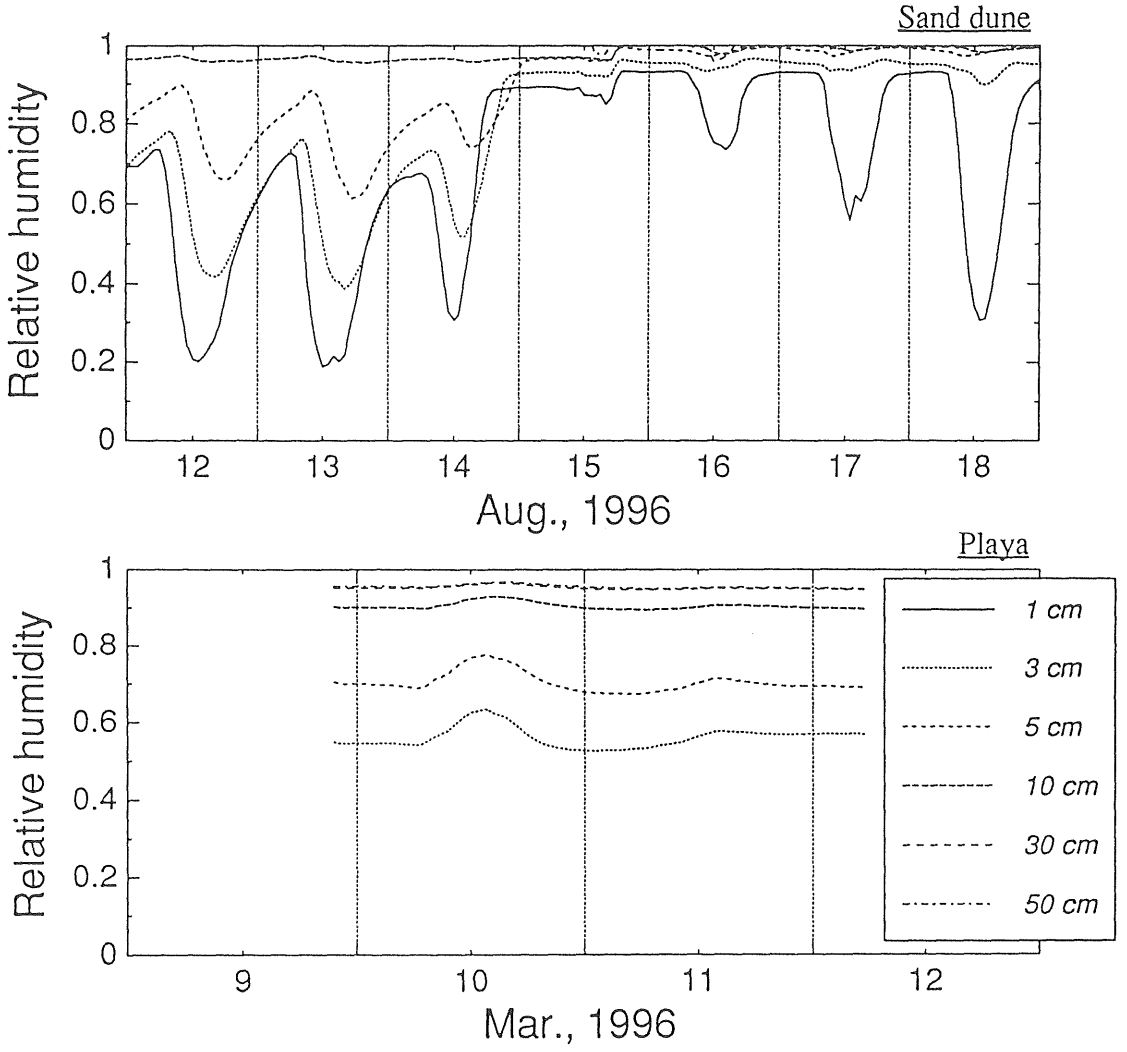

Figure 39 Temporal variation of relative humidity at several depths in the soil for the sand dune and the playa sites.

decrease in osmotic potential accompanying with the salt accumulation for the playa site. As mentioned in Section 5.3, soil water in the zone shallower than the depth of 5 cm is estimated to be saturated with NaCl. An equilibrium relative humidity of saturated aqueous solution for NaCl, however, is no less than 74 % [Greenspan, 1977]. Therefore the low humidity at the depth of 3 cm and 5 cm can not be explained by the decrease in osmotic potential only. Thus, there is a huge decrease in matric potential within the DSL for the playa site in spite of presence of liquid water supply into the DSL.

Figure 40 shows the time-space distribution of specific humidity within the soil for the sand dune and the playa sites. For the sand dune site, it can be seen that the peak of specific humidity profile in the daytime is positioned at around the bottom boundary of the DSL. In addition, in the forenoon, a change of humidity gradient can be seen within the DSL. These characteristics suggest that the main source of vapor in the daytime is located at the bottom boundary of the DSL, and that the evaporation of water can take place also within the DSL in the forenoon (not only at its bottom boundary). On the other hand, the figure for the playa site indicates the daytime peak of specific humidity positioned at a depth shallower than that of the bottom boundary of the DSL. Therefore, the evaporation of water mainly takes place not at the bottom boundary of the DSL but at a shallower zone for the playa site.

Although Figure 40 indicates large downward-gradients of specific humidity below the peak both for the sand dune site and the playa site, it should be noted that the magnitudes of downward vapor fluxes become considerably small relative to the upward vapor fluxes because of the small values of effective vapor diffusivity (in other words, less air-filled porosity) in the zone below the peak.

Figure 41 shows the relationship between the energy-balance based latent heat flux (LE) and the humidity-gradient based flux (LE_h) for the sand dune site. LE_h can be calculated

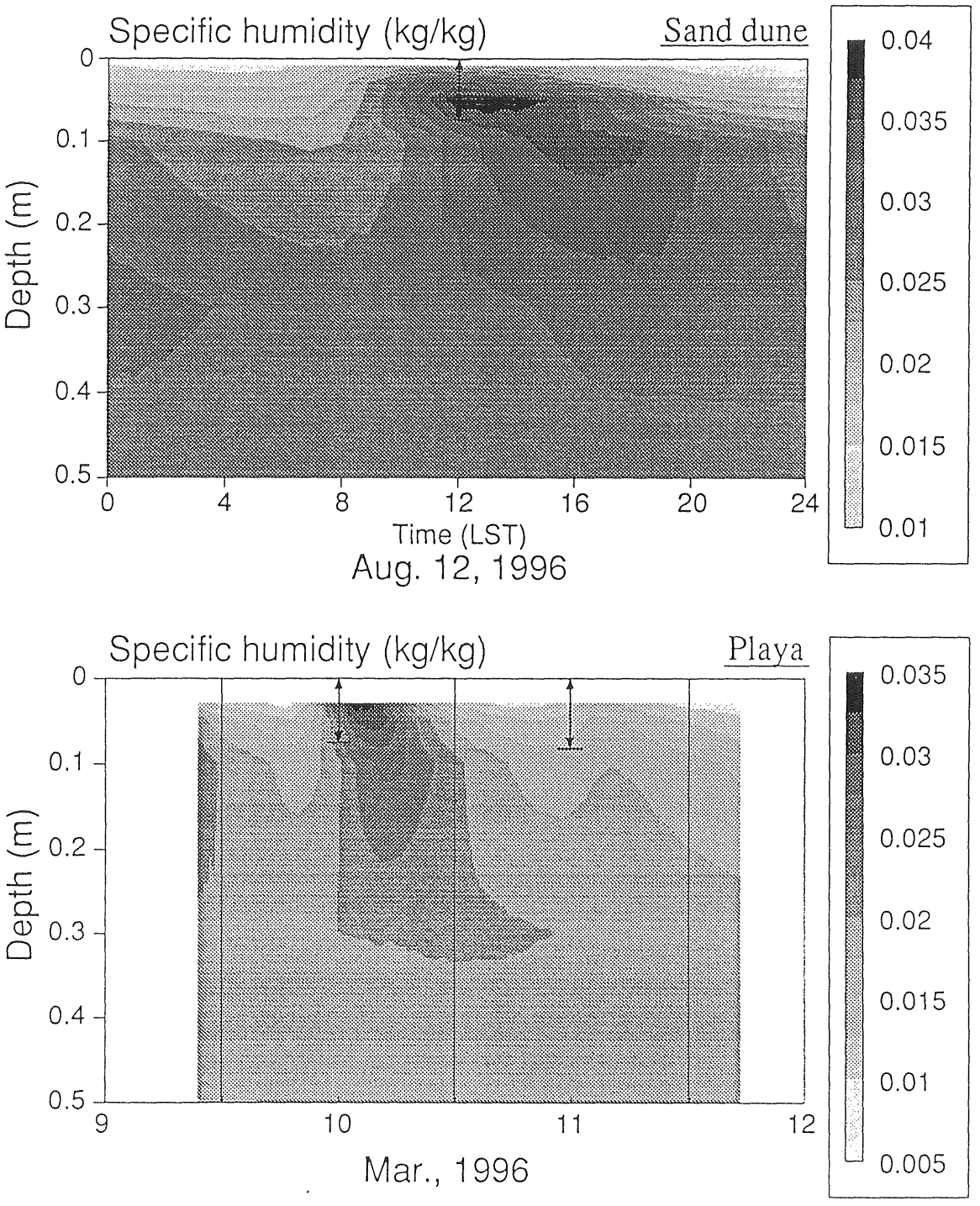

Figure 40 Time-space distribution of specific humidity in the soil for the sand dune and the playa site. Arrow denotes the thickness of the DSL. Note that the scale of horizontal axis is different between top and bottom columns.

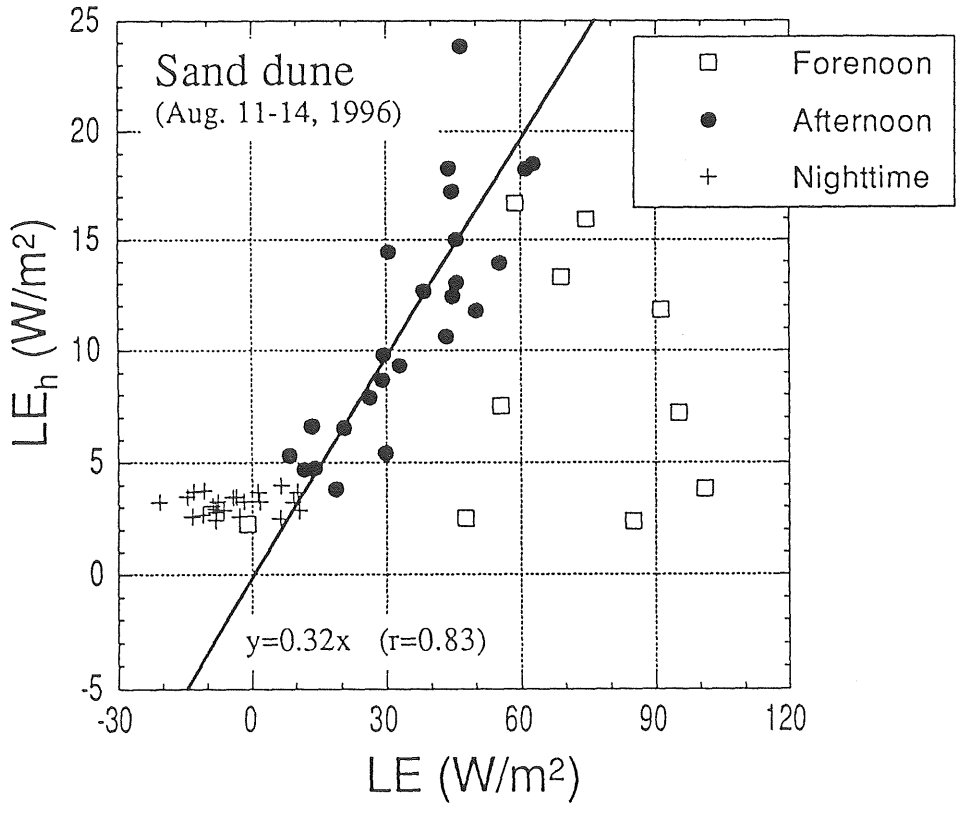

Figure 41 Comparison of latent heat flux derived by the Bowen ratio (LE) and that evaluated from humidity gradient in the soil (LE_h). In this analysis, forenoon data are as data of 7 - 11 LST; afternoon data, 12 - 17 LST; and nighttime data are as residuals. Regression line in the figure is for the afternoon data.

with the following equation:

$$LE_h = -l\rho D_{ve}\frac{\partial q}{\partial z} \tag{7.2}$$

where l is the latent heat for vaporization, ρ the density of the air, D_{ve} the effective vapor diffusivity in the soil (given by Equation (3.11)), q the specific humidity of the pore-air, and z is the depth.

In Figure 41, the data points in the afternoon distribute around a straight line ($LE_h = 0.32LE$). In contrast, LE_h is smaller than LE in the forenoon, and is larger than LE in the nighttime. These can be explained by hypothesis that there was condensation of vapor traveling up from the deeper layers during the nighttime and was subsequent re-evaporation of water within the DSL in the forenoon. In this hypothesis, however, there is a problem that the slope of the regression line for the afternoon data is not unity but is approximately one thirds. Thus, the actual rate of evaporation is three times as large as expected rate from the specific humidity gradient. A cause of this difference may be in the evaluation of effective vapor diffusivity. Although in the present analysis molecular diffusion was considered as an only mechanism of vapor transfer in the soil, there are several mechanisms suggested previously other than molecular diffusion. These include turbulent diffusion [Fukuda, 1955; Farrell et al., 1966; Scotter and Raats, 1969; Ishihara et al., 1992], advective transfer [Kazanskiy and Zolotokrylin, 1994], and thermal diffusion [Kobayashi, 1993]. Kobayashi [1993] confirmed that the thermal diffusion mechanism can be ignored in the DSL. However, influences of the former two mechanisms in common soil materials have not been clearly understood yet. Figure 41 may suggest that any other mechanism of vapor transport makes the effective vapor diffusivity three times larger than that by molecular diffusion only, although there is no definite information to specify the mechanism.

7.4 Summary

In this chapter, processes of water transport in the liquid and vapor phases within the soil and phase change of soil water were assessed by three independent means, i.e., stable isotopic analysis, water balance, and analysis of direct humidity measurements in the soil. Results are follows:

(1) Stable isotopic analysis of soil water showed that the liquid water transport region and vapor transport region could be distinguished clearly each other, particularly in coarse-textured soils. The boundary between the two regions almost corresponded to the bottom boundary of the DSL. At the same time, it was also shown for a fine-textured soil that the change of water fluxes of liquid phase to those of vapor phase occurred gradually and that there was non-negligible liquid water transport into the DSL.

(2) Analysis of water balance of surface soil layer indicated that the evaporation within the DSL was not negligible in the forenoon and also that a condensation occurred within the DSL in the late afternoon and the nighttime. Amounts of the evaporation and condensation within the DSL depended on soil types.

(3) Direct measurements of soil air humidity confirmed the presence of vapor transport in the DSL, and indicated the effect of the evaporation and condensation within the DSL on the humidity profile. In addition, it was suggested the presence of additional vapor transfer mechanisms other than the molecular diffusion.

Chapter 8

Variation of the effective evaporation zone

In the previous chapter, it was indicated that evaporation can actually take place below the soil surface. In the present chapter, variation of the location of the evaporation zone and its relation to the DSL will be investigated by applying a lumped parameter model, which assumes that evaporation occurs only at an extremely thin zone within the soil layer. Here the zone will be expressed as *effective evaporation zone.*

8.1 Model development and application

8.1.1 Formulation

By assuming no evaporation at the soil surface, energy budget at the surface can be expressed as

$$R_n = H + G_0, \tag{8.1}$$

where R_n is the net radiation, H the sensible heat flux, and G_0 the conductive heat flux into the soil. Energy budget equation at the effective evaporation zone can be given as

$$G_1 = LE + G_2, \tag{8.2}$$

where G_1 is the conductive heat flux from the layer between the soil surface and the effective evaporation zone (referred to as Layer 1) to the effective evaporation zone, LE the latent heat flux, and G_2 the conductive heat flux from the effective evaporation zone to the lower layer (referred to as Layer 2). The heat fluxes G_0 and G_1 are related as follows:

$$G_0 = G_1 + S_1, \tag{8.3}$$

where S_1 is the change rate of heat storage in the Layer 1. It should be noted that the soil heat flux G (in Equation (2.4)) corresponds to the sum of S_1 and G_2.

Latent heat flux from the effective evaporation zone to the atmosphere through the soil surface can be expressed as [Yamanaka et al., 1997]

$$LE = \frac{l\rho(q_{sat}(T_e) - h_a q_{sat}(T_a))}{r_{av} + r_{sv}}, \tag{8.4}$$

where l is the latent heat for vaporization, ρ the density of the air, q_{sat} the saturation specific humidity as a function of temperature, T_e the temperature at the effective evaporation zone, and h_a and T_a are the relative humidity and the temperature of the air at a certain level in the ASL, respectively. The resistance to the vapor transfer in the atmosphere (r_{av}) can be given by Equation (6.6), and the resistance in the soil (r_{sv}) can be given as

$$r_{sv} = z_e / D_{ve} f_e, \tag{8.5}$$

where z_e is the depth (not thickness) of the effective evaporation zone, D_{ve} the effective vapor diffusivity in the soil (given as Equation (3.11)), and f_e the enhancement factor for additional vapor diffusion process in the soil (see Section 7.3. This scheme (i.e. Equations (8.4) and (8.5)) assumes that the degree of the restriction of evaporation due to soil drying is determined by the depth of the effective evaporation zone.

The heat flux G_1 can be approximately given as

$$G_1 = \lambda_1 \frac{T_s - T_e}{z_e}, \tag{8.6}$$

where λ_1 is the thermal conductivity of the soil in the Layer 1, and T_s is the soil surface temperature.

S_1 and G_2 can be given as first order approximation (see Appendix B for their derivation), as follows:

$$S_1 = \frac{C_1 z_e}{2}\{\frac{\partial T_s}{\partial t} + \exp(-z_e/d_1)[\frac{\partial T_s}{\partial t}\cos(-z_e/d_1) - \omega(T_s - T_2)\sin(-z_e/d_1)]\} \tag{8.7}$$

$$G_2 = \frac{\lambda_2}{d_2}\{\exp(-z_e/d_1)[\frac{1}{\omega}\frac{\partial T_s}{\partial t}\cos(-z_e/d_1) - (T_s - T_2)\sin(-z_e/d_1)] + T_e - T_2\}, \tag{8.8}$$

where C_1 is the volumetric heat capacity of the soil in the Layer 1, ΔT_s the change of surface temperature at a time interval Δt, d_1 ($\equiv (\frac{2\lambda_1}{C_1\omega})^{1/2}$) the dumping depth for the Layer 1, ω ($= 2\pi/24/60/60$) the angular frequency of the diurnal temperature wave, λ_2 the thermal conductivity of the soil in the Layer 2, d_2 the damping depth for the Layer 2, and T_2 is the deep soil temperature in the Layer 2.

8.1.2 Solution and parameters

Equations (8.1) and (8.2) were solved simultaneously for z_e and T_e using Newton-Raphson method, when measured values of T_s, T_a, h_a, u, R_n, and H were given. Details of its procedure are given below.

Equations (8.1) and (8.2) can be rewritten as

$$f_1(x,y) = R_n - H - G_1(x,y) - S_1(x,y) \tag{8.9}$$

$$f_2(x,y) = G_1 - LE(x,y) - G_2(x,y), \tag{8.10}$$

where $x = z_e, y = T_e$. Here, it is assumed that

$$h_x = x^{i+1} - x^i \tag{8.11}$$

$$h_y = y^{i+1} - y^i, \tag{8.12}$$

where suffixes i and $i+1$ mean i-th and $(i+1)$-th approximate values, respectively. Then parameters h_x and h_y are obtained by the following equation:

$$\begin{bmatrix} h_x \\ h_y \end{bmatrix} = \mathrm{C}^{-1} \begin{bmatrix} f_1(x,y) \\ f_2(x,y) \end{bmatrix} \tag{8.13}$$

where the matrix C is often called *Jacobian*, and is expressed as follows:

$$\mathrm{C} = \begin{bmatrix} \frac{\partial f_1(x,y)}{\partial x} & \frac{\partial f_1(x,y)}{\partial y} \\ \frac{\partial f_2(x,y)}{\partial x} & \frac{\partial f_2(x,y)}{\partial y} \end{bmatrix} \tag{8.14}$$

The next approximate values of x and y are obtained by Equations (8.11) and (8.12), respectively, and then Equation (8.13) is recalculated. This iteration procedure is continued until absolute values of both h_x and h_y are become smaller than 1×10^{-3}.

During the course of the procedure, an iterative calculation was carried out because the atmospheric stability correction function in Equation (6.7) and roughness parameters in Equations (6.7) through (6.13) are implicit form. Then LE was estimated by Equation (8.4) using the obtained values of z_e and T_e, and G was also estimated as the sum of the calculation results of Equations (8.7) and (8.8). Flowchart of these calculation procedures is shown in Figure 42.

Values of the soil parameters used in the calculation were determined by Equations (3.9) and (3.10) based on the results of soil analysis. The values are summarized in Table 14. For the aerodynamical properties of the soil surface, the values summarized in Table 12 were used. The enhancement factor for additional vapor diffusion process in the soil (f_e) was assumed to be 3.0 by considering the results of humidity measurements within the soil (see Section 7.3). The value of T_2 was given by 24-hour moving average of temperature measured at the depth of 30 cm.

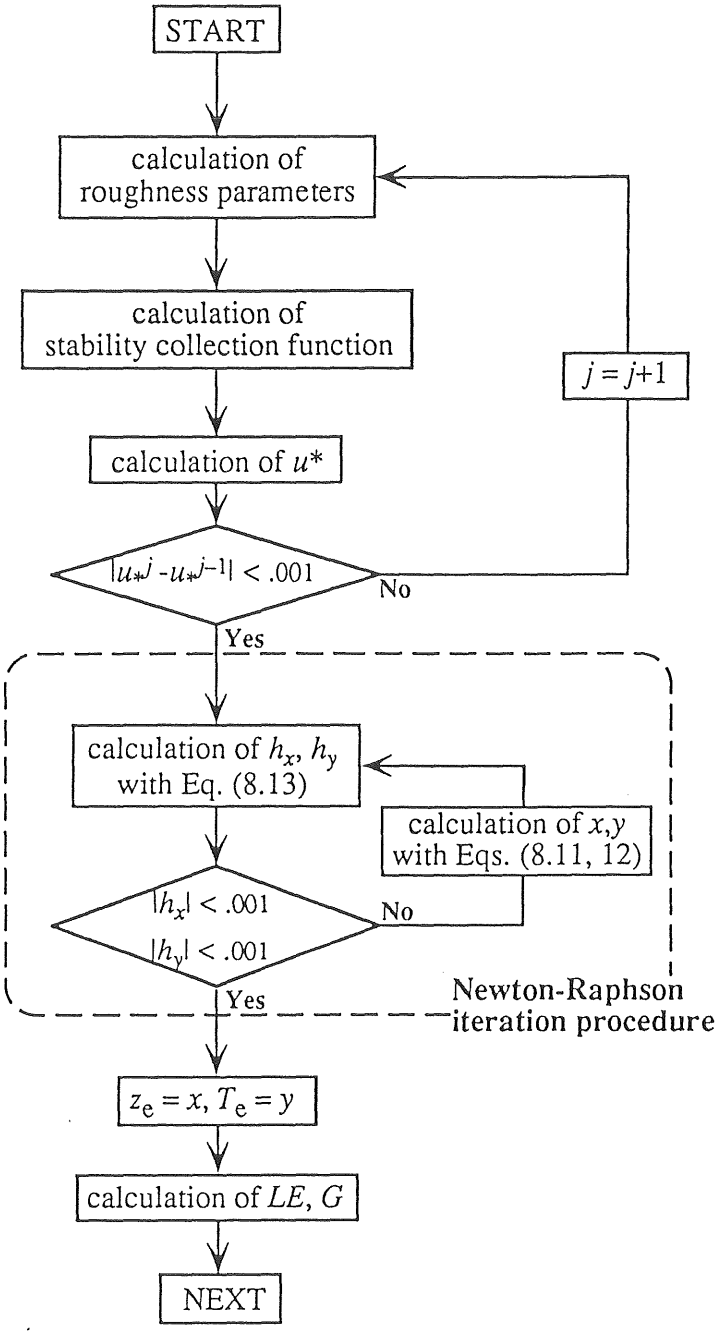

Figure 42 Flowchart of the energy balance model application.

Table 14 Representative values of water content (θ), thermal conductivity (λ), and volumetric heat capacity (C) in the Layers 1 and 2.

Site	θ_1 (m^3/m^3)	θ_2 (m^3/m^3)	λ_1 (W/mK)	C_1 (MJ/m^3K)	λ_2 (W/mK)	C_2 (MJ/m^3K)
Fallow	0.02	0.125	0.2	1.1	0.75	1.6
Sand dune	0.005	0.03	0.3	1.1	0.5	1.2
Playa	0.05	0.25	0.2	1.0	0.8	1.9

8.2 Validity of the flux estimation

Figures 43 through 45 show the comparisons of temporal variation in latent heat flux and soil heat flux between observation and model estimation for the three sites. From the figures, it can be seen that the estimated results simulate quite well diurnal and interdiurnal variations in both latent heat flux and soil heat flux at all sites.

Statistics of comparison between observed and estimated fluxes are summarized in Table 15. The table indicates very good agreements between observed and estimated fluxes, and also that the degree of agreement hardly depend on the observation sites. This suggests the validity of the model used and its wide applicability independent of soil type, climate, and other conditions. Also, this suggests that the degree of the restriction of evaporation can be controlled by the depth of the effective evaporation zone.

8.3 Relationship between the effective evaporation zone and the DSL

Figure 46 shows temporal variations in the estimated depth of the effective evaporation zone (z_e) and the thickness of the DSL (δ_{DSL}) at the three observation sites, and diurnal variations of those on an intensive observation day at each site is shown in Figure 47. In the figures, only the data in the period from 07 LST to 17 LST are presented because of large uncertainty in z_e estimation when low value of $(R_n - H)$ or downward latent heat flux (i.e. dew formation) was appeared.

Figure 46 indicates that interdiurnal evolution of z_e corresponds well to that of the thickness of the DSL for the fallow site and sand dune site, while the value of z_e at noon is somewhat smaller than the thickness of the DSL. From Figure 47, it can be seen for the fallow and sand dune sites that the value of z_e in the early morning is clearly smaller than the thickness of the DSL, then gradually increases and reaches to the same magnitude of

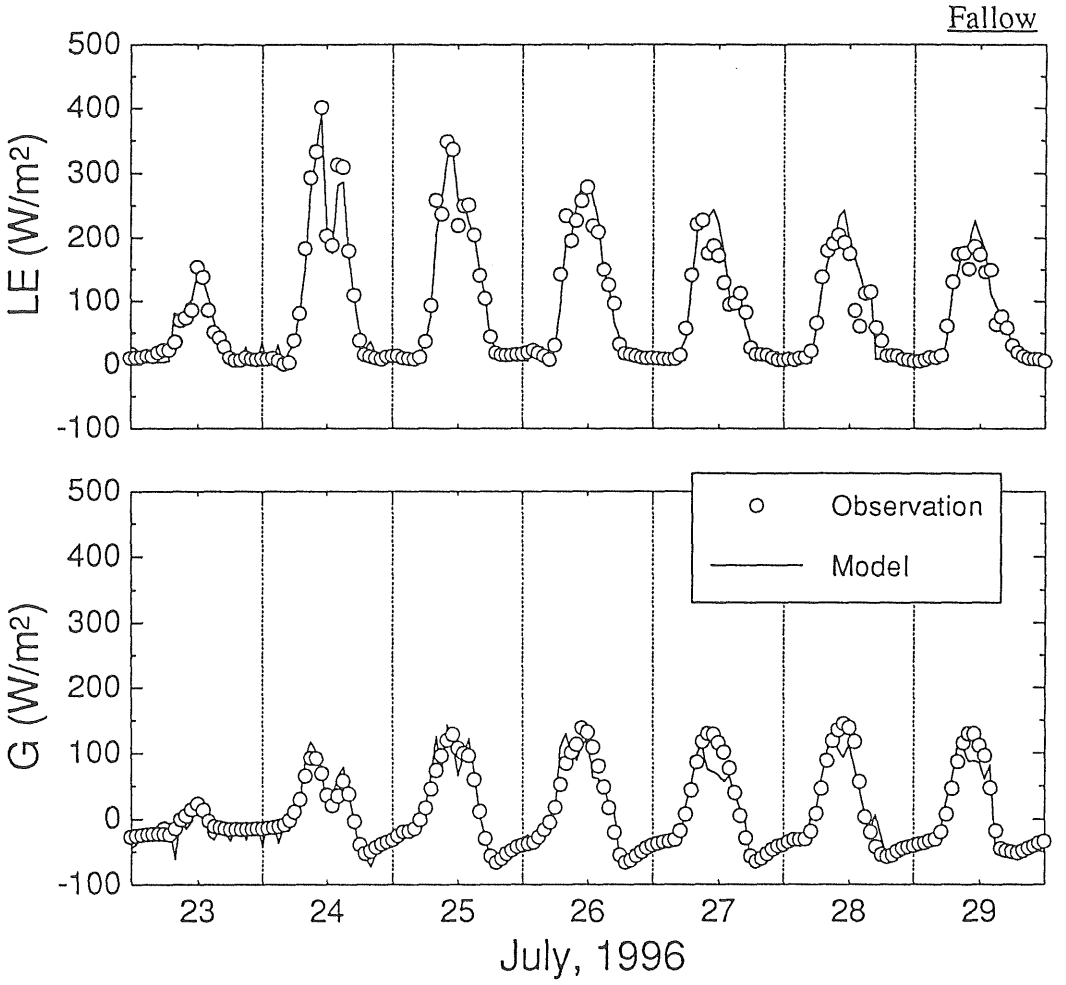

Figure 43 Comparison of the temporal variations of latent heat flux and soil heat flux between field observation and model estimation for the fallow site.

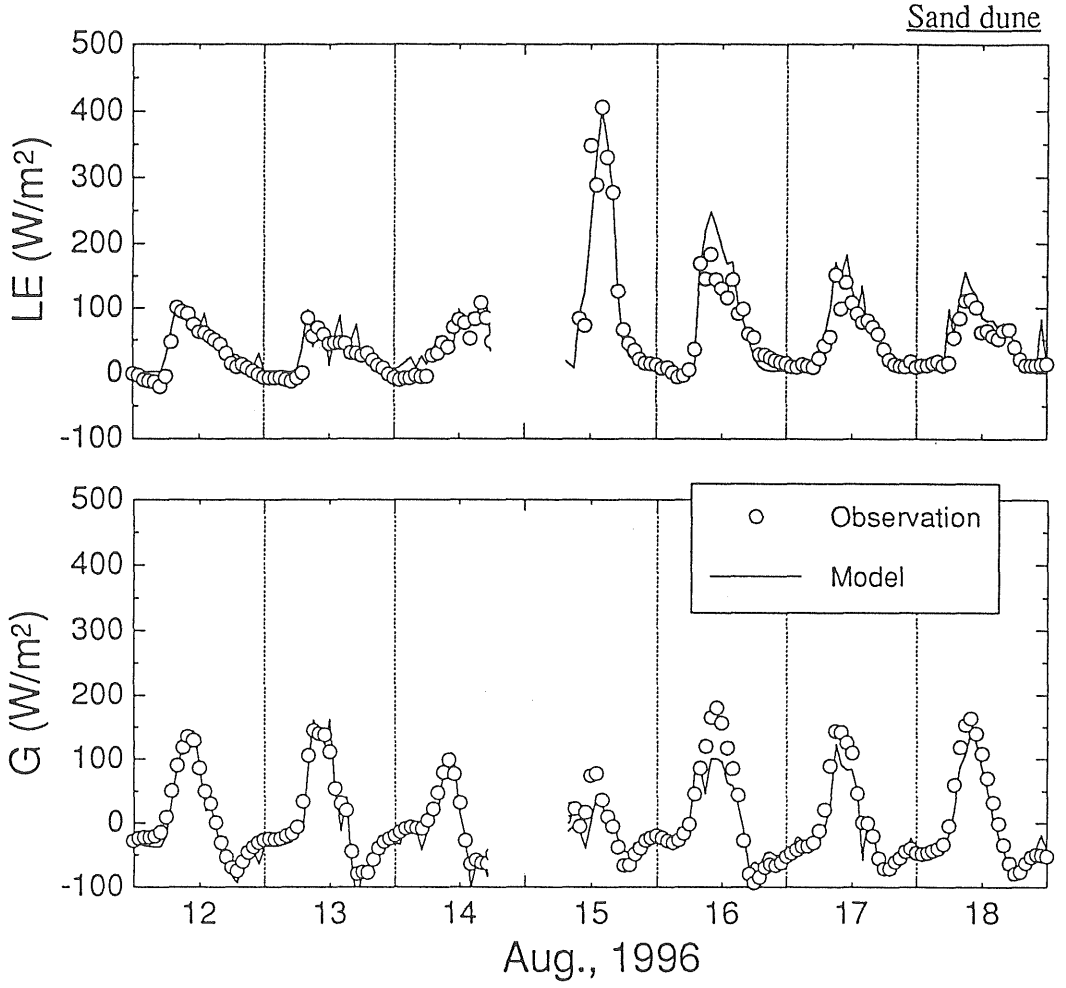

Figure 44 Comparison of the temporal variations of latent heat flux and soil heat flux between field observation and model estimation for the sand dune site.

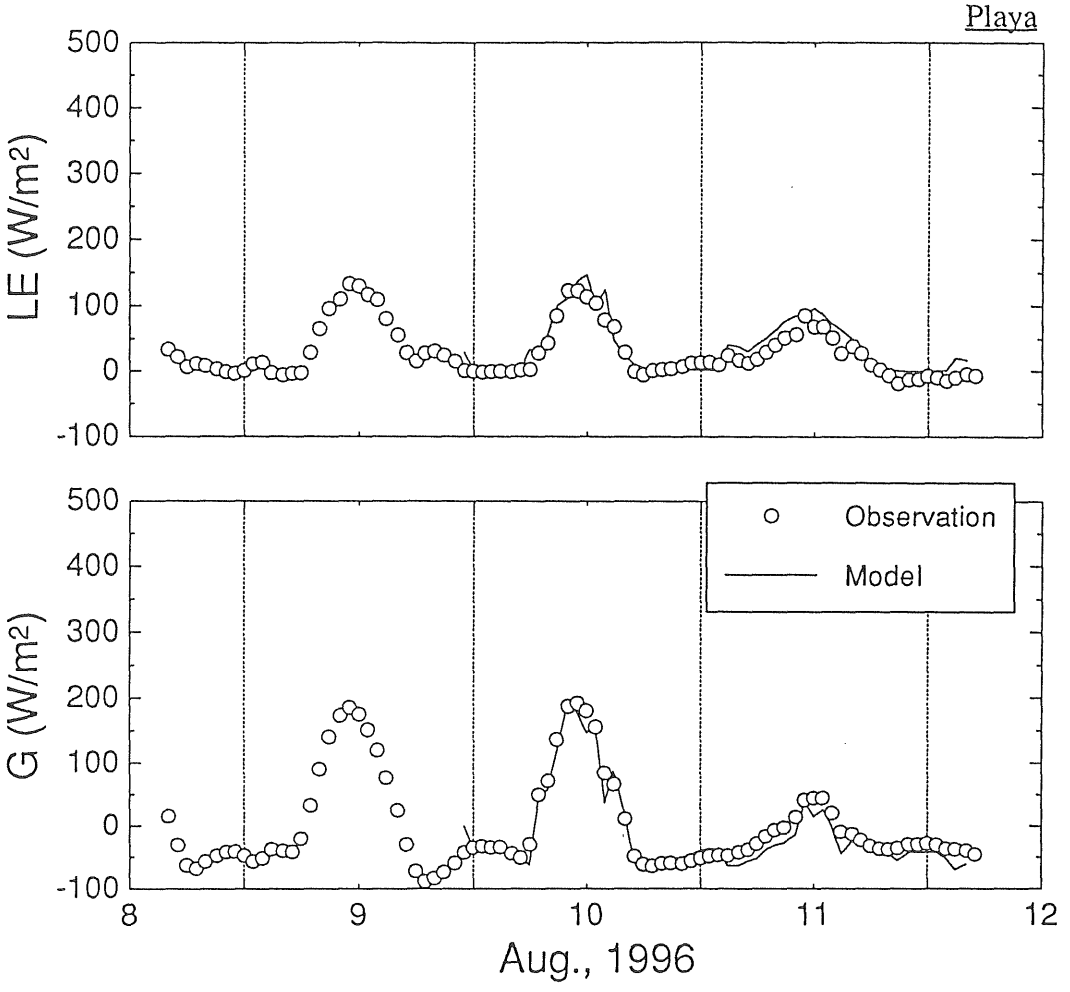

Figure 45 Comparison of the temporal variations of latent heat flux and soil heat flux between field observation and model estimation for the playa site.

Table 15 Statistics for comparisons of fluxes between model estimation (F_m) and field observation (F_b).

	Regression constants for $F_m = aF_b + b$		Correlation coefficient	MAD $\langle \mid F_m - F_b \mid \rangle$	RMSD $\sqrt{\langle (F_m - F_b)^2 \rangle}$
	a	b	r	(W/m^2)	(W/m^2)
Fallow					
LE	0.962	5.643	0.967	14.0	19.5
G	0.957	-2.127	0.920	14.0	19.5
Sand dune					
LE	1.067	5.862	0.952	16.6	23.5
G	0.858	-7.841	0.950	16.6	23.5
Playa					
LE	1.043	9.577	0.938	14.0	21.7
G	0.961	-9.493	0.972	14.0	21.7

MAD: mean absolute difference, RMSD: root mean square difference

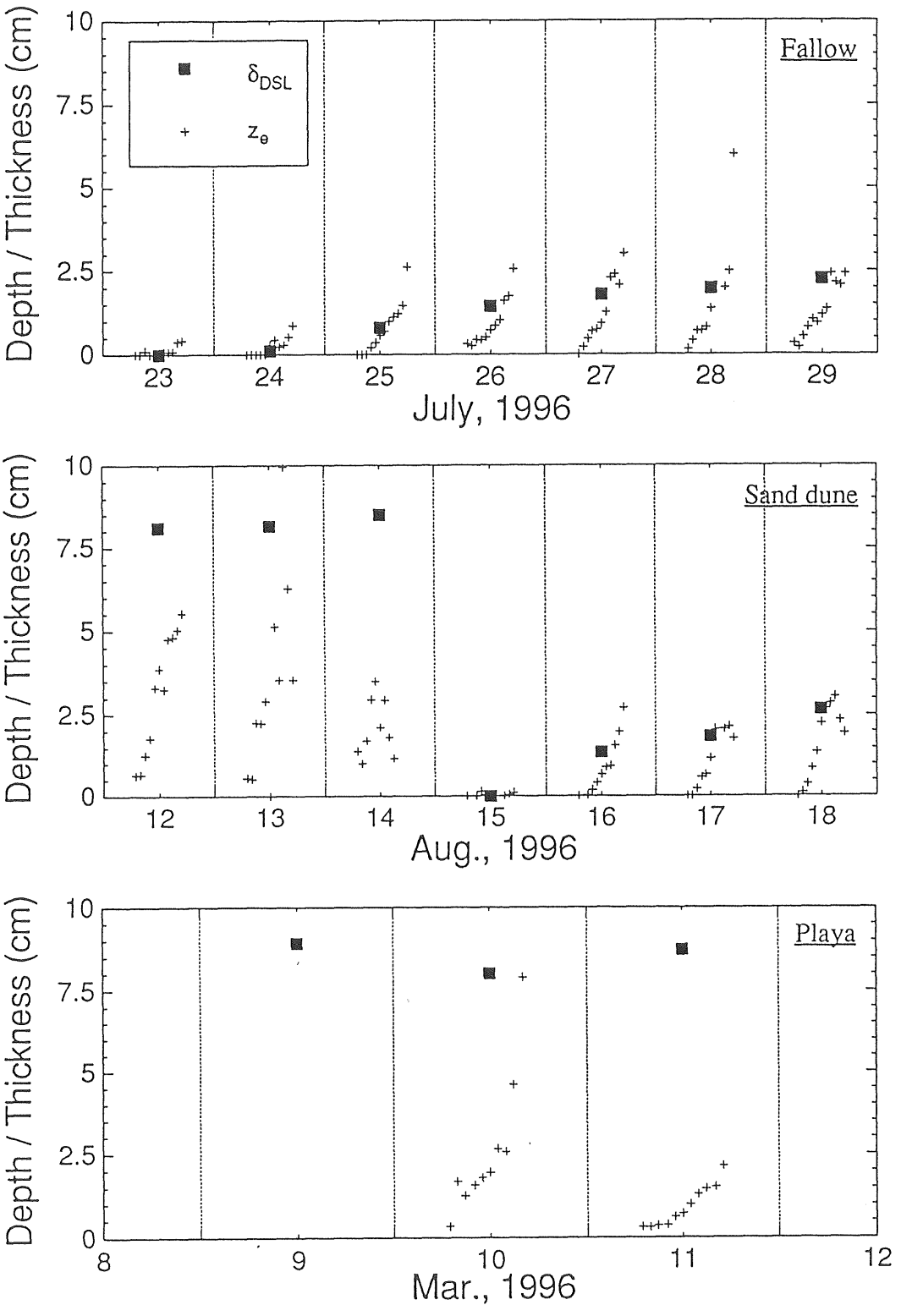

Figure 46 Temporal variations of observed thickness of the DSL and estimated depth of the effective evaporation zone for the three sites.

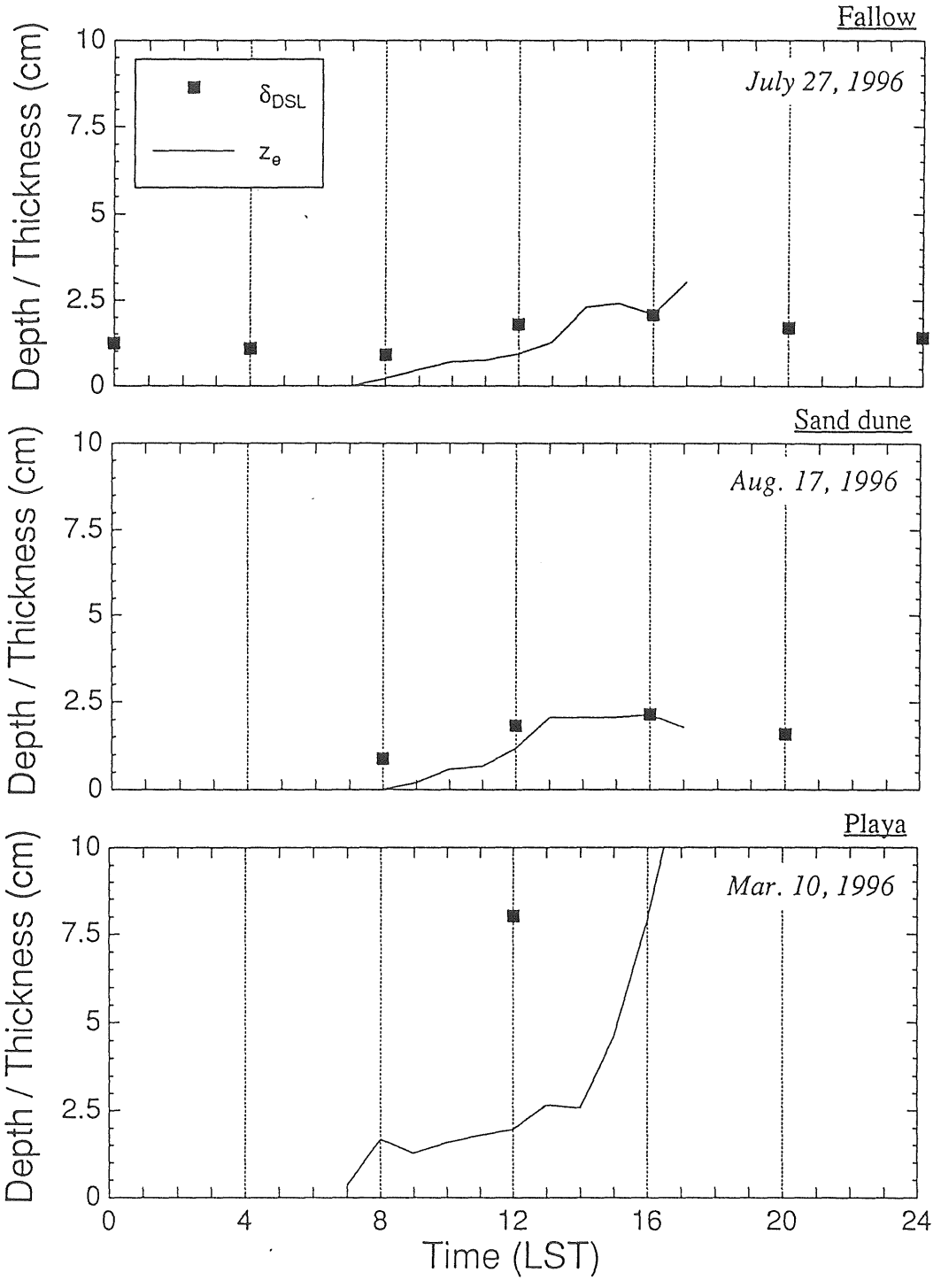

Figure 47 Diurnal variation patterns of observed thickness of the DSL and estimated depth of the effective evaporation zone for the three sites.

the thickness of the DSL in the afternoon. This suggests that the evaporation of soil water occurs within the DSL (particularly near the soil surface) in the forenoon, and that the evaporation at the bottom boundary of the DSL dominates in the afternoon.

On the other hand, only for the playa site, it is clear that the value of z_e is smaller than the thickness of the DSL and that the increase in z_e during the daytime occurs more gradually than that for the other sites. Although the z_e value may be somewhat underestimated because the effect of cracks on vapor transport was not taken into account, z_e would not reach to 8 cm since the depth of the cracks was no more than 2 cm. This suggests that at the playa site the evaporation takes place not at the bottom boundary of the DSL but at the upper part of the DSL throughout the daytime. A cause of this may be partly a large volume of water stored in the DSL and partly a non-negligible liquid water transport in the DSL (see Section 7.1).

8.4 Summary

A lumped parameter model for energy balance was applied to the data obtained by field observations. The following results were obtained:

(1) Latent heat and soil heat fluxes estimated by the model agreed very well with those observed. This suggests that the degree of the restriction of evaporation during soil drying was controlled by the depth of the effective evaporation zone.

(2) The effective evaporation zone was located within the DSL in the forenoon, and was at the bottom boundary of the DSL. For a fine-textured soil, however, it remains at the shallower part of the DSL throughout the daytime.

Chapter 9

Discussion

9.1 Process of evaporation with dual sources

Analysis of surface energy balance has indicated that evaporation from soils comes to be restricted with the development of the DSL, but that the degree of its restriction is smaller in the forenoon than in the afternoon (Sections 6.2 and 6.3). Vertical profiles of isotopic composition of soil water (Section 7.1) and humidity measurements in the soil (Section 7.3) suggested that below the DSL water is transported upward mainly in the liquid phase, and that the vapor transport dominates in the DSL. Therefore, it was expected that the evaporation takes place mainly at the bottom boundary of the DSL throughout the day. On the other hand, water budget of the surface soil (Section 7.2) and an application of energy balance model to observation data (Section 8.3) suggested that evaporation also takes place within the DSL in the forenoon, and that the condensation occurs there in the late afternoon and in the nighttime. Such a process was also found in a theoretical investigation (Section 3.4). Although there are some differences among soils, the facts mentioned above suggest that the evaporation from a dry bare soil has dual sources as illustrated in Figure 48.

Assumption of the process of evaporation with dual sources may be able to explain the

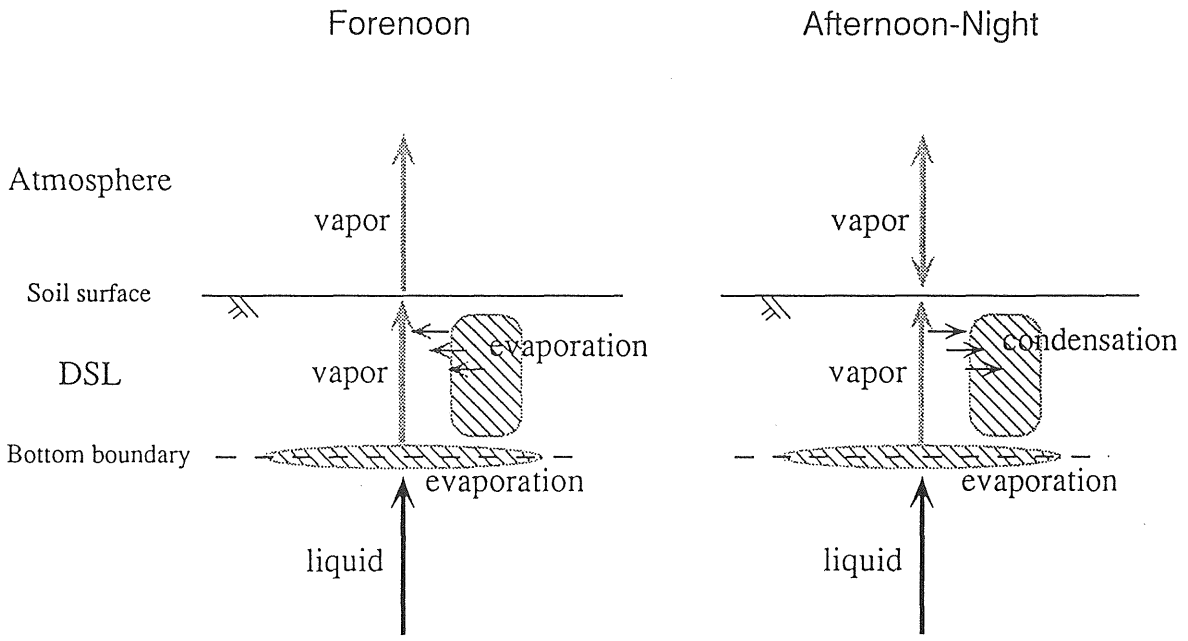

Figure 48 Schematic illustration of the evaporation process with dual sources.

cause of the difference in the r_s - θ relationship between diurnal and inter-diurnal time scales, or of the hysteresis in the relationship (Section 6.3). It has been demonstrated that the evaporation at the bottom boundary of the DSL is closely related with the movement of an inflection of the water content profile (Type-A in Figure 49), and that the evaporation within the DSL is related with the water content variation above the inflection (Type-B in Figure 49). In fact, the variations of water content profile as illustrated in Figure 49 were observed in detail by Nomura and Inoue [1977]. What is remarkable is that the Type-A variation of water content profile is significant for both diurnal and inter-diurnal variations in r_s while the Type-B variation is significant only for the diurnal variation in r_s. Therefore, it can be said that the r_s - θ relationship for the noon data reflects the effect of Type-A variation of water content on r_s, and the relationship for the IOD data contains the effects of both Type-A variation and Type-B variation.

However, to accept the process of evaporation with dual sources, the following two questions should be examined: one is why the dominant phase of water flux is changed from liquid phase to vapor phase at the bottom boundary of the DSL, and the other is why evaporation can occur within the DSL in spite of the lack of the liquid water supply from deeper soil layers. These questions would be directly related to the mechanisms of evaporation from each source.

9.1.1 Mechanism of evaporation at the bottom boundary of the DSL

Figure 50 shows the relationships between the matric head and conductivities for the three soils used in the model calculation in Chapter 3. In the figure, the hydraulic conductivity is reduced with the decrease of matric head while the vapor conductivity maintains a constant level in a wide range of matric head. (Note the vapor conductivity could slightly vary with temperature variation.) As a result, the magnitude of the hydraulic conductivity

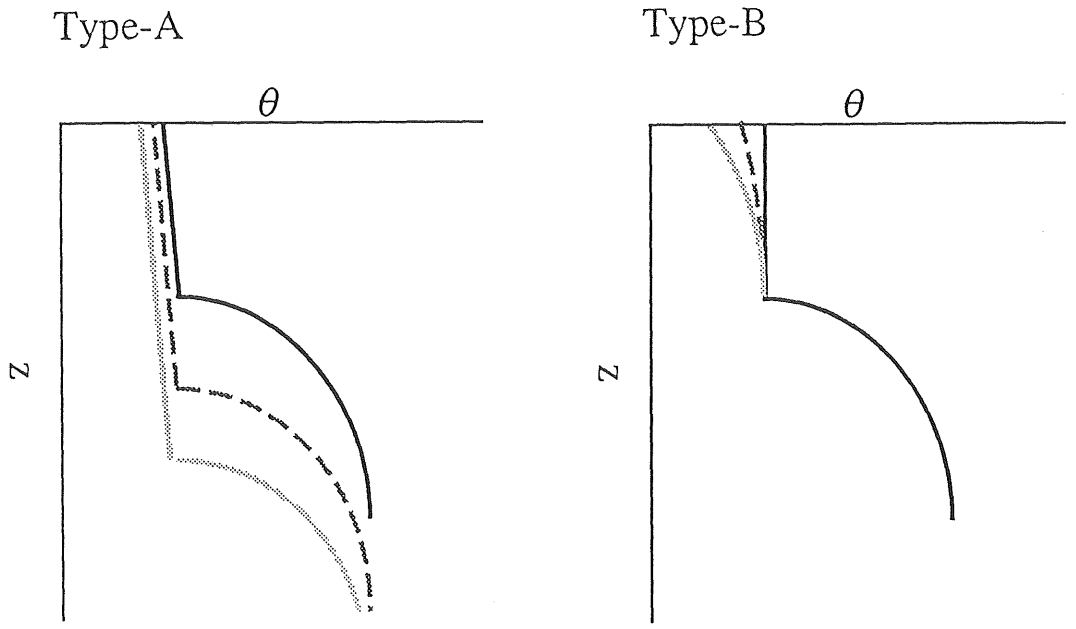

Figure 49 Schematic illustration of the variation of the water content profile due to evaporation.

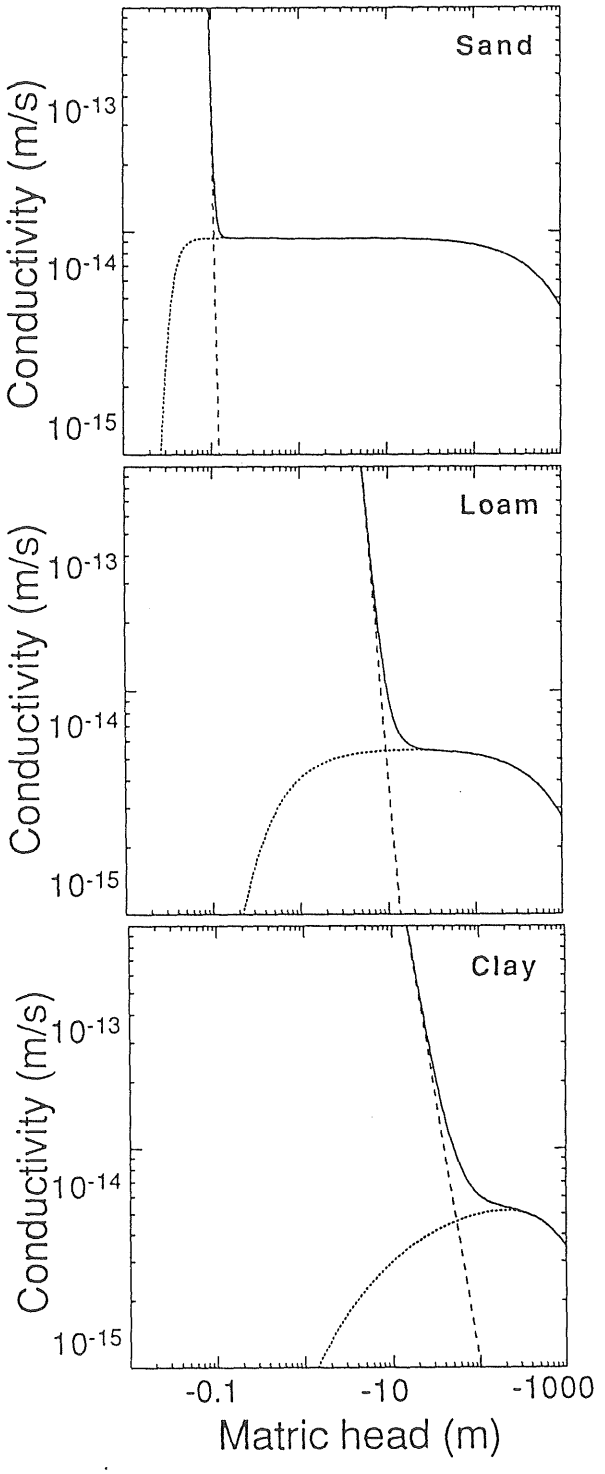

Figure 50 Relationship between matric head and conductivities for three soils, used in the high resolution model (see Chapter 3). Broken and dotted lines denote unsaturated hydraulic conductivity and vapor conductivity (under isothermal conditions), respectively, and solid line denotes the sum of those.

becomes smaller than that of vapor conductivity at a certain value of the matric head during soil drying. This value of matric head for each soil approximately agreed to that at the depth of the inflection (i.e., the bottom boundary of the DSL) in simulated water content profile. These features suggest that the water transport in vapor phase is more efficient than that in liquid phase within the DSL. Phenomenologically, it can be explained that the upward liquid water transport from deeper soil layers ceases at the bottom boundary of the DSL, and that resulting steep gradient of matric head enhances not the liquid water transport but the vapor water transport.

Figure 50 also indicates a difference among soils. The slope of hydraulic conductivity against matric head is gentler for fine-textured soil than for coarse-textured soil. Therefore, it is expected that for fine-textured soil the phase of water flux is more gently changed from liquid to vapor than for coarse-textured soil. In fact, this expectation was supported from model calculations (Section 3.3) and also from field measurements of isotopic compositions of soil water (Section 7.1).

Thus, it can be concluded that the change of the phase of water flux at the bottom boundary of the DSL is caused by the change in efficiency of water transport in liquid and vapor phase, and that the change of the phase of water flux takes place gradually at a wider region of the soil profile at around the bottom boundary of the DSL for fine-textured soil because of its gentler slope of hydraulic conductivity against matric head. The slope of hydraulic conductivity is closely relating with the value of specific water capacity [e.g., van Genuchten, 1980].

9.1.2 Mechanism of evaporation within the DSL

In general, the liquid and vapor phases of water within the soil pore are in thermodynamic equilibrium conditions, as expressed by Equation (2.9). From the equation, it is expected that the decrease of relative humidity, which is caused by a rise in soil temperature or by

an outflow of water vapor from a system introduces the decrease of matric head through an evaporation of liquid water. If there is sufficient liquid water supply to a system, no decrease in matric head makes liquid water freely evaporate, and relative humidity of pore air would be maintained at almost unity. However, in the case of no liquid water supply, it would be expected that evaporation transiently occurs until matric head is adjusted to equilibrium with pore air humidity and then evaporation ceases. On the contrary, the increase of relative humidity due to a decrease in soil temperature or an inflow of water vapor into a system could introduce a transient condensation of vapor, even though the relative humidity is considerably smaller than unity. (Note that the saturation vapor pressure or specific humidity is defined for free water surfaces.) It is worthwhile examining more quantitatively whether the evaporation within the DSL actually takes place by the mechanisms presented above.

By applying the chain rule to the following equation as a rewritten form of Equation (2.9):

$$\psi = \frac{RT}{g} \log(q/q_{sat}(T)), \tag{9.1}$$

the change rate of volumetric water content within the DSL can be expressed as,

$$\frac{\partial \theta}{\partial t} = [log(\frac{q}{q_{sat}(T)})\frac{\partial T}{\partial t} + \frac{T}{q}\frac{\partial q}{\partial t} - \frac{T}{q_{sat}(T)}\frac{\partial q_{sat}(T)}{\partial t}]\frac{R}{g}\frac{d\theta}{d\psi}, \tag{9.2}$$

where $d\theta/d\psi$ is often called the specific water capacity. In this equation, order of the first term of the right hand side is negligibly small relative to that of the other terms for common situations. Although the second term of the right hand side is not always negligible, it is expected to be smaller than the third term at the upper region of the DSL and is eliminated in the present analysis. Finally Equation (9.2) can be rewritten by finite difference approximation as follows:

$$\triangle\theta = -\frac{d\theta}{d\psi}\frac{RT}{gq_{sat}(T)}\triangle q_{sat}(T). \tag{9.3}$$

Figure 51 shows the relationship between $\Delta\theta$ and $\Delta q_{sat}(T)$ evaluated based on the data of 4-hour interval on the IOD at each observation site. Average values from 0 to 1 cm depth

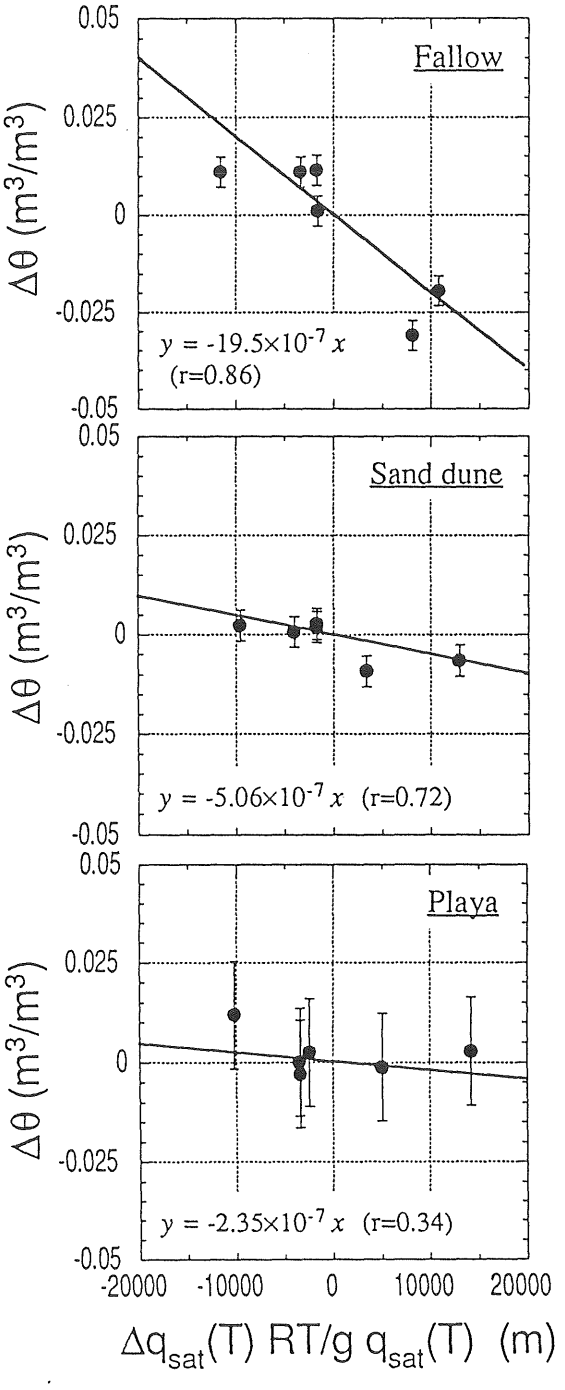

Figure 51 Relationship between changes in surface water content and soil temperature, evaluated by data on IOD for the three sites.

were used for the fallow site and the sand dune site, and 0 to 5 cm depth for the playa site. The figure indicates a good negative correlation between the changes of water content and of soil temperature. Absolute value of the slope of regression line corresponds to the specific water capacity (see Equation (9.3)). The values of specific water capacity obtained from the slope values for the fallow site and the sand dune site are quite reasonable for those under soil dryness of pF 4 to 5 for sand and sandy loam, respectively [van Genuchten, 1980; Campbell et al., 1993]. Thus, these suggest the validity of the concept that the evaporation within the DSL takes place by the mechanisms mentioned above. Nevertheless, for the playa site the specific water capacity estimated from the slope of regression line is too small relative to that expected from the moisture retention data in the previous works, even though the correlation coefficient (r) is very small due to an inhomogeneity in horizontal moisture distribution. The slope value for the playa site may be underestimated due to the effect of non-negligible liquid water transport into the upper DSL. Considering the discussion in previous section, it is reasonable to conclude only for the playa site that the two types of evaporation (i.e., evaporation at the bottom boundary of the DSL and evaporation within the DSL) tend to combine over the lower part of the DSL.

9.2 Redefinition of the DSL

In addition to the above discussion, it is necessary to reexamine the physical properties and definition of the DSL.

As indicated in Figure 50, any soils commonly have a matric head level (or a water content level) where the conductivity of liquid water is less than the conductivity of vapor water. As a result, when soil drying progresses from the soil surface to deeper depth, a soil layer where water can not be transported in the liquid phase is formed at around the soil surface. This would be a mechanism of the DSL formation. For sandy soils, the bottom boundary of the layer is clear because the the reversal of the magnitude of the

two conductivities occurs at a narrow band of matric head. Therefore, it is reasonable to assume that there is no liquid water transport within the DSL, and this has been the definition of the DSL. For clayey soils, however, the reversal of the conductivities occurs gradually at a relatively wide band of matric head so that the bottom boundary of the layer is not very clear. In the present study, the bottom boundary of the DSL, which is determined by difference in color between the DSL and the underlying layer, was located below the upper limit of the liquid water transport region at the playa site (Section 7.1). In other words, observed results suggest that water can move in liquid phase for a clayey soil even in the DSL. At the same time, the results also suggest that there is a reduction of the humidity in the DSL even for a clayey soil. This reduction can not be explained solely by an effect of the decrease in osmotic potential with salt accumulation at the surface soil (Sections 5.3 and 7.3), and is appeared to be caused by the huge decrease in matric head due to an insufficient liquid water supply to it. Thus, in order to make the definition universal by including fine-textured soils, the DSL should be redefined as the layer in which a reduction of relative humidity occurs due to lack of or insufficient liquid water supply from deeper layers. The color difference between the DSL and an underlying layer, which had been commonly used as the simplest measure of the bottom boundary of the DSL, may reflect an insufficient mobility of liquid water, while it is necessary to be investigated further from an aspect of the relationship between the liquid water mobility and optical properties of soil matrix.

Chapter 10

Conclusions

(1) For bare soils, evaporation of soil water takes place at the bottom boundary of the DSL throughout the day. In addition to this, evaporation also occurs within the DSL in the forenoon. Waters evaporating within the DSL are those transported in the vapor phase from below the DSL and/or from the atmosphere and condensed in the previous afternoon and nighttime. The former type of evaporation is caused by a deficit of or insufficient liquid water supply from deeper soil layers, and the latter type of evaporation is introduced by change in the conditions of equilibrium between the liquid and vapor phases of water in the DSL mainly due to diurnal variation of solar radiation.

(2) For coarse-textured soils, the phase of water transported upward changes at a narrow zone around the bottom boundary of the DSL, and the amounts of evaporation and condensation occurring within the DSL is small. In contrast, for fine-textured soils, the liquid water transport is not negligible even in the DSL, and two types of evaporation combine over a wider zone. The dependency of the structure and temporal behavior of the evaporation zone upon the soil texture is related with the difference in specific water capacity ($d\theta/d\psi$) among soils.

(3) Degree of the restriction of evaporation during soil drying depends strongly on the depth of a dominant part of the evaporation zone and increases with the development of

the DSL. In the forenoon, however, the flux of evaporation into the atmosphere does not decrease very much due to a contribution of the evaporation of water within the DSL. The movement of the location of this effective evaporation zone affects the energy partitioning of available energy and induces an asymmetric diurnal variation in energy fluxes at the soil surface.

(4) The DSL should be redefined as the layer in which a reduction of relative humidity occurs due to lack of or insufficient liquid water supply from deeper soil layers and the layer has whitish color relative to that of the underlying soil.

Acknowledgements

The author wishes to express his gratitude to his adviser, Professor Tsuneharu Yonetani, and his former adviser, Dr. Atsushi Takeda, for their guidance and encouragement during the graduate work and research. Special thanks are extended to Dr. Jun Shimada for his continuing guidance and helpful support throughout the course of this research, and to Dr. Tadashi Tanaka, Dr. Norio Tase and Professor Shinkichi Kishi, for their guidance and valuable comments. The author is also grateful to his B.S. adviser, Professor Isamu Kayane, for giving a guide to this research.

The author is indebted to Dr. Michiaki Sugita and Professor C.M. Madduma Bandara (University of Peradeniya, Sri Lanka) for reviewing the manuscript and providing helpful comments. Thanks are also expressed to Dr. Tokuo Kishii, Dr. Yasuhisa Kuzuha, and other staff members of National Research Institute for Earth Science and Disaster Prevention, for making available facilities and supporting analyses, and to Dr. Fumi Sugita (Chiba University of Commerce) for her technical advice while conducting numerical simulations. The author is grateful to Dr. Makoto Taniguchi (Nara University of Education) and the staff members of CSIRO Division of Water Resources, Australia, for their supporting field observation at the playa site. In addition, thanks are also extended to the staff members of Institute of Geoscience, University of Tsukuba, and the author's colleagues, for their supports and discussion.

Finally, the author would like to thank his son Kaoru, daughter Miwa, and wife Sachiko, for their support and encouragements.

Reference

Abramopoulos, F., Rosenzweig, C. and Choudhury, B. (1988): Improved ground hydrology calculations for global climate models (GCMs): Soil water movement and evapotranspiration. *J. Climate*, **1**, 921-941.

Abramova M.M. (1969): Movement of moisture as a liquid and vapor in soils of semi-deserts. In *Proceedings of the Wageningen Symposium on Water in the Unsaturated Zone*, IAHS-Unesco, Belgium, **2**, 781-789.

Allison, G.B. and Barnes, C.J. (1983): Estimation of evaporation from non-vegetated surfaces using natural deuterium. *Nature*, **301**, 143-145.

Allison, G.B. and Barnes, C.J. (1985): Estimation of evaporation from the normally "dry" Lake Frome in South Australia. *J. Hydrol.*, **78**, 229-242.

Allison, G.B., Barnes, C.J. and Hughes, M.W. (1983): The distribution of deuterium and oxygen-18 in dry soils: 2, Experimental. *J. Hydrol.*, **64**, 377-397.

Barnes, C.J. and Allison, G.B. (1983): The distribution of deuterium and oxygen-18 in dry soils: 1, Theory. *J. Hydrol.*, **60**, 141-156.

Barnes, C.J. and Allison, G.B. (1984): The distribution of deuterium and oxygen-18 in dry soils: 3, Theory for non-isothermal water movement. *J. Hydrol.*, **74**, 119-135.

Barnes, C.J. and Allison, G.B. (1988): Tracing of water movement in the unsaturated zone using stable isotopes of hydrogen and oxygen. *J. Hydrol.*, **100**, 143-176

Barnes, C.J. and Walker, G.R. (1989): The distribution of deuterium and oxygen-18 during unsteady evaporation from a dry soil. *J. Hydrol.*, **112**, 55-67.

Barnes, C.J., Allison, G.B. and Hughes, M.W. (1989): Temperature gradients on stable isotope profiles in dry soils. *J. Hydrol.*, **112**, 69-87.

Barton, I.J. (1979): A parameterization of the evaporation from non-saturated surfaces. *J. Appl. Meteorol.*, **18**, 43-47.

Baumgartner, A. and Reichel, E. (1975): *The World Water Balance : Mean Annual Global, Continental and Maritime Precipitation, Evaporation and Runoff.* Elsevier, Amsterdam, 179 pp.

Benoit, G.R. and Kirkham, D. (1963): The effect of soil surface conditions on evaporation of soil water. *Soil Sci. Soc. Am. Proc.*, **27**, 495-498.

Blake, G.R. (1965): Particle density. In Black, C.A. (ed.): *Methods of Soil Analysis: Part 1*, American Society of Agronomy, Madison, 371-373.

Bresler, E. and Laufer, A. (1974): Anion exclusion and coupling effects in nonsteady transport through unsaturated soils: 2, Laboratory and numerical experiments. *Soil Sci. Soc. Amer. Proc.*, **38**, 213-218.

Brutsaert, W. (1975): The roughness length for water vapor, sensible heat, and other scalars. *J. Atmos. Sci.*, **32**, 2028-2031.

Brutsaert, W. (1982): *Evaporation into the Atmosphere: Theory, History and Applications.* Kluwer Academic Pub., Dordrecht, 299 pp.

Brutsaert, W. and Chan,F.K.-F. (1978): Similarity functions D for water vapor in the unstable atmospheric boundary layer. *Boundary-Layer Meteorol.*, **14, 441-456.**

Brutsaert, W. and Chen, D. (1996): Diurnal variation of surface fluxes during thorough drying (or sever drought) of natural prairie. *Water Resour. Res.*, **32**, 2013-2019.

Budyko, M.I. (1948): *Evaporation under Natural Conditions.* GIMIZ, Leningrad, English Translation, Israel Progr. Sci. Translations, Jerusalem (1963), 130 pp.

Budyko, M.I. (1956): *Heat Balance of the Earth's Surface*, Gidrometeoizdat, Leningrad, 255 pp. (in Russian)

Budogovsky, A.I. (1964): *Evapotranspiration in plowland* (*Kochi no Jo-hassan*). Japanese Translation, Hatachi-Nougyou-Kenkyuukai, Tokyo (1965), 170 pp.

Bureau of Meteorology, Australia (1994): Kalgoorlie-Boulder Climate Averages 1939-1992. Bureau of Meteorology, Australia, Perth.

Businger, J.A. and Buettner, K.J.K (1961): Thermal contact coefficient (a term proposed for use in heat transfer). *J. Meteorol.*, **18**, 422.

Camillo, P.J. and Gurney, R.J. (1986): A resistance parameter for bare soil evaporation models. *Soil Sci.*, **141**, 90-105.

Camillo, P.J., Gurney, R.J. and Schmugge, T.J. (1983): A soil and atmospheric boundary layer model for evapotranspiration and soil moisture studies. *Water Resour. Res.*, **19**, 371-380.

Campbell, G.S. (1985): *Soil Physics with Basic: Transport Models for Soil-Plant System.* Elsevier, New York, 150 pp.

Campbell G.S., Jungauer, Jr., J.D., Shiozawa, S. and Hungerford, R.D. (1993): A one-parameter equation for water sorption isotherms of soils. *Soil Sci.*, **156**, 302-305.

Carson, T.N., Dodd, J.K., Benjamin, S.G. and Cooper, J.N. (1980): Satellite estimation of the surface energy balance, moisture availability and thermal inertia. *J. Appl. Meteorol.*, **20**, 67-87.

Cass, A., Campbell, G.S. and Jones, T.L. (1984): Enhancement of thermal water vapor diffusion in soil. *Soil Sci. Soc. Am. Proc.*, **48**, 25-32.

Chanzy, A. and Bluckler, L. (1993): Significance of soil surface moisture with respect to daily bare soil evaporation. *Water Resour. Res.*, **29**, 1113-1125.

Choshi Local Meteorological Observatory (1980): Climate of Chiba prefecture (*Chiba-ken no Kiko*). Choshi Local Meteorological Observatory, Choshi. (in Japanese)

Choudhury, B.J. and Monteith, J.L. (1988): A four-layer model for heat and budget of homogeneous land surfaces. *Quart. J. Roy. Meteorol. Soc.*, **114**, 373-398.

Coleman, M.L., Shepherd, T.J., Durham, J.J., Rouse, J.E. and Moore, G.R. (1982): Reduction of water with zinc for hydrogen isotope analysis. *Anal. Chem.*, **54**, 993-995.

Connel, L.D. and Bell, P.R.F. (1993): Modeling moisture movement in revegetating waste heaps: 1, Development of a finite element model for liquid and vapor transport. *Water Resour. Res.*, **29**, 1435-1443.

Connel, L.D., Bell, P.R.F. and Haverkamp, R. (1993): Modeling moisture movement in revegetating waste heaps: 2, Application to oil shale wastes. *Water Resour. Res.*, **29**, 1445-1455.

Craig, H. (1961): Standard for reporting concentration of deuterium and oxygen-18 in natural waters. *Science*, **113**, 1833-1834.

Daamen, C.C. and Simmonds, L.P. (1996): Measurement of evaporation from bare soil and its estimation using surface resistance. *Water Resour. Res.*, **32**, 1393-1402.

Davies, J.A. and Allen, C.D. (1973): Equilibrium, potential and actual evaporation from cropped surfaces in Southern Ontario. *J. Appl. Meteorol.*, **12**, 649-657.

Day, P.R. (1965): Particle fractionation and particle-size analysis. In Black, C.A. (ed.): *Methods of Soil Analysis: Part 1*, American Society of Agronomy, Madison, 545-567.

Deardorff, J.W. (1977): A parameterization of the ground surface moisture content for use in atmospheric prediction models. *J. Appl. Meteorol.*, **16**, 1182-1185.

de Vries, D.A. (1963): Thermal properties of soils. In van Wijk, W.R. (ed): *Physics of Plant Environment*, North-Holland Publishing Co., Amsterdam, 210-235.

Dickinson, R.E. (1984): Modeling evapotranspiration for three-dimensional global climate models. In *Climate processes and Climate Sensitivity*, Amer. Geophys. Union, Geophys. Monogr., 58-72.

Edelfsen, N.E. and Anderson, A.B.C. (1943): The thermodynamics of soil moisture. *Hilgardia*, **16**, 31-299.

Epstein, S. and Mayeda, T. (1953): Variation of ^{18}O content of waters from natural sources. *Geochim. Cosmochim. Acta*, **4**, 213-224.

Farrell, D.A., Greacen, E.L. and Gurr, C.G. (1966): Vapor transfer in soil due to air turbulence. *Soil Sci.*, **102**, 305-313.

Fritton, D.D., Kirkham, D. and Shaw, R.H. (1967): Soil water chloride redistribution under various evaporation potentials. *Soil Sci. Soc. Am. Proc.*, **31**, 599-603.

Fritton, D.D., Kirkham, D. and Shaw, R.H. (1970): Soil water evaporation, isothermal diffusion, and heat and water transfer, *Soil Sci. Soc. Am. Proc.*, **34**, 183-189.

Fuchs, M. and Tanner, C.B. (1967): Evaporation from drying soil. *J. Appl. Meteorol.*, **6**, 852-857.

Fukuda, H. (1955): Air and vapor movement in soil due to wind gustiness. *Soil Sci.*, **79**, 249-256.

Fukuhara,T, Pinder, J.F. and Sato, K. (1990): An approach to fully coupled heat and moisture transfer analysis in saturated-unsaturated porous media during surface evaporation. *J. Hydraulic, Coastal and Environ. Engineering*, **423**, 111-120. (in Japanese)

Fukuhara, T., Sato, K. and Baba, T. (1992): Movement of water vapor in sand column and mechanism of evaporation. *Ann. J. Hydraulic Engineering, JSCE*, **36**, 453-458. (in Japanese)

Fukuhara, T., Takano, Y. and Sato, K. (1994): Evaporation in sand column under diurnal temperature variation. *Ann. J. Hydraulic Engineering, JSCE*, **38**, 119-124. (in Japanese)

Fukumoto, M. and Hirota, T. (1994): The effect of surface soil moisture on heat balance at a bare soil surface. *J. Japan Soc. Hydrol. and Water Resour.*, **7**, 393-401. (in Japanese)

Furley, P.A. (1994): Tropical moist forests: Transformation or conservation? In Roberts, N. (ed.): *The Changing Global Environment*, Blackwell, Oxford, 304-331.

Gardner, H.R., and Hanks, R.J. (1966): Evaluation of the evaporation zone in soil by measurement of heat flux. *Soil Sci. Soc. Am. Proc.*, **30**, 425-428.

Gonfiantini, R. (1978): Standard for stable isotope measurements in natural compounds. *Nature*, **271**, 534-536.

Goudie, A. (1994): Dryland Degradation. In Roberts, N. (ed.): *The Changing Global Environment*, Blackwell, Oxford, 351-368.

Greenspan, L. (1977): Humidity fixed points of binary saturated aqueous solutions. *J. Res. Nat. Bureau Stds.*, **81A**, 89-96.

Gurney, R.J. and Hsu, A.Y. (1990): Relating evaporative fraction to remotely sensed data at the FIFE site. In *Proceedings of the AMS Symposium on FIFE, anahime, CA*, American Meteorological Society, Boston, 112-116.

Haltiner, G.J. and Martin, F.L. (1957): *Dynamical and Physical Meteorology.* McGraw-Hill, New York.

Hanks, R.J., Gardner, H.R. and Fairbourn, M.L. (1967): Evaporation of water from soils as influenced by drying with wind or radiation. *Soil Sci. Soc. Am. Proc.*, **31**, 593-598.

Heller, J.P. (1968): The drying through the top surface of a vertical porous column. *Soil Sci. Soc. Am. Proc.*, **32**, 778-786.

Hide, J.C. (1954): Observation on factors influencing the evaporation of soil moisture. *Soil Sci. Soc. Am. Proc.*, **18**, 234-239.

Hillel, D. (1971): *Soil and Water: Physical Principles and Processes.* Academic Press, New York, 288 pp.

Hillel, D. (1980): *Applications of soil Physics.* Academic Press, San Diego, 385 pp.

Hiyama, T., Shimada, J. and Kotoda, K. (1993): Evaluation of formation process of the dry surface layer by means of capacitance humidity sensor. *Bull. Environ. Res. Center, Univ. Tsukuba*, **7**, 75-83. (in Japanese)

Hiyama, T., Sugita, M. and Kayane, I. (1995): Variability of surface fluxes within a complex area observed during TABLE 92. *Agr. For. Meteorol.*, **73**, 189-207.

Holmes, R.M. (1959): A modulated soil moisture budget. *Mon. Wea. Rev.*, **87**, 101-106.

Hubble, G.D., Isbell, R.F. and Northcote, K.H. (1983): Features of Australian soils. In *Soils: an Australian view point*, Division of Soils, CSIRO, Melbourne / Academic Press, London, 17-47.

Hwang, S.-J. (1985): Effects of the soil moisture on the net radiation flux and soil heat flux at the ground surface. *Geograph. Rev. Japan*, **58A**, 39-46.

Ibaraki Prefecture (1987): Basic investigations for land classification (Tochi-Bunrui-Kihon-Chosa): 'Sawara'. Ibaraki Prefecture, Mito. (in Japanese)

Idso S.B., Jackson, R.D., Reginato, R.J., Kimball, B.A. and Nakayama, F.S. (1975): The dependence of bare soil albedo on soil water content. *J. Appl. Meteorol.*, **14**, 109-113.

Ishihara, Y., Shimojima, E and Harada, H. (1989): On the evaporation from bare land with an underlying restricted water table. *Annuals, Disas. Prev. Res. Inst., Kyoto Univ.*, **32B-2**, 281-295. (in Japanese)

Ishihara, Y., Shimojima, E. and Harada, H. (1992): Water vapor transfer beneath bare soil where evaporation is influenced by a turbulent surface wind. *J. Hydrol.*, **131**, 63-104.

Iwata, S. (1984): Japanese translation of Hillel, D. (1971): *Soil and Water: Physical Principles and Processes* (*Dojyo-Butsurigaku-Gairon: Tsuchi to Mizu no Kagaku*). Yogendo, Tokyo, 288 pp. (in Japanese)

Iwata, S, Tabuchi, T, and Warkentin, B. P. 1994. *Soil-Water Interactions: Mechanisms and Applications* (*2nd ed.*). Marcel Dekker, New York, 440 pp.

Japan Meteorological Agency (1991): *Climatic Table of Japan.* Japan Meteorological Agency, Tokyo, 478 pp.

Johnson, J.E. (1954): *Physical Meteorology.* John Wiley and Sons, New York.

Kasubuchi, T. (1982): Heat conduction of soil. *Report of Nat. Inst. Agr. Sci.*, **33B**, 1-54. (in Japanese)

Kayane, I. (1967): Recent problems in evapotranspiration studies. *Tenki*, **14**, 271-284. (in Japanese)

Kayane, I. (1973): *Cycle of Waters* (*Mizu no Junkan*). Kyoritsu-Shuppan, Tokyo, 230 pp. (in Japanese)

Kazanskiy, A.B. and Zolotokrylin, A.N. (1994): On the missing component in the equation for the land surface heat balance as applied to the heat exchange between the desert or semidesert surface and the atmosphere. *Boundary-Layer Meteorol.*, **71**, 189-195.

Kemp, P.R., Cornelius, J.M. and Reynolds, J.F. (1992): A simple model for predicting soil temperatures in desert ecosystems. *Soil Sci.*, **153**, 280-287.

Kendall, C. and Coplen, T.B. (1985): Multisample conversion of water to hydrogen by Zn for stable isotope determination. *Anal. Chem.*, **57**, 1437-1440.

Kim, C.P., Stricker, J.N.M. and Torfs, P.J.J.F. (1996): An analytical framework for the water budget of the unsaturated zone. *Water Resour. Res.*, **32**, 3475-3484.

Kimball, B.A., Jackson, R.D., Reginato, R.J., Nakayama, F.S. and Idso S.B. (1976): Comparison of field-measured and calculated soil-heat-fluxes. *Soil Sci. Soc. Am. J.*, **40**, 18-25.

Kobayashi, T. (1993): Effects of thermal gradients on the evaporation from a dry soil surface. *J. Japan Soc. Hydrol and Water Resour.*, **6**, 31-35. (in Japanese with English abstract)

Kobayashi, T., Matsuda, A., Kamichika, M. and Sato. T. (1986): Studies of the dry surface layer of sand dune field: 1, Modeling of the dry surface layer of sand under isothermal steady conditions. *J. Agr. Meteorol.*, **42**, 113-118.

Kobayashi, T., Matsuda, A., and Kamichika, M. (1987): Studies of the dry surface layer of sand dune field: 2, Effect of soil temperature gradients on the water content profiles in the dry surface layer. *J. Agr. Meteorol.*, **43**, 121-126.

Kobayashi, T., Matsuda, A. and Kamichika, M. (1989): A simple method for estimating the rate of evaporation from a dry sand surface. *J. Agr. Meteorol.*, **44**, 269-274.

Kobayashi, T., Matsuda, A., Kamichika, M. and Yamamura, Y. (1991a): Why the thickness of the dry surface layer in sand dune fields exhibits a diurnal variation? *J.Agr. Meteorol.*, **47**, 3-9.

Kobayashi, T., Takemasa, T., Hayashi, S., Miyagawa, K. and Kominami, Y. (1991b): A model of the growth of the dry surface layer in sand dune fields. *J. Agr. Meteorol.*, **47**, 151-157.

Kondo, J. (1994): *Meteorology of Water Environment (Mizu-Kankyo no Kisho-gaku)*. Asakura Shoten, Tokyo, 337 pp. (in Japanese)

Kondo,J. and Watanabe,T. (1992): Studies on the bulk transfer coefficients over a vegetated surface with a multilayer energy budget model. *J. Atmos. Sci.*, **49**, 2183-2199.

Kondo, J., Saigusa, N. and Sato, T. (1990): A parameterization of evaporation from bare soil surfaces. *J. Appl. Meteorol.*, **29**, 385-389.

Kondo, J., Saigusa, N. and Sato, T. (1992): A model and experimental study of evaporation from bare-soil surfaces. *J. Appl. Meteorol.*, **31**, 304-312.

Korzoun, et al. (eds.) (1977): *Atlas of World Water Balance.* USSR National committee for the International Hydrological Decade, UNESCO Press, Paris.

Kuzuha, Y., Ishihara, Y. and Shimojima, E. (1988): A numerical simulation on the evaporation in a bare land: In the case of a restricted groundwater table. *Annuals, Disas. Prev. Res. Inst., Kyoto Univ.*, **31B-2**, 255-274. (in Japanese)

Lee, T.J. and Pielke, R.A. (1992): Estimating the soil surface specific humidity. *J. Appl. Meteorol.*, **31**, 480-484.

Letey, J., Kemper, W.D. and Noonan, L. (1969): The effect of osmotic pressure gradients on water movement in unsaturated soil. *Soil Sci. Soc. Am. Proc.*, **33**, 15-18.

Lin, J.D. (1980): On the force-restore method for prediction of ground surface temperature. *J. Geophys. Res.*, **85**, 3251-3254.

Lvovitch, M.I. (1973): The global water balance. *Trans. Am. Geophys. Union*, **54**, 28-42.

Mahfouf, J.F. and Noilhan, J. (1991): Comparative study of various formulations of evaporation from bare soil using in situ data. *J. Appl. Meteorol.*, **30**, 1354-1365.

Mahrt, L. and Pan, H. (1984): A two-layer model of soil hydrology. *Boundary-Layer Meteorol.*, **29**, 1-20.

Manabe, S. (1969): The atmospheric circulation and the hydrology of the earth's surface. *Mon. Wea. Rev.*, **97**, 739-774.

Marlatt, W.E., Havens, A.V., Willits, N.A. and Brill, G.D. (1961): A comparison of computed and measured soil moisture under snap beans. *J. Geophys. Res.*, **66**, 535-541.

Maruyama, E. (1962): Study on the evaporation from a soil. *J. Meteorol. Res.*, **14**, 1-32.

Matsuda, A., Kamichika, M. and Ando, T. (1977): Vertical distribution of temperature near the ground surface in a sand dune area. *Bull. Sand Dune Res. Inst., Tottori Univ.*, **16**, 9-13. (in Japanese)

McCumber, M.C. and Pielke, R.A. (1981): Simulation of the effects of surface fluxes of heat and moisture in a mesoscale numerical model. Part1: Soil layer. *J. Geophys. Res.*, **86**, 9929-9938.

McInnes, K.J. (1981): Thermal conductivities of soils from dryland wheat regions of Eastern Washington. M.S. Thesis, Washington State University, Pullman.

Melayah, A., Bruckler, L. and Bariac, T. (1996a): Modeling the transport of water stable isotopes in unsaturated soils under natural conditions: 1. Theory. *Water Resour. Res.*, **32**, 2047-2054.

Melayah, A., Bruckler, L. and Bariac, T. (1996b): Modeling the transport of water stable isotopes in unsaturated soils under natural conditions: 2. Comparison with field experiments. *Water Resour. Res.*, **32**, 2055-2065.

Menenti, M. (1984): Physical aspects and determination of evaporation in deserts applying remote sensing Techniques. Report 10 (special issue). Inst. Land and Water Manag. Res., Wageningen, The Netherlands, 202 pp.

Millington, R.J. (1959): Gas diffusion in porous media. *Science*, **130**, 100-102.

Milly, P.C.D. (1982): Moisture and heat transport in hysteretic, inhomogeneous porous media: A matric head-based formulation and a numerical model. *Water Resour. Res.*, **18**, 489-498.

Milly, P.C.D. (1992): Potential evaporation and soil moisture in general circulation models. *J. Climate*, **5**, 209-226.

Monteith, J.L. (1973): *Principles of Environmental Physics.* American Elsevier, New York, 241 pp.

Nakagawa, S. (1982): Seasonal and diurnal variations of albedo for a field of pasture. *J. Japanese Assoc. Hydrol. Sci.*, **12**, 7-12.

Nakagawa, S. (1984): Study on evapotranspiration from pasture. *Environ. Res. Center Papers, Univ. of Tsukuba*, No. 4, 87 pp.

Nakano,M. (1991): *Mass Movement in Soil* (*Tsuchi no Bussitsu-Ido-Gaku*). Univ. of Tokyo Press, Tokyo, 189 pp. (in Japanese)

Nakano, M., Miyazaki, T., Shiozawa, S. and Nishimura, T. (1995): *Physical and Environmental Analysis of Soils.* Univ. of Tokyo Press, Tokyo, 236 pp. (in Japanese)

Nappo, C.J. (1975): Parameterization of surface moisture and evaporation rate in a planetary boundary layer model. *J. Appl. Meteorol.*, **14**, 289-296.

Nichols, W.E. and Cuenca, R.H. (1993): Evaluation of the evaporative fraction for parameterization of the surface energy balance. *Water Resour. Res.*, **29**, 3681-3690.

Nimmo, J.R. (1991): Comment on the treatment of residual water content in "A consistent set of parametric models for the two-phase flow of immiscible fluids in the subsurface "by Luckner, L. et al., *Water Resour. Res.*, **27**, 661-662.

Nkedirim, L.C. (1972): A note on the albedo of surfaces. *J. Appl. Meteorol.*, **11**, 867-874.

Noilhan, J. and Planton, S. (1989): A simple parameterization of land surface processes for meteorological models. *Mon. Wea. Rev.*, **117**, 536-549.

Nomura, Y. and Inoue, M. (1979): Development of dry sand layer after the cessation of spray irrigation and its characteristics. *Bull. Sand Dune Res. Inst., Tottori Univ.*, **18**, 27-33. (in Japanese)

O'Kane, J.P. (1991): Implications for remote sensing of natural switching from atmosphere-controlled to soil-controlled evaporation or infiltration. In Schmugge, T.J. and Andre, J.-C. (eds.): *Land Surface Evaporation: Measurement and Parameterization*, Springer-Verlag, New York, 371-381.

Owe, M. and van de Griend, A.A. (1990): Daily surface moisture model for large area semi-arid land application with limited climate data. *J. Hydrol.*, **121**, 119-132.

Passerat de Silans, A. (1986): Transferts de masse et de chaleur dans un sol stratifié soumis à une excitation atmosphérique naturelle. Comparison modèles-expérience. These de Doctorat de l'Institut National Polytechnique de Grenoble.

Passerat de Silans, A., Bruckler, L., Thony J.L. and Vauclin, M. (1989): Numerical modeling of coupled heat and water flows during drying in a stratified bare soil: Comparison with field observations. *J. Hydrol.*, 105, 109-138.

Penman, H.L. (1941): Laboratory experiments on evaporation from fallow soil. *J. Agric. Sci.*, **31**, 454-465.

Penman, H.L. (1948): Natural evaporation from open water, bare soil, and grass. *Proc. Roy. Soc. London*, **193A**, 120-146.

Petterssen, S. (1959): On the influence of heat exchange on motion and weather systems. Scientific Report, No. 10, University of Chicago, Chicago.

Philip, J.R. (1957): Evaporation, and moisture and heat fields in the soil. *J. Meteorol.*, **14**, 354-366.

Philip, J.R. and de Vries, D.A. (1957): Moisture movement in porous materials under temperature gradients. *Trans. Am. Geophys. Union*, **38**, 222-232.

Pohn, H.A., Offield, T.W. and Watson, K. (1974): Thermal inertia mapping from satellites: Discrimination of geologic units in Oman. *J. Res. U.S. Geol. Surv.*, **2**, 147-158.

Pratt, D.A. and Ellyett, C.D. (1979): The thermal inertia approach to mapping of soil moisture and geology. *Remote Sens. Environ.*, **8**, 151-168.

Priestley, C.H.B. (1959): *Turbulent Transfer in the Lower Atmosphere.* University of Chicago Press, Chicago.

Priestley, C.H.B. and Taylor, R.J. (1972): On the assessment of surface heat flux and evaporation using large-scale parameters. *Mon. Wea. Rev.*, **100**, 81-92.

Qayyum, M.A. and Kemper, W.D. (1962): Salt concentration gradients in soils and their effects on moisture movement and evaporation. *Soil Sci.*, **93**, 333-342.

Revesz, K. and Woods, P.H. (1990): A method to extract soil water for stable isotope analysis. *J. Hydrol.*, **115**, 397-406.

Ronen, D., Yechieli, Y. and Shatkay, M. (1996): Characterization of water and solute transport in the unsaturated zone of a hypersaline environment. *Water Resour. Res.*, **32**, 3264-3275.

Ross, P.J., Williams, J. and Bristow, K.L. (1991): Equation for extending water-retention curves to dryness. *Soil Sci. Soc. Am. J.*, **55**, 923-927.

Rowntree, P.R. and Bolton, J.A. (1983): Simulation of the atmospheric response to soil moisture anomalies over Europe. *Quart. J. Roy. Meteorol. Soc.*, **109**, 501-526.

Sasamori, T. (1970): A numerical study of atmospheric and soil boundary layer. *J. Atmos. Sci.*, **27**, 1122-1137.

Sato, K., Fukuhara, T., Munakata, M. and Bories, S. (1990): Fundamental study on migration and accumulation of solute in unsaturated zone of soil column by evaporation. *J. Hydraulic, Coastal and Environ. Engineering*, **424**, 135-144. (in Japanese)

Scotter, D.R. and Raats, P.A.C. (1969): Dispersion of water vapor in soil due to air turbulence, *Soil Sci.*, **108**, 170-176.

Sellers, W.D. (1965): *Physical Climatology.* Univ. of Chicago Press, Chicago, 272 pp.

Sellers, P.J., Mintz, Y., Sud, Y.C. and Dalcher, A. (1986): A simple biosphere model (SiB) for use within general circulation models. *J. Atmos. Sci.*, **43**, 505-531.

Sepaskhah, A.R. and Boersma, L. (1979): Thermal conductivity of soils as a function of temperature and water content. *Soil Sci. Soc. Am. J.*, **43**, 439-444.

Shimada, J., Yamanaka, T., Tanaka, T., and Nandakumar, V. (1997): Role of soil water in the regional hydrological process in Sri Lanka. In Taniguchi, M. (Ed.), *Subsurface Hydrological Responses to Land Cover and Land Use Changes.* Kluwer, Boston, 35-46.

Shimojima, E., Curtis, A.A. and Turner, J.V. (1990): The mechanism of evaporation from sand columns with restricted and unrestricted water tables using deuterium under turbulent air flow conditions. *J. Hydrol.*, **117**, 15-54.

Shinjo, A. and Shirai, K. (1978): A problem about soil moisture and temperature changes in a case of finite soil type for an airtight container: A study of simultaneous transfer of heat and moisture in a soil (1). *Trans. Japanese Soc. Irrig. Dran. Reclam. Engineering*, **74**, 1-6. (in Japanese)

Shukla, J. and Mintz, Y. (1982): Influence of land surface evapotranspiration on the earth's climate. *Science*, **15**, 1498-1501.

Shurbaji, A.M. and Phillips, F.M. (1995): A numerical model for the movement of H_2O, $H_2^{18}O$, and ^2HHO in the unsaturated zone. *J. Hydrol.*, **171**, 125-142.

Shurbaji, A.M., Phillips, F.M., Campbell, A.R. and Knowlton, R.G. (1995): Application of a numerical model for simulating water flow, isotope transport, and heat transfer in the unsaturated zone. *J. Hydrol.*, **171**, 143-163.

Shuttleworth, W.J., Gurney, R.J., Hsu, A.Y. and Ormsby (1989): FIFE: The variation in energy partition at surface flux sites, In Rango, A. (ed.): *Remote Sensing and Large-Scale Global Processes (Proceedings of the IAHS Third International Assembly, Baltimore, MD, May 1989)*, IAHS Publ., 186, 67-74.

Slatyer, R.O. and McIlroy, I.C. (1961): *Practical Microclimatology.* CSIRO, Melbourne, 310 pp.

Sophocleous, M. (1979): Analysis of water and heat flow in unsaturated-saturated porous media. *Water Resour. Res.*, **15**, 1195-1206.

Sugita, M. and Brutsaert, W (1991): Daily evaporation over a region from lower boundary layer profiles measured with radiosondes. *Water Resour. Res.*, **27**, 747-752.

Sugita, M., Hiyama, T., Endo, N. and Tian, S.-F. (1995): Flux determination over a smooth surface under strongly unstable conditions. *Boundary-Layer Meteorol.*, **73**, 145-158.

Sun, S.-F. (1982): Moisture and heat transport in a soil layer forced by atmospheric conditions. M.S. Thesis, Dept. of Civil Engineering, University of Connecticut, 72 pp.

Takano, Y., Fukuhara, T. and Kurokawa, K. (1997): Heat and moisture transfer in soils and evaporation-drying process at arid region in Middle East: Meteorological observation and measurement of heat and moisture in soils at U.A.E.. *Ann. J. Hydraulic Engineering, JSCE*, **41**, 221-226.

Takeda, S. (1993): Restriction of evaporation caused by dry sand layer on Syounai dune. *J. Groundwater Hydrol.*, **35**, 217-225.

Thornthwaite, W.C. and Mather, J.R. (1955): The water balance. Publications in Climatology VIII(1), 86 pp.

Tottori Prefecture (1975): Basic investigations for land classification (Tochi-Bunrui-Kihon-Chosa): 'Tottorihokubu-Tottorinanbu'. Tottori Prefecture, Tottori.

van de Griend, A.A. and Owe, M. (1994): Bare soil surface resistance to evaporation by vapor diffusion under semiarid conditions. *Water Resour. Res.*, **30**, 181-188.

van de Griend, A.A., Camillo, P.J. and Gurney, R.J. (1985): Discrimination of soil physical parameters, thermal inertia, and soil moisture from diurnal surface temperature fluctuations. *Water Resour. Res.*, **21**, 997-1009.

van Genuchten, M.T. (1980): A closed-form equation for predicting the hydraulic conductivity of unsaturated soils. *Soil Sci. Soc. Am. J.*, **44**, 892-898.

van Hylckama, T.E.A. (1966): Evaporation from vegetated and fallow soils. *Water Resour. Res.*, **2**, 99-103.

van Keulen, H. and Hillel, D. (1974): A simulation study of the drying phenomenon. *Soil Sci.*, **118**, 270-273.

van Wijk, W.R. and Derksen, W.J. (1963): Sinusoidal temperature variation in a layered soil. In van Wijk, W.R. (ed): *Physics of Plant Environment.* North-Holland Publishing Co., Amsterdam, 171-209.

Veihmeyer, F.J. and Hendrickson, A.H. (1955): Does transpiration decreases as the soil moisture decreases. *Trans. Am. Geophys. Union*, **36**, 425-448.

Ward, R.C. (1967): *Principles of Hydrology.* McGraw-Hill, London, pp.

Walker, J. and Rowntree, P.R. (1977): The effect of soil moisture on circulation and rainfall in a tropical model. *Quart. J. Roy. Meteorol. Soc.*, **103**, 29-46.

Walker, G.R., Hughes, M.W., Allison, G.B. and Barnes, C.J. (1988): The movement of isotopes of water during evaporation from a bare soil surface. *J. Hydrol.*, **97**, 181-197.

Walker, G.R., Woods, P.H. and Allison, G.B. (1994): Interlaboratory comparison of methods to determine the stable isotope composition of soil water. *Chem. Geol. (Isot. Geosci. Sect.)*, **111**, 297-306.

Warrick, A.W. and Nielsen, D.R. (1980): Spatial variability of soil physical properties in the field. In Hillel, D. (ed.) (1980): *Applications of Soil Physics.* Academic Press, San Diego, 319-344.

Westcot, D.W. and Wierenga, P.J. (1974): Transfer of heat by conduction and vapor movement in a closed soil system. *Soil Sci. Soc. Am. Proc.*, **38**, 9-14.

Wetzel, P.J. and Chang, T.J. (1987): Concerning the relationship between evapotranspiration and soil moisture. *J. Climate Appl. Meteorol.*, **26**, 18-27.

Whitford, W.G. (1989): Abiotic controls on the functional structure of soil food webs. *Biol. Fertil. Soils*, **8**, 1-6.

Yamanaka, T and Shimada, J. (1997): Simple but reliable method to extract soil water for stable isotope analysis. *J. Japan Soc. Hydrol. Water Resour.*, **10**, 181-184.

Yamanaka, T. and Takeda, A. (1994a): Fundamental study of water and energy exchanges at the dry bare soil surface: 1, Numerical experiments by using quasi-steady-state theoretical scheme. *Proc. Ann. Meeting Japanese Assoc. Hydrol. Sci.*, **8**, 92-95. (in Japanese)

Yamanaka, T. and Takeda, A. (1994b): Fundamental study of water and energy exchanges at the dry bare soil surface: 2, Wind tunnel experiment on the dependency of evaporation on wind speed. *Proc. Ann. Meeting Japanese Assoc. Hydrol. Sci.*, **8**, 96-97. (in Japanese)

Yamanaka, T., Hiyama, T. and Shimada, J. (1994): Behavior of the water vapor in the sandy soil during the bare soil evaporation. *J. Japanese Assoc. Hydrol. Sci.*, **24**, 31-46. (in Japanese with English abstract)

Yamanaka, T., Sugita, F. and Takeda, A. (1995a): An experimental study on relative humidity at the soil surface: Is bulk a method effective? *Bull. Environ. Res. Center, Univ. Tsukuba*, **20**, 55-67. (in Japanese)

Yamanaka, T., Sugita, F. and Takeda, A. (1995b): Restriction of evaporation and surface

energy balance variation during soil drying. *Proc. Ann. Meeting Japanese Assoc. Hydrol. Sci.*, **9**, 70-73. (in Japanese)

Yamanaka, T., Takeda,A. and Shimada, J. (1996): Evaporation beneath the soil surface: Field observation and numerical experiments. In *Proceedings of IGBP/BAHC-LUCC Joint Inter-Core Projects Symposium on Interactions between the Hydrological Cycle and Land Use/Cover*, 196-199.

Yamanaka, T., Takeda, A., and Sugita, F. (1997): A modified surface-resistance approach for representing bare-soil evaporation: Wind-tunnel experiments under various atmospheric conditions. *Water Resour. Res.*, **33**, 2117-2128.

Yasuda, N and Toya, T. (1981): Evaporation from nonsaturated surface and surface moisture availability. *Pap. Meteorol. Geophys.*, **32**, 89-98.

Yasunari, T., Kitoh, A. and Tokioka, T. (1991): Local and remote responses to excessive snow mass over Eurasia appearing in the northern spring and summer climate -A study with the MRI-GCM. *J. Meteorol. Soc. Japan.*, **69**, 473-487.

Ye, Z. and Pielke, R.A. (1993): Atmospheric parameterization of evaporation from non-plant-covered surfaces. *J. Appl. Meteorol.*, **32**, 1248-1258.

Yeh, T.C., Wetherald, R.T. and Manabe, S. (1984): The effect of soil moisture on the short term climate and hydrology change: A numerical experiment. *Mon. Wea. Rev.*, **112**, 474-490.

Appendix A

Theory for distribution of isotopic compositions of soil water

By assuming an isothermal system under quasi-steady state conditions, Barnes and Allison [1983] derived the following mathematical model which describes the vertical profiles of isotopic compositions of soil water:

Vapor transport region

$$\delta_i = \alpha_i^{*-1}\{\delta_i^a + \epsilon_i^* + [\eta_i(1+\delta_i^{res}) + \delta_i - \delta_i^a]\}/[z/(z+h_a\bar{z})] \tag{A.1}$$

Liquid water transport region

$$\delta_i = (\delta_i^{ef} + \delta_i^{res})\exp(-f(z)/\hat{z}_i) + \delta_i^{res} \tag{A.2}$$

where δ_i is the isotopic delta value for species i (suffix a means the value of the vapor in the atmosphere; res the value of input water (i.e., deep soil water or antecedent precipitation); ef the value at the evaporating front), α_i^* the equilibrium isotope fractionation factor, ϵ_i^* ($\equiv 1-\alpha_i^*$) the equilibrium enrichment, η_i ($\equiv D_v/D_{vi}-1$) the diffusion ratio excess, D_v the vapor diffusivity, z the depth, h_a the relative humidity in the atmosphere, $\bar{z}$ ($\equiv \rho_{vsat}D_{ve}/\rho_l E$) the penetration depth, ρ_{vsat} the saturation vapor density, D_{ve} effective vapor diffusivity, ρ_l the density of liquid water, E the evaporation rate, $\hat{z}_i$ ($\equiv D_{lei}/E$) the decay

length, D_{lei} the effective liquid water diffusivity for species i, and depth function $f(z)$ is defined as

$$f(z) = \bar{\theta} \int_{z_{ef}}^{z} dz/\theta \tag{A.3}$$

in which θ and $\bar{\theta}$ are the volumetric water content and its average over z_{ef} to z, respectively.

Although this analytical model have been modified for applying to non-isothermal and quasi-steady state conditions [Barnes and Allison, 1984], isothermal and non-steady-state conditions [Barnes and Walker, 1989], and now numerical models were developed for non-isothermal and non-steady-state conditions [Shurbaji and Phillips, 1995; Melayah et al., 1996], original version of Barnes and Allison [1983] model (i.e., Equations (A.1) and (A.2)) is known to well simulate the shape of isotopic profile.

Figures A1-A4 show the vertical profiles of δD and $\delta^{18}O$ in soil water and their δ-diagram representation, calculated with Equations (A.1) and (A.2) for some different conditions. Figure A1 indicates that the isotopic profiles have a peak at a certain depth below the soil surface, and that data above the peak are plotted on a line in δ-diagram and data below the peak are plotted on another line. Comparison between Figures A1 and A2 suggests that when evaporation rate is small (i.e., the soil is in drier conditions), the location of the peak is deeper, but the two lines in the δ-diagram do not change. Comparison between Figures A1 and A3 suggests that the difference in isotopic compositions of input water is reflected in the slope and offset of the two line in δ-diagram. On the other hand, comparison between Figures A1 and A4 suggests the difference in isotopic compositions of the vapor in the atmosphere is reflected in the line for the data above the peak, but is hardly reflected in the line for the data below the peak.

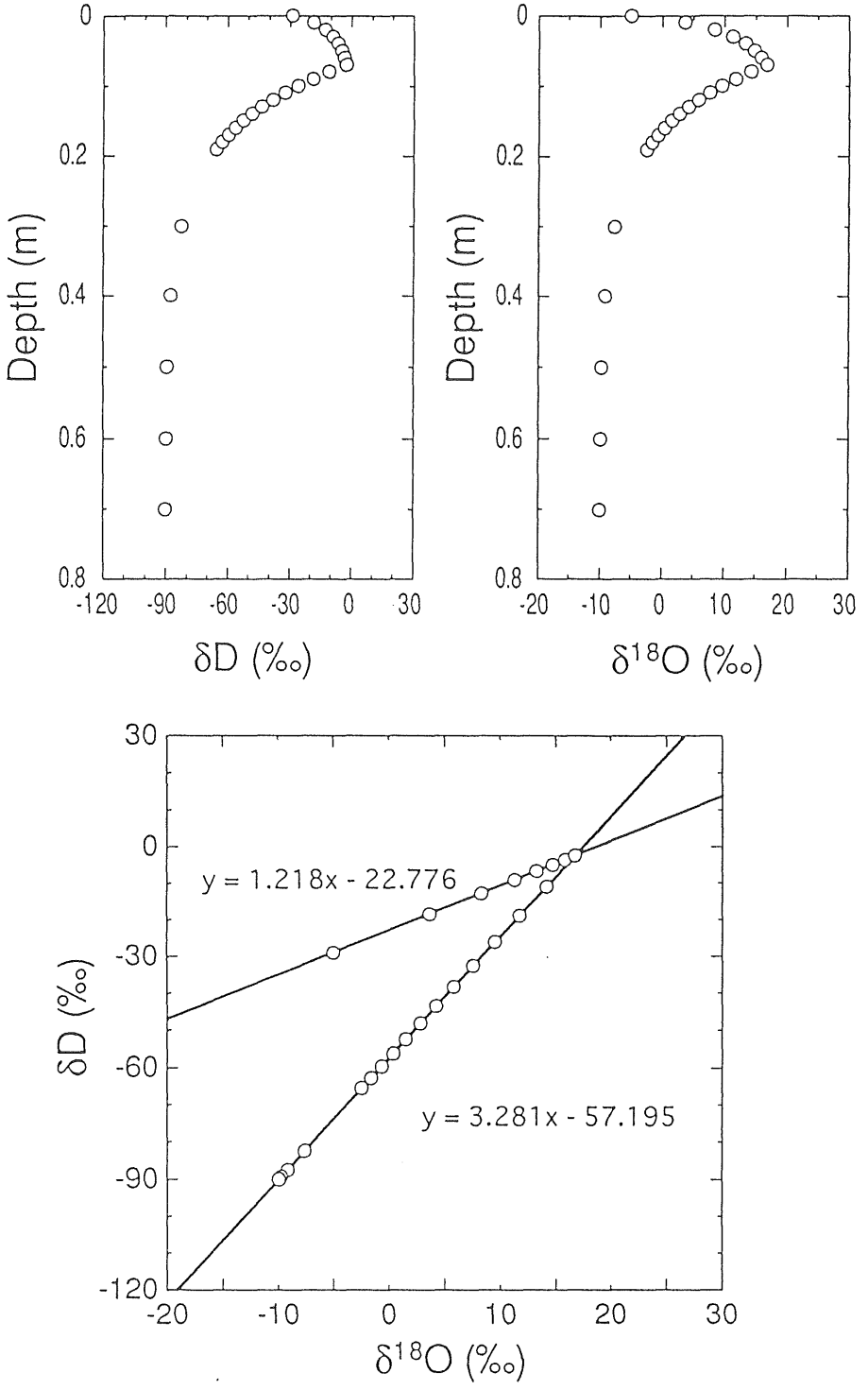

Figure A1 Vertical distribution of isotopic compositions of soil water and its δ-diagram, calculated by the model of Barnes and Allison [1983] with E = 0.1 mm/d, δD^{res} = -90 ‰, $\delta^{18}O^{res}$ = -10 ‰, δD^{a} = -100 ‰, and $\delta^{18}O^{a}$ = -14 ‰.

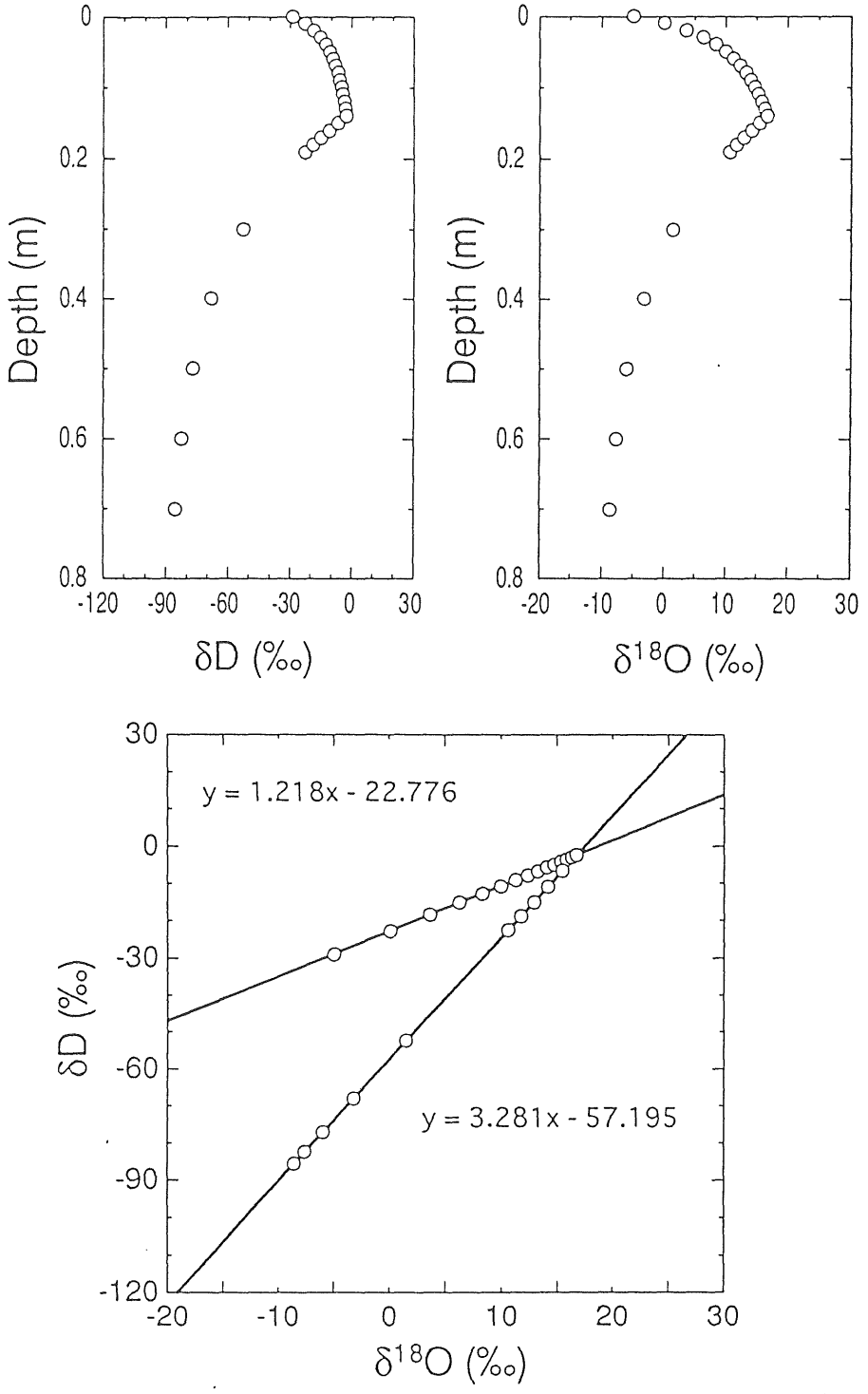

Figure A2 Calculated vertical distribution of isotopic compositions of soil water and its δ-diagram (calculation conditions are identical to those in Figure A1 except for E = 0.05 mm/d).

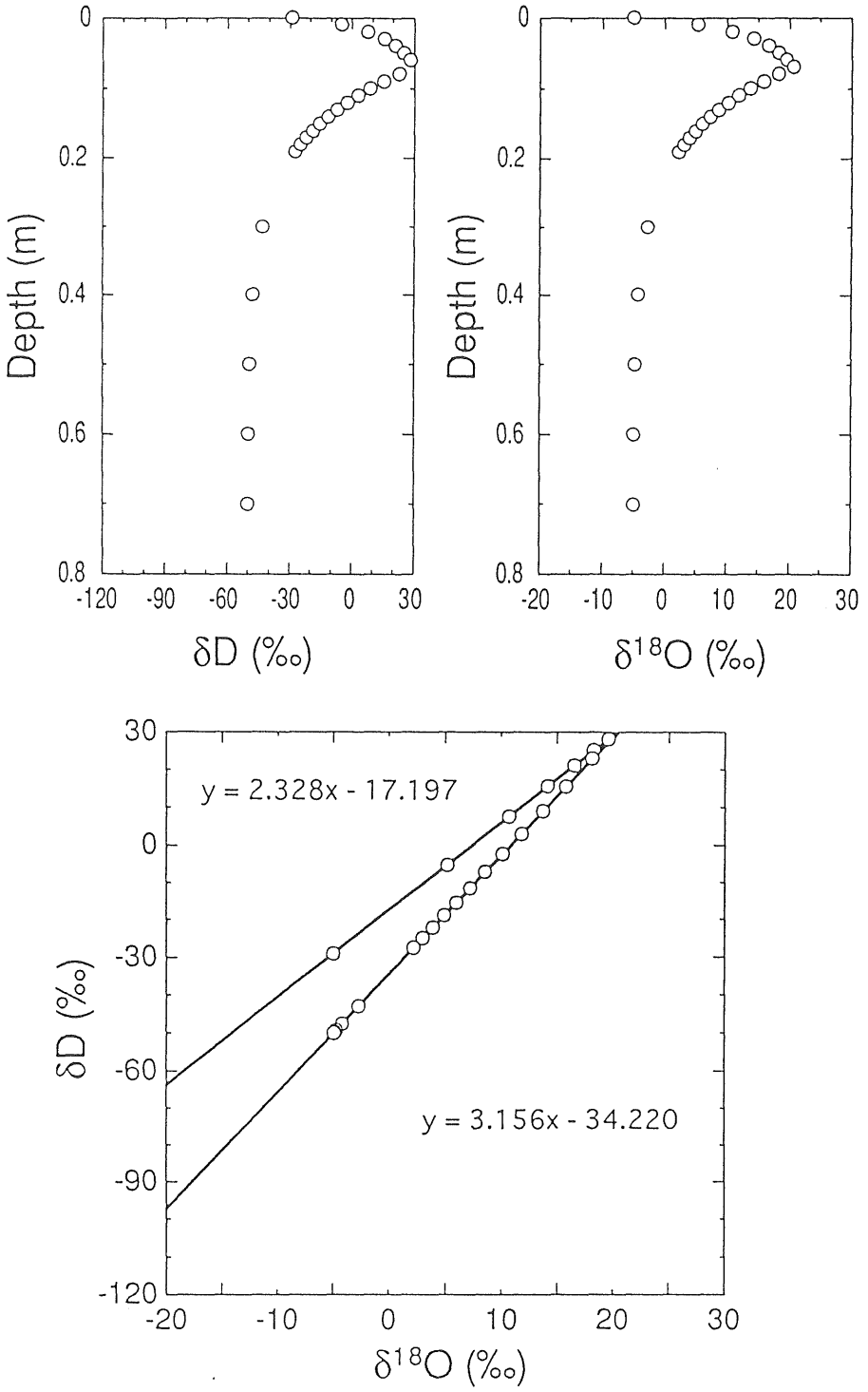

Figure A3 Calculated vertical distribution of isotopic compositions of soil water and its δ-diagram (calculation conditions are identical to those in Figure A1 except for δD^{res} = -50 ‰ and $\delta^{18}O^{res}$ = -5 ‰).

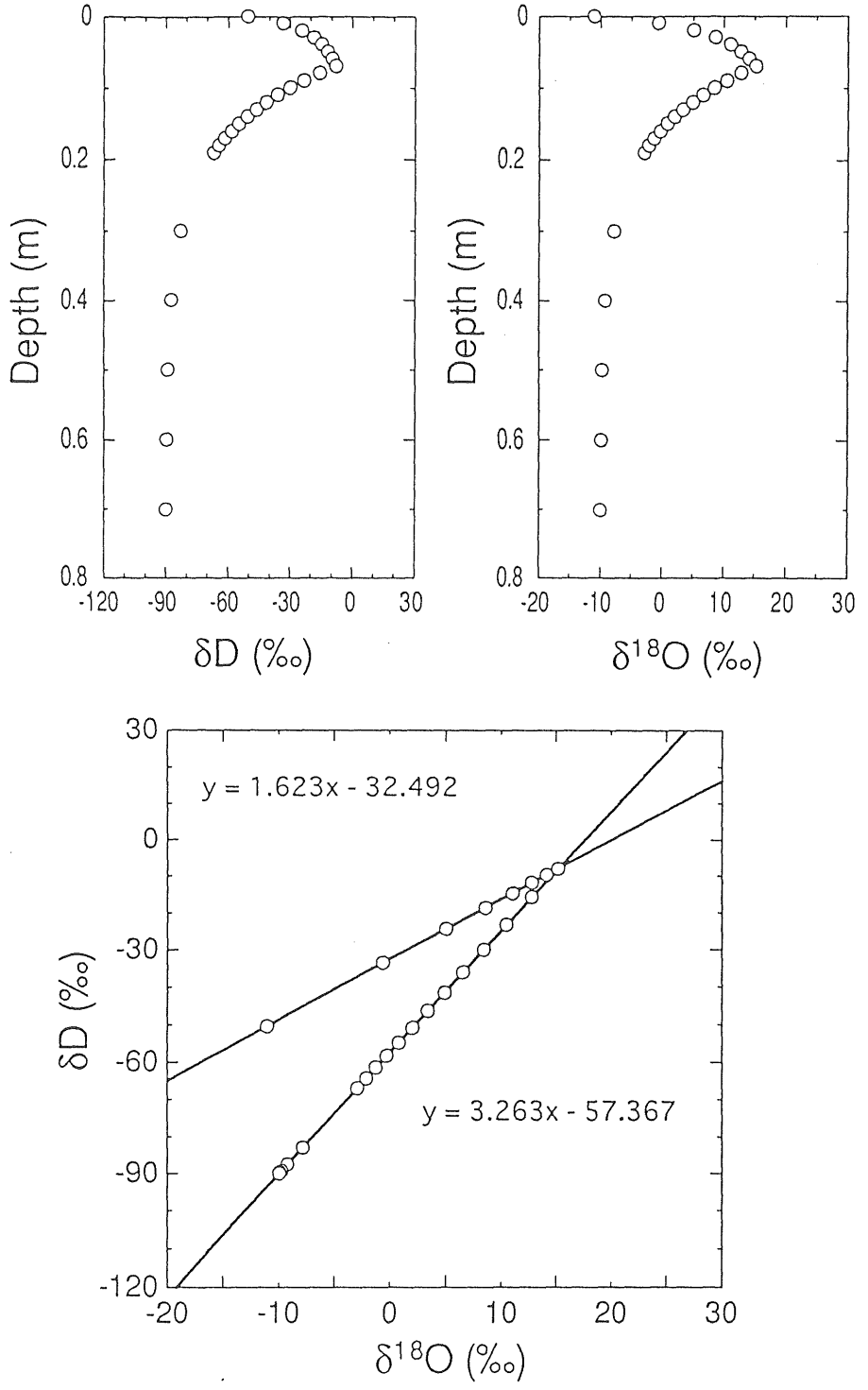

Figure A4 Calculated vertical distribution of isotopic compositions of soil water and its δ-diagram (calculation conditions are identical to those in Figure A1 except for δD^a = -120 ‰ and $\delta^{18}O^a$ = -20 ‰).

Appendix B

Derivation of equations for the conductive heat flux and heat storage in the soil

If the soil is homogeneous, so that the thermal conductivity does not vary with depth, the one dimensional heat conduction equation can be expressed as follows:

$$\frac{\partial T}{\partial t} = \frac{\lambda}{C}\frac{\partial^2 T}{\partial z^2}, \tag{B.1}$$

where T is the temperature, t the time, λ the thermal conductivity, C the volumetric heat capacity of the soil, and z the depth. Here, it is assumed that the surface temperature T_s is given by

$$T_s = \bar{T} + A_T \sin(\omega t), \tag{B.2}$$

where $\bar{T}$ is the mean soil temperature, A_T the amplitude of the surface temperature wave, and ω is the angular frequency of temperature oscillation ($= 2\pi/24 \times 60 \times 60$ for diurnal cycle). With the above boundary condition, Equation (B.1) can be solved for the simple case of a homogeneous semi-infinite soil as follows [Sellers, 1965, pp. 135-138; Lin, 1980]:

$$T(z,t) = \bar{T} + A_T \exp(-z/d)\sin(\omega t - z/d), \tag{B.3}$$

where d ($\equiv (2\lambda/C\omega)^{1/2}$) is the dumping depth, and the conductive heat flux $G_c(z,t)$ ($= -\lambda\partial T/\partial t$) can be derived by differentiating (B.3) with respect to z and t and then eliminating A_T by (B.3) as

$$G_c(z,t) = \frac{\lambda}{d}\left(\frac{1}{\omega}\frac{\partial T(z,t)}{\partial t} + T(z,t) - \bar{T}\right). \tag{B.4}$$

Differentiating Equations (B.2) and (B.3) with respect t give

$$\frac{\partial T_s}{\partial t} = A_T\omega\cos(\omega t) \tag{B.5}$$

$$\frac{\partial T(z,t)}{\partial t} = A_T\omega\exp(-z/d)\cos(\omega t - z/d) \tag{B.6}$$

$$= A_T\omega\exp(-z/d)\cos(\omega t)\cos(-z/d)$$

$$-A_T\omega\exp(-z/d)\sin(\omega t)\sin(-z/d). \tag{B.7}$$

Substituting Equations (B.2) and (B.5) into (B.7) gives

$$\frac{\partial T(z,t)}{\partial t} = \frac{\partial T_s}{\partial t}\exp(-z/d)\cos(-z/d) - \omega\exp(-z/d)\sin(\omega t)\sin(-z/d)(T_s - \bar{T}). \tag{B.8}$$

Finally, substituting (B.8) into (B.4) gives

$$G_c(z,t) = \frac{\lambda}{d}\{\exp(-z/d)[\frac{1}{\omega}\frac{\partial T_s}{\partial t}\cos(-z/d) - (T_s - \bar{T})\sin(-z/d)] + T(z,t) - \bar{T}\}. \tag{B.9}$$

On the other hand, change rate of heat storage (S) within the surface soil layer of the thickness of δ_s can be approximately given as

$$S = \frac{C\delta_s}{2}\left(\frac{\partial T_s}{\partial t} + \frac{\partial T(\delta_s,t)}{\partial t}\right) \tag{B.10}$$

By substituting Equations (B.5) and (B.7) into Equation (B.10), the following equation can be obtained:

$$S = \frac{C\delta_s}{2}\{\frac{\partial T_s}{\partial t} + \exp(-\delta_s/d)[\frac{\partial T_s}{\partial t}\cos(-\delta_s/d) - \omega(T_s - \bar{T})\sin(-\delta_s/d)]\}. \tag{B.11}$$

Equations (B.9) and (B.11) correspond to Equations (8.8) and (8.7), respectively.